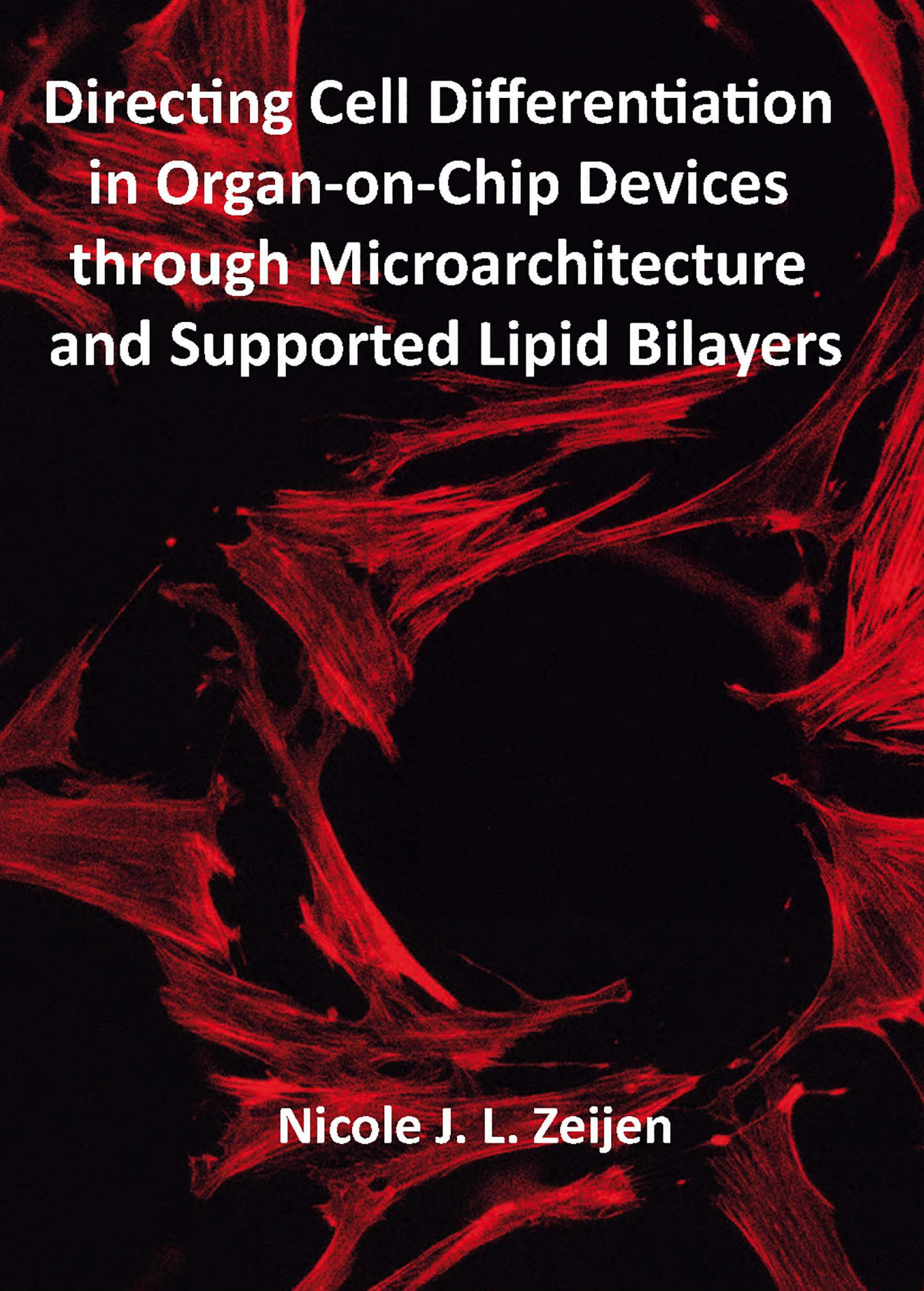
Directing Cell Differentiation in Organ-on-Chip Devices through Microarchitecture and Supported Lipid Bilayers
Nicole J. L. Zeijen

DIRECTING CELL DIFFERENTIATION IN ORGAN-ON-CHIP DEVICES THROUGH MICROARCHITECTURE AND SUPPORTED LIPID BILAYERS

Nicole Jeane Louise Zeijen

DIRECTING CELL DIFFERENTIATION IN ORGAN-ON-CHIP DEVICES THROUGH MICROARCHITECTURE AND SUPPORTED LIPID BILAYERS

DISSERTATION

to obtain
the degree of doctor at the Universiteit Twente,
on the authority of the rector magnificus,
prof. dr. ir. A. Veldkamp,
on account of the decision of the Doctorate Board
to be publicly defended
on Friday 4 June 2021 at 16.45 hours

by

Nicole Jeane Louise Zeijen

born on the 13th of October, 1984
in Oldenzaal, The Netherlands

This dissertation has been approved by:

Supervisor

prof. dr. ir. P. Jonkheijm

Co-supervisors

dr. A.D. van der Meer
dr. M.L. Bennink

Cover design: Nicole Zeijen
Printed by: Gildeprint
Lay-out: Nicole Zeijen
ISBN: 978-90-365-5190-8
DOI: 10.3990/1.9789036551908

© 2021 Nicole Jeane Louise Zeijen, The Netherlands. All rights reserved. No parts of this thesis may be reproduced, stored in a retrieval system or transmitted in any form or by any means without permission of the author. Alle rechten voorbehouden. Niets uit deze uitgave mag worden vermenigvuldigd, in enige vorm of op enige wijze, zonder voorafgaande schriftelijke toestemming van de auteur.

Graduation Committee:

Chair / secretary:	prof. dr. J.L. Herek
Supervisor:	prof.dr.ir. P. Jonkheijm
Co-supervisors:	dr. A.D. van der Meer
	dr. M.L. Bennink
Committee Members:	prof. dr. P.C.J.J. Passier
	prof. dr. N. Sommerdijk
	prof. dr. J.J.L.M. Cornelissen
	prof. dr. R.K. Truckenmüller

Chapter 1

Instructing cell differentiation in organ-on-chip devices through microarchitecture and supported lipid bilayers

Abstract

To realistically model a specific tissue or organ *in vitro*, it is key to create a cellular environment that is very close to the one found *in vivo*. When cells in a model are exposed to similar environmental triggers as they are *in vivo*, the cells can differentiate or mature into relevant cell types, and they can be triggered to organize themselves into a 3D network, reminiscent of an organ. Current literature states that an arrangement of cells that is similar to the *in vivo* organization results in more realistic cell responses in the *in vitro* models than when the cells are grown in a 2D cell culture. Physical and chemical cues can be incorporated to achieve cell culture models that mimic more closely the *in vivo* environment. The coating on, the stiffness of and the microstructure of the substrate on which the cells are deposited are instrumental to instruct cell differentiation of stem cells towards the desired cell types. Optimization of physical and chemical cues leads to better cellular network formation, which is the subject of the research described in this thesis. In this chapter, an overview is given of the possibilities of how microarchitecture and molecular coatings can be used to create a more realistic microenvironment in 3D cell culture models of tissues and organs.

1

1.1. Introduction

The development of complex multicellular organisms from a single fertilized cell is a highly organized process. This process is key in the phase of embryogenesis and continues to play a role throughout the entire lifespan of an organism, as even adults still have several stem cells available. Most notable are mesenchymal stem cells (MSCs) and hematopoietic stem cells in the bone marrow, satellite cells in skeletal muscle tissue, and neural stem cells (NSCs) in the brain. These stem cells are limited in the cell types they can differentiate into and their function is, as far as is known, to replenish the tissues when needed (for muscle, brain and bone) or to replenish blood cells. The differentiation of these stem cells into mature cell types is influenced by chemical and physical signals from their environment. This includes cell-cell contacts, the interaction of cells with their surrounding extracellular matrix (ECM), also known as cell-ECM interactions, and concentration gradients of soluble factors (chemotaxis).

The differentiation of stem cells towards a specific cell type depends on an intricate combination of chemical and physical cues from the environment of stem cells. Several molecular cues are found to be major triggers for a cellular pathway, leading to the desired differentiation of stem cells to a specific cell type. When effective, the resulting culture resembles a tissue with cell-cell and cell-ECM interactions that occur in *in vivo* tissue.

1.2. Why do we need *in vivo*-like models?

Insight in how the human body organizes tissues and organs, down to a cellular level, is very valuable. It provides a chance to study the mechanisms of diseases and can help to find or optimize strategies for treatment and prevention of those diseases. For the study of tissues and organs in a laboratory and to be able to manipulate these, there is a need for *in vitro* modelling of the *in vivo* environment. *In vitro* modelling gives the opportunity to make changes to the chemical and physical cues to establish which ones can effectively instruct cell differentiation and which ones are instrumental in the course of a disease. Disease models are used to gain insight in disease mechanisms and can also be used for testing and validating pharmaceuticals.[1] Research furthermore states that studies that used models based on human cells provide insights that are more in line with human *in vivo* results when compared with animal test models.[2,3] *In vitro* models also allow for real time analysis, which is very complicated to achieve in animal models[2,4] Therefore, it is generally

believed that i*n vitro* models will contribute to the reduction in the use of animals in biomedical and pharmacological research.

1.3. *In vitro* models of tissues and organs

The functionality of organ and tissue models depends very much on the design of the environment in which the cells are placed. As cultured cells respond to their surroundings, the design and the material of the microenvironment have a major influence on the morphology of the cells and on the cell-cell interactions within the model.[5]

1.3.1. Cells used in in vitro models

It is possible to use commercially available cell lines for *in vitro* modelling of tissue and organs. These cell lines are usually derived from tumour tissue and will therefore grow without restriction, resulting in models that approach the behaviour of the modelled *in vivo* tissue. Tumour-derived cells often still have tissue-specific characteristic behaviour, such as the tumour cell line Caco-2, which is derived from the colon and still displays enterocytic differentiation.[6,7] In advanced 3D *in vitro* modelling, these cell lines are now used mostly as disease models.[8]

Cells that are versatile and derived from healthy tissue are induced pluripotent stem cells (iPSCs) (**Figure 1.1**)[9]. These are made by dedifferentiation of fibroblasts or other adult cells and resemble the embryonic blastocyst cells. These cells have been shown to be able to differentiate into many mature cell types when exposed to appropriate differentiation induction media and therefore they are often used in organ and tissue models. iPSCs are more representative of *in vivo* tissue than tumour-derived cell lines, because the differentiation of iPSCs resembles the differentiation of embryonic or adult stem cells. However, this differentiation is less stable, with variation from culture to culture and concerns about genetic instability.[10–13]

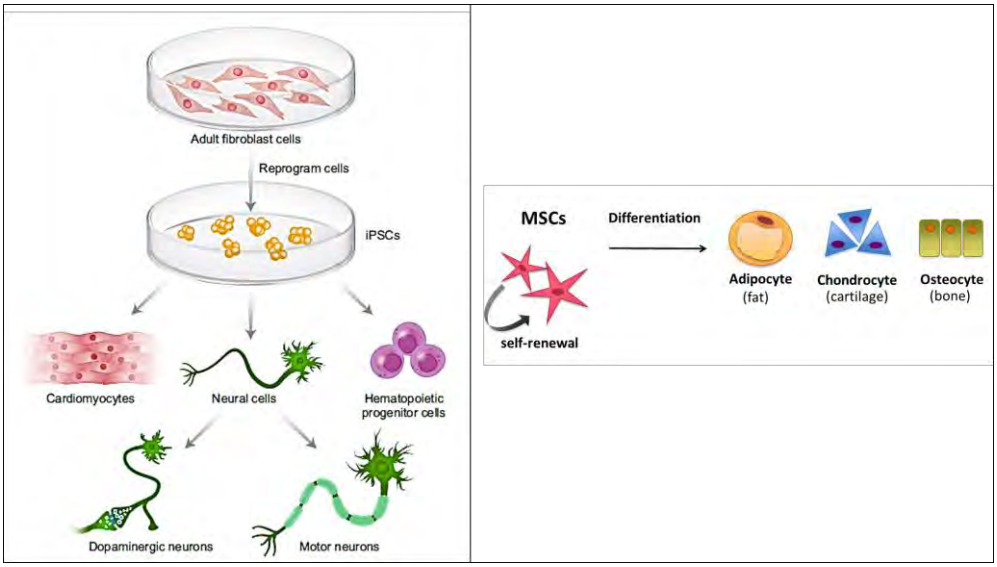

Figure 1.1 Adult stem cells: fibroblast cells taken from the human body can be reprogrammed to iPSCs and subsequently be induced to differentiate into multiple mature cell types[14] and the mesenchymal stem cells which can differentiate in three different tissues.[15] Reproduced with permission.

Not all models with (healthy) mature cells need dedifferentiated adult cells as starting material. Some cell types are stable when harvested and cultured *in vitro* and will grow to fill the model to the desired extend. These primary cells are adult cells that are harvested from healthy or diseased tissue and used without the need for differentiation, such as epithelial, endothelial and stromal cells, and tumour cells. These cells are patient-derived and can therefore be used for personalised medicine.[16]

Other adult cells that can be used are MSCs. These are available from the bone marrow and are destined for supporting tissue such as bone, cartilage and adipose tissue (**Figure 1.1**). These primary stem cells have the ability for self-renewal and their multipotency with adipogenic, osteogenic and chondrogenic cell fates makes them very suitable for models that use or study differentiation.[17] Cartilage development has a role in regenerative medicine as this tissue does not regenerate *in vivo* The application with MSCs could be a solution to this. Most interestingly, adipose tissue and bone are opposites in stiffness and the differentiation of MSCs is informative on the influence of the microenvironment on cell fate.

1.3.2. 2D models

Epithelial and endothelial cells have a 2D cell organization *in vivo*, where the cells form a monolayer on a basal membrane. Many organs that are relevant in the uptake of substances have an epithelial layer, separating one bodily compartment from another, or the outside world. This situation has been integrated in 2D *in vitro* models using a Transwell® culture plate where the epithelial cells are cultured on a permeable membrane and the substance of interest is added on top of the epithelial layer in the culture medium (**Figure 1.2**). The presence of the substance is then measured in the culture medium below the epithelial layer. Another use for the single cell layer model is to measure how signalling occurs across the cell layer as is done in blood-brain-barrier studies to find molecular cues that compromise the integrity of the barrier.[18,19]

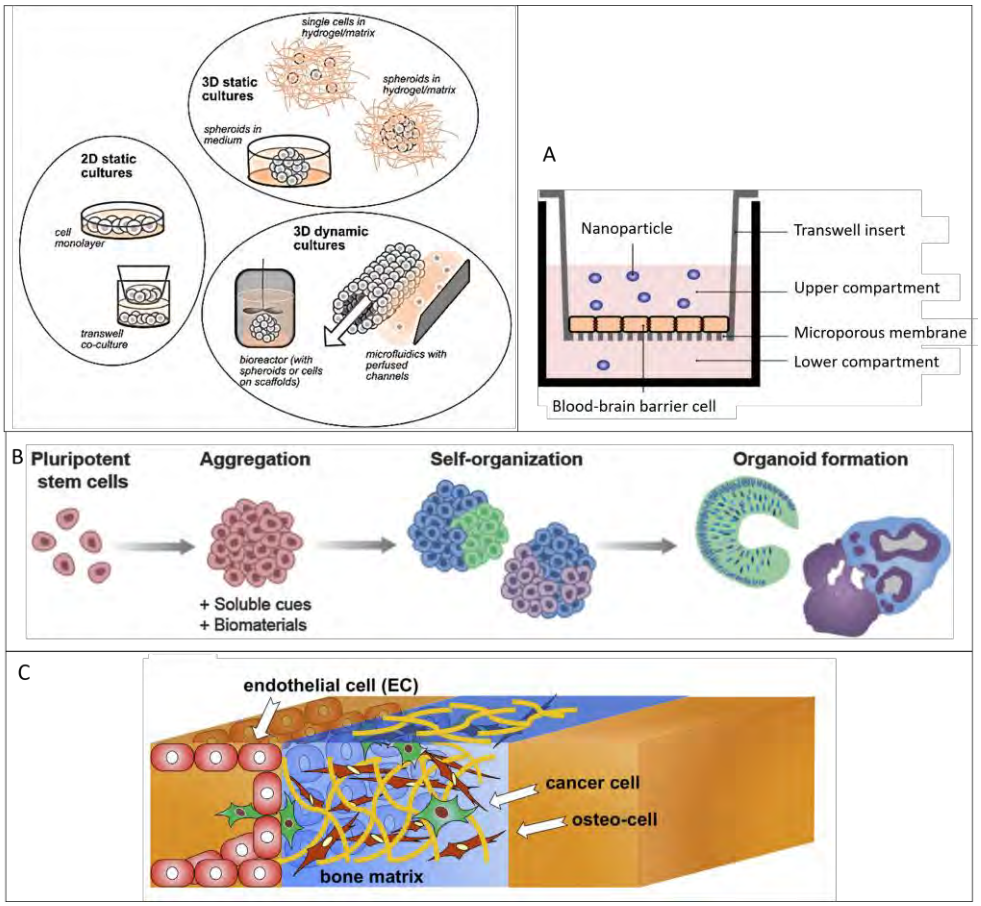

Figure 1.2 Methods of culturing cells in models:[20] A) 2D model with Transwell™ system used for studying the transport of nanoparticles across the blood-brain-barrier. The Transwell™ system separates two compartments by a porous membrane which allows culture of the barrier cells on one side.[19] B) Aggregation of stem cells can lead to the cell differentiation and cell organization within an organoid. This self-organized rudimentary organ is then used as a model[21] C) organoids, in which multiple cell types are combined in a microfluidic device. In this examples two cell types are suspended in hydrogel (cancer cell and osteo-cell) and one cell type in the flow channel (endothelial cell).[22] Reproduced with permission.

1.3.3. 3D Spheroids

To achieve a more *in vivo*-like 3D organization of cultured cells, it is possible to pack cells together in a hanging drop or on a low-attachment plate and let the cells clump together.[23] This forms a spheroid with a maximum size. As the aggregate becomes larger, the innermost cells become necrotic due to lack of diffusion of nutrients, oxygen and waste products. Spheroids are useful in studies where the difference in

nutrient concentration is a factor, such as in tumour formation, and in studies using liver spheroids to assess liver toxicity or to mimic hepatic metabolism to reflect *in vivo* phenotype and functionality.[2,4,24]

Spheroids are simplistic in their construction: they are only comprised of cells and culture medium. Once formed, they can grow either in suspension in non-adhering culture flasks, they can be suspended in a hydrogel or the spheroids can be placed in well plates to adhere and further develop, in which the spheroid has the function to trigger differentiation. [23,25]

1.3.4. Organoids

Organs, such as the intestine, always consist of more than one cell type In the small intestine we find enterocytes that have the absorption of nutrients to the bloodstream as primary function, goblet cells that provide a protective mucus layer and crypt cells (Paneth cells) which replenish both the enterocytes and the goblet cells in the epithelial layer of the intestine. To model this cell specialization and organization, an organoid has been made of either minced tissue sections or stem cells and combined with molecular cues to induce specific differentiation[26] The cells or tissue sections are suspended in hydrogels to obtain a 3D structure, often after they are formed into spheroids (**Figure 1.2**). The cells are then influenced by each other by the formation of cell-cell contacts to achieve the desired organization and form a rudimentary version of the organ.[21]

In an organoid, the hydrogel provides the necessary chemical cues, as well as serving as support system to keep the spheroids intact and not spread out on a surface. Frequently used hydrogels are Matrigel® and collagen type I. Matrigel® is an ill-defined derivative of mouse sarcoma cells and its composition varies greatly from batch to batch. It provides growth factors as molecular cues, as it is derived from a tumour. A major feature of the tissue models is to establish an *in vivo*-like cell organization. This can be, for example, the combination of multiple cell types, such as the lung model in which endothelial cells were combined with alveolar pneumocytes type I to mimic the air-blood barrier. Or it can be to provide a third dimension to the cell culture. This can be done by suspending the cells in hydrogels such as collagen or Matrigel®. These hydrogels do allow for cell invasion, as often used in research to metastases but they do not allow for deposition of the tissue ECM by the cells.

1.3.5. Bioprinting

Instead of relying on cell-cell contact formation to organize different cell types, it is possible to 3D-print different cell types at predetermined locations in the culture and achieve a tissue model inside the hydrogel. The hydrogel functions as binder to prevent the cells from diffusing away into the culture medium and to provide a starting point for cellular organization. It is also possible to deposit biomolecules to specifically adhere cells on certain locations on substates or hydrogels (**Figure 1.3**). The layering of different cell types has been achieved[27] using bioprinting, however the spatial control to place different cell types adjacent to each other is still somewhat limited.[28]

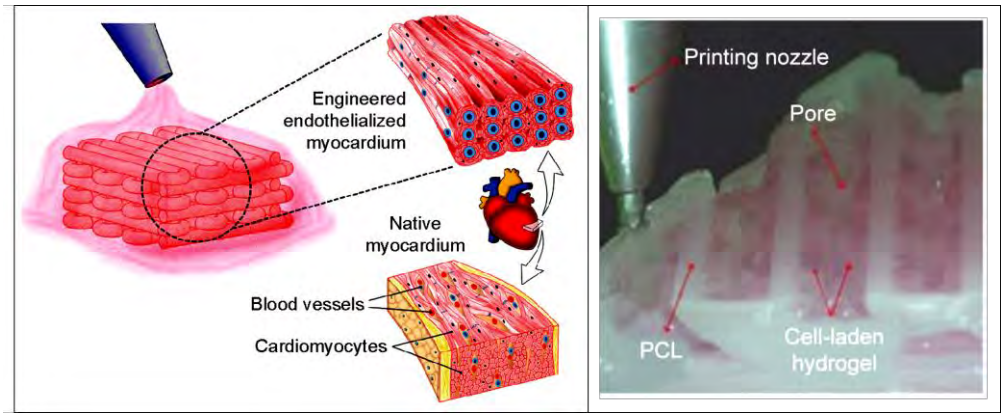

Figure 1.3 Bioprinting: A) schematic depiction of the printed layers of cardiomyocytes and endothelial cells, both suspended in hydrogel, to mimic the highly organised and vascularised myocardium; and B) an example of PCL supporting material printed together with a cell-laden hydrogel.[29] Reproduced with permission.

1.3.6. Organ-on-Chip Devices

An organ-on-chip (OoC) is a microfluidic device where cells are cultured in one or several microchannels (**Figure 1.2C**). In a microfluidic device it is relatively straightforward to include active flow to influence cell self-organization or even differentiation.[30–34] The goal is to mimic the functionality of an organ or tissue and the microfluidic device can be designed at will to, for example, introduce a chemical gradient using multiple channels or to deliver chemicals by adding extra channels at the sides of the cell-containing channels.[35] Multiple channels can also be used to

separate two cell types or media separated by a membrane. The two layers of cells on opposite sides of the membrane is suited for modelling natural barriers of interest, such as the blood-brain barrier[18,34] or the alveolar blood-air barrier[36] as they are combined with flow and, in the case of the alveolar blood barrier, mechanical movement (**Figure 1.4**).

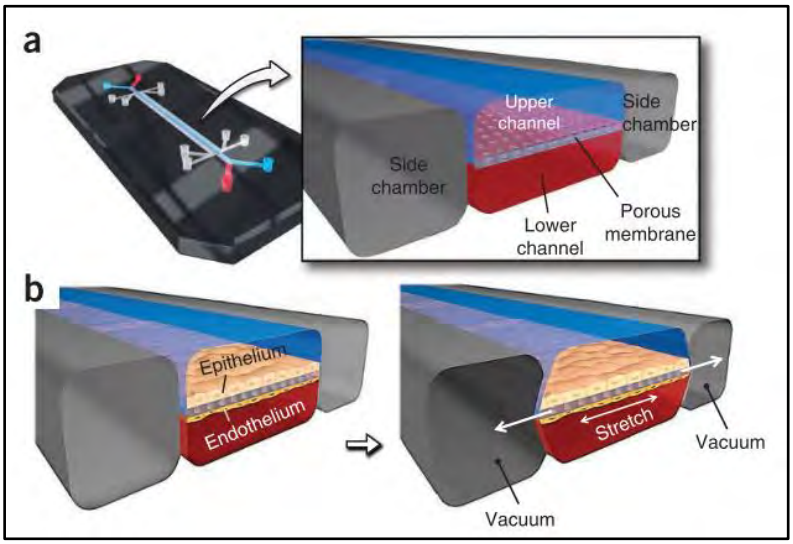

Figure 1.4 Lung-on-Chip where two cell types are cultured on sides of a membrane within fluidic channels, in order to mimic the epithelial barrier of the alveoli.[37] Reproduced with permission.

There are several relevant chemical and mechanical microenvironments that can be incorporated in such OoC device models. These include chemical gradients, barriers, mechanical strain, flow, 3D architecture and electrical stimulation.[38]

1.4. Mimicking the tissue microenvironment *in vitro*

In tissue modelling, one of the aims is to replace the differentiation induction medium by a suitable substrate that can instruct the cells to differentiate into the desired cell type. Such substrates would incorporate specific requirements such as substrate stiffness and substrate-attached ligands that more closely mimic cell-cell and/or cell-ECM interactions (**Figure 1.5**). In addition, the microstructure needs to

provide support for cellular network formation.[26] The design of the microarchitecture combined with the chemical surface provide the cells with the physical and chemical cues they need to develop, differentiate or function as required. These properties of the model are key to *in vitro* modelling of *in vivo* microenvironment and they are the subject of many studies. The cues are different for different tissues and finding the essential cues and then implement these in the models remains a challenge. Not all techniques for adding chemical cues are compatible with the techniques for physical cues, and the number of possible techniques is extensive. The aim in this research is to find not only suitable cues to implement in the model, but also to find a technique that can be controlled reproducibly and can be varied in composition to make it widely applicable in *in vitro* models.

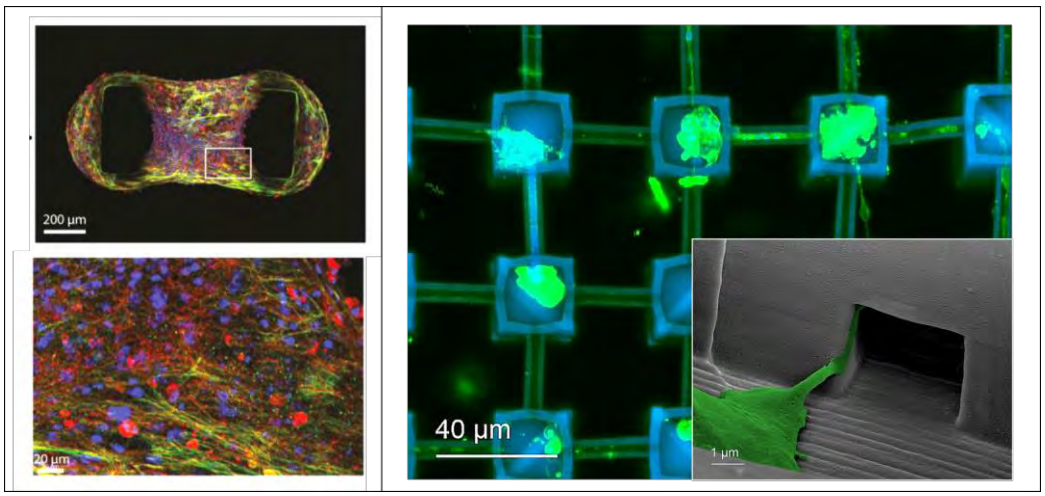

Figure 1.5 Structured cell microenvironment in order to induce the natural morphology of cells. Cardiomyocytes are cultured around two posts to trigger the pulling force of the muscle cells, stained for α-actinin (red), cardiac troponin T (green) and nucleus (blue).[39] Neurons cultured in a structure which separates the neurons combined with channels to stimulate the formation of long axons to connect the neurons (insert).[40] Reproduced with permission

1.4.1. Modelling the architecture of the microenvironment

Models can be made for structured or non-structured tissues. For example, the liver has a specific structure of blood vessels and bile ducts, but metabolic liver cells

themselves are all the same throughout the liver and will perform the same action regardless of neighbouring cells. On the other hand, the brain is a highly structured tissue, with many supporting cells and cellular organization to perform its functions.[18]

1.4.2. Modelling the cell-cell interactions

Cells communicate with each other and thereby influence each other.[41] In the models, cells are organized to facilitate formation of cell-cell interactions. Cells can be seeded on a more complex matrix, however, the addition of a 3D matrix does not necessarily result in a 3D cell culture, as the cells can form a single layer on the matrix. Organoids force cells together to form a network and trigger cell-cell interactions. It is this cell-cell interaction that can be mimicked and enforced by molecular cues in hydrogels.

1.4.3. Extracellular matrix

The choice of the substrate material that forms the main structure of the model are key to achieve a cellular network. Substrate stiffness and type of ligands in the substrate coating largely influence cell morphology and cell differentiation.

The substrate material for the model is effectively the substrate material on which the ECM-cell interaction occur and mimic the *in vivo* types of interactions. This substrate material can be varied in stiffness, topology and in biocompatibility and cell-specific ligands. An option is to use decellularised tissue as the substrate material to seed the cells onto.[42,43] This procedure requires a tissue section for each model to decellurise, while during the removal of cells molecular cues are often lost. Also, this type of model does not help in the study for gaining more detailed insight in the role some cues play in modelling tissue or organs.[43]

Another option is the use of resorbable substrate materials. These types of materials will function as a support and, when functionalised, chemical influence on the cells for a limited amount of time after which they are resorbed by the cells. These materials can be used in implants where they are meant to guide or speed up the healing process.[44,45]

Not resorbable, but completely bioinert is polydimethylsiloxane (PDMS). PDMS is widely used in the microfluidics and OoCs as it can be shaped in many possible ways, creating the desired channels and microarchitecture for the model. There is also some variability possible in the stiffness of PDMS, as it is made by combining an

elastomer with a curing agent. The lower the concentration of curing agent, the softer the PDMS will become because of lack of crosslinks.[46]

To make different microarchitectures, materials can be woven or spun into a web, they can be cast with salt that, upon dissolving, leave a porous material behind, they can be cast in a mold or milled to produce a microarchitecture (**Figure 1.6**). Each of these methods has its own influence on the cells that are cultured on it. The porosity of woven materials and the organization of the deposited materials can have an enormous impact on the morphology of the cells.[5]

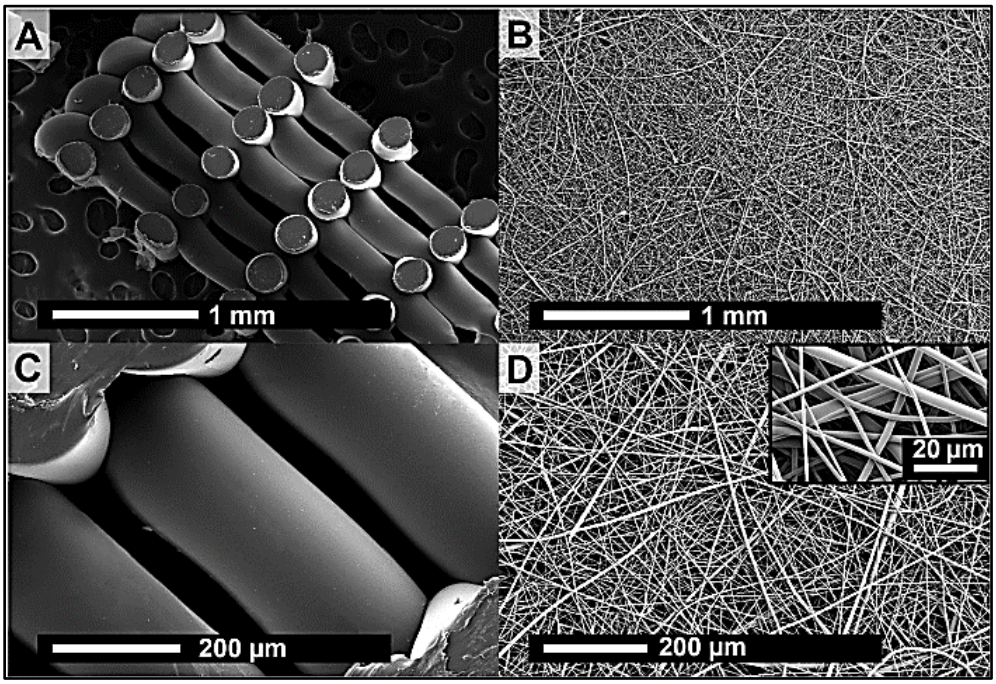

Figure 1.6 Several methods are possible to create a mesh to serve as ECM.[47] Reproduced with permission.

As many models would prefer to model more complex tissues such as skin and intestine by using the self-organization of stem cells, to initiate and guide differentiation of the stem cells in the desired direction is a decisive step to achieve. While cell-cell and cell-ECM interactions *in vivo* are often too complex and sometimes even unknown to reconstitute *in vitro*, studies often focus on finding the regulating receptors and ligands and other key cues that induce the desired differentiation. These molecular ligands can be attached to the solid structure directly[48] and often click chemistry is used in the form of the biologically compatible

poly ethylene glycol (PEG) system (**Figure 1.7**). The microgel contains PEGylated ligand molecules[49] or the hydrogel contains locations on which the different PEGylated ligands can bind and unbind under the influence of UV-light.[26]

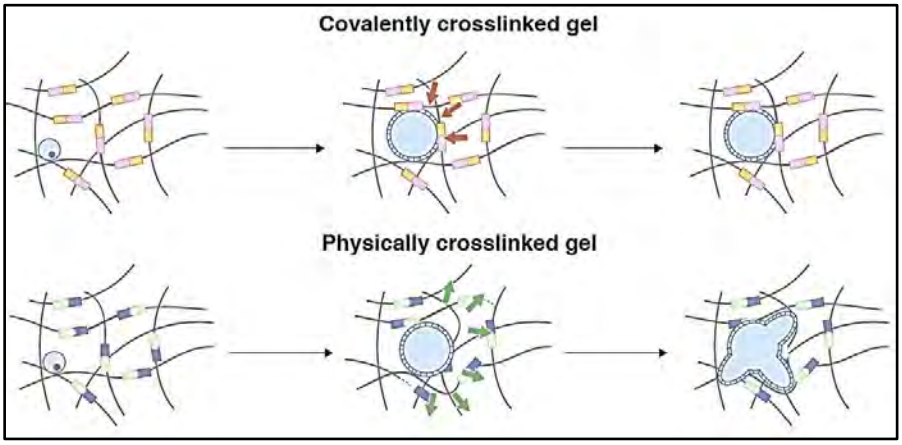

Figure 1.7 Binding molecular cues to the PEG containing cell environment to mimic cell-ECM interaction and hereby influence the cell fate.[26] Reproduced with permission.

Other techniques of introducing the chemical cues to the surface include direct covalent binding of the molecules to the surface, or by coating the surface with a hydrogel.

1.5. Supported lipid bilayers as cell-instructive coating

Cell-instructive coatings can be made of surface absorbed fibronectin. Although this is a very effective method to induce cell adhesion, it lacks the possibility to tune the adhesion ligand density, mobility and the type of ligands.[50] A type of coating is supported lipid bilayer (SLB) coating that can be tailored relatively easily by the choice of the lipid molecules that are the component of these SLBs.[51] An SLB is a lipid bilayer (or phospholipid bilayer) consisting of a thin polar membrane made of two layers of lipid molecules. These membranes are flat sheets that form a continuous substrate coating. SLBs are made of lipids with a hydrophilic phosphate head and a hydrophobic tail consisting of two fatty acid chains. Phospholipids with certain head groups can alter the surface chemistry of a bilayer and can, for example, serve as signals as well as anchors for other molecules in the membranes of cells.[52] The lipids

can also affect SLB properties, for instance by determining the phase of the bilayer. The bilayer can adopt a solid gel phase state at lower temperatures but undergo phase transition to a fluid state at higher temperatures, and the chemical properties of the lipids' tails influence at which temperature this occurs. The packing of lipids within the bilayer also affects its mechanical properties, that can be of influence how cells interact with the substrate.[51]

1.6. Aim and Scope of the Thesis

Models of tissues or organs are highly informative for studies in cell biology, toxicology and biomedical research, provided they are a realistic mimic of *in vivo* tissues. In this thesis, the interactions between hMSCs and the fabricated microenvironment is studied. Microarchitecture in OoC devices is combined with a functional coating of the device substrate to instruct the stem cells' morphology and differentiation.

In chapter 2, several designs will be made for the microarchitecture in microfluidic devices and used for studying their effect on hMSC morphology and whether these OoC devices support a 3D hMSC network.

The influence on hMSC morphology of the type of lipids in supported lipid bilayers that are applied to PDMS films is shown in chapter 3. The stiffness of the PDMS substrate is varied and these PDMS films will be covered with different types of SLBs that vary in ligand mobility and density.

In chapter 4 we combine the microfabricated OoC device including an optimized design for hMSC network formation with a cell-instructive supported lipid bilayer coating. The supported lipids bilayer will be functionalised with cell-adhesive and cell-differentiation ligands as cell-instructive cues.

In chapter 5, human pluripotent stem cell-derived cardiomyocytes will be cultured in our microfluidic OoC device for several days. Changes in the formation of beating clusters of cardiomyocytes as well as the survival of this high metabolizing cell type in a confined space of the microfluidic device is studied.

1.7. References

1. Skardal, A., Shupe, T. & Atala, A. Organoid-on-a-chip and body-on-a-chip systems for drug screening and disease modeling. *Drug Discov. Today* **21**, 1399–1411 (2016).
2. Esch, E. W., Bahinski, A. & Huh, D. Organs-on-chips at the frontiers of drug discovery. *Nat. Rev. Drug Discov.* **14**, 248–260 (2015).
3. Fitzgerald, K. A., Malhotra, M., Curtin, C. M., O' Brien, F. J. & O' Driscoll, C. M. Life in 3D is never flat: 3D models to optimise drug delivery. *J. Control. Release* **215**, 39–54 (2015).
4. Lauschke, V. M., Hendriks, D. F. G., Bell, C. C., Andersson, T. B. & Ingelman-Sundberg, M. Novel 3D culture systems for studies of human liver function and assessments of the hepatotoxicity of drugs and drug candidates. *Chem. Res. Toxicol.* **29**, 1936–1955 (2016).
5. Leferink, A. M., van Blitterswijk, C. & Moroni, L. Methods of monitoring cell fate and tissue growth in three-dimensional scaffold-based strategies for in vitro tissue engineering. *Tissue Eng. Part B Rev.* **22**, ten.TEB.2015.0340 (2016).
6. Jumarie, C. & Malo, C. Caco-2 cells cultured in serum-free medium as a model for the study of enterocytic differentiation in vitro. *J. Cell. Physiol.* **149**, 24–33 (1991).
7. Wang, L., Nagesha, D. K., Selvarasah, S., Dokmeci, M. R. & Carrier, R. L. Toxicity of CdSe nanoparticles in Caco-2 cell cultures. *J. Nanobiotechnology* **6**, 11 (2008).
8. Mirabelli, P., Coppola, L. & Salvatore, M. Cancer cell lines are useful model systems for medical research. *Cancers (Basel).* **11**, (2019).
9. Parrotta, E. I., Scalise, S., Scaramuzzino, L. & Cuda, G. Stem cells: The game changers of human cardiac disease modelling and regenerative medicine. *Int. J. Mol. Sci.* **20**, (2019).
10. Lako, M., Armstrong, L. & Stojkovic, M. Induced pluripotent stem cells: It looks simple but can looks deceive? *Stem Cells* **28**, 845–850 (2010).
11. Volpato, V. & Webber, C. Addressing variability in iPSC-derived models of human disease: Guidelines to promote reproducibility. *DMM Dis. Model. Mech.* **13**, (2020).
12. Shafa, M. *et al.* Long-term stability and differentiation potential of cryopreserved cGMP-compliant human induced pluripotent stem cells. *Int. J. Mol. Sci.* **21**, 1–17 (2020).
13. Attwood, S. & Edel, M. iPS-Cell technology and the problem of genetic instability—can it ever be safe for clinical use? *J. Clin. Med.* **8**, 288 (2019).
14. Borger, D. K. *et al.* Induced pluripotent stem cell models of lysosomal storage disorders. *DMM Dis. Model. Mech.* **10**, 691–704 (2017).
15. EuroStemCell. Mesenchymal stem cells: the 'other' bone marrow stem cells.
16. Chen, C. S. 3D biomimetic cultures: the next platform for cell biology. *Trends Cell Biol.* **26**, 798–800 (2016).

17. Mushahary, D., Spittler, A., Kasper, C., Weber, V. & Charwat, V. Isolation, cultivation, and characterization of human mesenchymal stem cells. *Cytom. Part A* **93**, 19–31 (2018).

18. Griep, L. M. *et al.* BBB on CHIP: Microfluidic platform to mechanically and biochemically modulate blood-brain barrier function. *Biomed. Microdevices* **15**, 145–150 (2013).

19. Åberg, C. Quantitative analysis of nanoparticle transport through in vitro blood-brain barrier models. *Tissue Barriers* **4**, (2016).

20. Cortini, M., Baldini, N. & Avnet, S. New advances in the study of bone tumors: A lesson from the 3D environment. *Front. Physiol.* **10**, 1–8 (2019).

21. Jackson, E. L. & Lu, H. Three-dimensional models for studying development and disease: moving on from organisms to organs-on-a-chip and organoids. *Integr. Biol. (Camb).* 672–683 (2016) doi:10.1039/c6ib00039h.

22. Bersini, S. *et al.* A microfluidic 3D invitro model for specificity of breast cancer metastasis to bone. *Biomaterials* **35**, 2454–2461 (2014).

23. Theunissen, P. T. *et al.* Complementary detection of embryotoxic properties of substances in the neural and cardiac embryonic stem cell tests. *Toxicol. Sci.* **132**, 118–130 (2013).

24. Gomez-Lechon, M. J., Tolosa, L., Conde, I. & Donato, M. T. Competency of different cell models to predict human hepatotoxic drugs. *Expert Opin. Drug Metab. Toxicol.* **10**, 1553–1568 (2014).

25. van Dartel, D. A. M., Zeijen, N. J. L., de la Fonteyne, L. J. J., van Schooten, F. J. & Piersma, A. H. Disentangling cellular proliferation and differentiation in the embryonic stem cell test, and its impact on the experimental protocol. *Reprod. Toxicol.* **28**, 254–261 (2009).

26. Blondel, D. & Lutolf, M. P. Bioinspired hydrogels for 3d organoid culture. *Chimia (Aarau).* **73**, 81–85 (2019).

27. Hedström, U. *et al.* Bronchial extracellular matrix from COPD patients induces altered gene expression in repopulated primary human bronchial epithelial cells. *Sci. Rep.* **8**, 1–13 (2018).

28. Brassard, J. A. & Lutolf, M. P. Engineering stem cell self-organization to build better organoids. *Cell Stem Cell* **24**, 860–876 (2019).

29. Zhang, B. *et al.* 3D bioprinting: a novel avenue for manufacturing tissues and organs. *Engineering* **5**, 777–794 (2019).

30. Jang, K.-J. *et al.* Human kidney proximal tubule-on-a-chip for drug transport and nephrotoxicity assessment. *Integr. Biol.* **5**, 1119–1129 (2013).

31. Yourek, G., McCormick, S. M., Mao, J. J. & Reilly, G. C. Shear stress induces osteogenic differentiation of human mesenchymal stem cells. *Regen. Med.* **5**, 713–724 (2010).

32. Julaey, M., Hosseini, M. & Amani, H. Stem cells culture bioreactor fluid flow, shear

stress and microcarriers dispersion analysis using computational fluid dynamics. *J. Appl. Biotechnol. Reports* **3**, 425–431 (2016).

33. Scaglione, S. *et al.* Effects of fluid flow and calcium phosphate coating on human bone marrow stromal cells cultured in a defined 2D model system. *J. Biomed. Mater. Res. - Part A* **86**, 411–419 (2008).

34. Bhatia, S. N. & Ingber, D. E. Microfluidic organs-on-chips. *Nat. Biotechnol.* **32**, 760–772 (2014).

35. Baker, B. M., Trappmann, B., Stapleton, S. C., Toro, E. & Chen, C. S. Microfluidics embedded within extracellular matrix to define vascular architectures and pattern diffusive gradients. *Lab Chip* **13**, 3246–3252 (2013).

36. Huh, D. *et al.* Reconstituting organ-level lung functions on a chip. *Science (80-.).* **328**, 1662–1668 (2010).

37. Huh, D. *et al.* Microfabrication of human organs-on-chips. *Nat. Protoc.* **8**, 2135–2157 (2013).

38. Huh, D., Torisawa, Y., Hamilton, G. a., Kim, H. J. & Ingber, D. E. Microengineered physiological biomimicry: Organs-on-Chips. *Lab Chip* **12**, 2156 (2012).

39. Dostanic, M. *et al.* A miniaturized EHT platform for accurate measurements of tissue contractile properties. *J. Microelectromechanical Syst.* **29**, 881–887 (2020).

40. Fendler, C. *et al.* Microscaffolds by direct laser writing for neurite guidance leading to tailor-made neuronal networks. *Adv. Biosyst.* **3**, 1800329 (2019).

41. Ingber, D. E. Reverse Engineering Human Pathophysiology with Organs-on-Chips. *Cell* **164**, 1105–1109 (2016).

42. Flynn, L. E., Prestwich, G. D., Semple, J. L. & Woodhouse, K. A. Proliferation and differentiation of adipose-derived stem cells on naturally derived scaffolds. *Biomaterials* **29**, 1862–1871 (2008).

43. Sánchez-Romero, N., Schophuizen, C. M. S., Giménez, I. & Masereeuw, R. In vitro systems to study nephropharmacology: 2D versus 3D models. *Eur. J. Pharmacol.* **790**, 36–45 (2016).

44. Hench, L. L. & Polak, J. M. Third-generation biomedical materials. *Science* **295**, 1014–1017 (2002).

45. Wojak-Ćwik, I. M. *et al.* Synergistic effect of bimodal pore distribution and artificial extracellular matrices in polymeric scaffolds on osteogenic differentiation of human mesenchymal stem cells. *Mater. Sci. Eng. C* **97**, 12–22 (2019).

46. Drebezghova, V. *et al.* Network mesh nanostructures in cross-linked poly(dimethylsiloxane) visualized by AFM. *Macromol. Chem. Phys.* **221**, 1–7 (2020).

47. Leferink, A. M. *et al.* Differentiation capacity and maintenance of differentiated phenotypes of human mesenchymal stromal cells cultured on two distinct types of 3D polymeric scaffolds. *Integr. Biol.* **7**, 1574–1586 (2015).

48. Pati, F. *et al.* Ornamenting 3D printed scaffolds with cell-laid extracellular matrix for

bone tissue regeneration. *Biomaterials* **37**, 230–241 (2015).

49. Allazetta, S., Kolb, L., Zerbib, S., Bardy, J. & Lutolf, M. P. Cell-instructive microgels with tailor-made physicochemical properties. *Small* **11**, 5647–5656 (2015).

50. Bosmans, R. P. G. *et al.* Supramolecular protein immobilization on lipid bilayers. *Chemistry* **21**, 18466–18473 (2015).

51. Koçer, G. & Jonkheijm, P. Guiding hMSC adhesion and differentiation on supported lipid bilayers. *Adv. Healthc. Mater.* **6**, 1600862 (2017).

52. Verheijden, M. L. Supramolecular Binding of Vesicles, Viruses and Cells to Biomimetic Lipid Bilayers. (University of Twente, 2018). doi:10.3990/1.9789036545501.

Chapter 2

Biomimetic trabecular niche promotes hMSC differentiation in a Bone-on-chip microdevice

Abstract

This chapter reports a microfluidic device with a biomimetic microarchitecture consisting of an array of pillars for culture and differentiation of hMSCs. The PDMS surface of the microfluidic device was coated with cell-adhesive protein fibronectin to optimise cell culture. Where other studies rely on hydrogels or topography to culture their cells in 3D, in our device a microarchitecture of pillars was used to promote the formation of a (near) 3D network of hMSCs with enough locations for adhesion and the possibility to grow in more directions than would be possible in a 2D culture. Successful differentiation into osteoblasts was demonstrated by ALP and osteocalcin expression and the presence of calcium deposits in the microdevices. The microarchitecture of the device can be the base for surface chemistry using ligands to direct hMSC in differentiation substituting the use of osteogenic medium.

2.1. Introduction

Bone that is cultured *in vitro* has many potential uses. *In vitro* cultured bone is of interest for biomedical research to better understand cancer metastasis[1] and to study the toxicity response of bone to heavy metals[2]. While to understand cancer metastasis a bone model is required that allows for infiltrating bone by cancerous cells, toxicity response studies require a bone model that allows for extracellular matrix (ECM) deposition, bone formation and remodelling. Bone models can also be used in regenerative medicine to promote wound healing or to serve as implant attachments.[3–6] This use of *in vitro* grown bone for biomedical research calls for bone models that allow the infiltration of native cells and that have the capacity to take a load, as bone will not form properly without a minimum of stress.[7–9]

Any microarchitecture or environment that is used for constructing *in vitro* bone models needs to be biologically compatible to prevent cytotoxicity or immune response inhibiting the remineralization of the inserted artificial bone tissue. For this reason most models for bone metastasis use collagen I-based hydrogels loaded with a small number of osteoblasts or bone-like cells to observe cell-cell interactions.[1] However, in toxicological bone models the environment of the cells is investigated and this must therefore be deposited by the osteoblasts. In the case of heavy metal poisoning bone stores the heavy metals, as during the remodelling of bone osteoblasts continuously deposit new ECM consisting of hydroxyapatite and collagen I and incorporate the heavy metals from the bloodstream. [10–15] To realistically model this ECM deposition, an *in vitro* bone model is needed that does not contain a hydrogel, as osteoblasts will not deposit ECM if their environment already meets their requirements.[16,17] The best way to achieve a model in which cells deposit ECM during the assay is by modelling bone from scratch using human mesenchymal stem cells (hMSCs). hMSCs can be differentiated into osteoblasts at which point these cells deposit bone hydroxyapatite and collagen I[1,4,18–20] preferably in a (near) 3D culture environment to represent tissue formation and remodelling more realistically than in 2D culture environments.[21] hMSCs that are cultured in 3D environments show morphologies that are closer to that what is observed *in vivo*, i.e. hMSCs that express fewer focal adhesions than hMSCs that are cultured in 2D environments.[22–25]

Several types of (near) 3D environments have been recently described in literature.[1,26–29] For example, introduction of surface topography in cell culture materials has a major impact on cell attachment and cell differentiation when

producing bone tissue *in vitro*.[27] Other research described the use of woven and porous microarchitectures to fabricate a biomimetic bone environment for hMSCs.[28]

Whereas most organ-on-a-chip systems use a Matrigel® or hydrogels to provide structure to the cell culture to obtain a 3D (or near 3D) approximation of *in vivo*,[1,29,30] only a relatively low concentration of cells is present in these hydrogel matrices, which prevents the formation of densely connected tissues. This inhibits the cells to create their own ECM as they would *in vivo*.[31] Hydrogels that are suitable to differentiate hMSC into bone need additional signalling to activate differentiation.[25] There are some reports of the use of cell spheroids to mimic bone *in vitro*.[31] Such spheroids are embedded in a hydrogel, usually to combine the hMSCs or osteoblasts with another cell type.[31,32] Bersini *et al*. used a hydrogel of collagen I to suspend osteo-cells to study the interaction with infiltrating cancer cells.[1] As natural bone is composed of 30% collagen I, this model is an accurate approximation of bone for this type of metastasis studies.[33] Hydrogels that have been made of collagen I or gelatin[34] in combination with hydroxyapatite-mimetic microarchitectures such as ceramics or hydroxyapatite in a gel were also explored.[18,34,35] Ceramic or polymer-based porous structures are usually coated with collagen I or gelatine to induce cell adherence.[28,34,35] Hydroxyapatite is the major component of human bone, however, as the choice of the material to fabricate a (near) 3D environment for bone it restricts the hMSCs in their ability to form bone.[31] Other studies have used a hydroxyapatite source to make a woven microarchitecture consisting of calcium in cellulose or used complete bone chips in fibrin.[6,12,36] The hMSC culture in a hydroxyapatite containing microarchitecture is successful in promoting cell viability and adherence and the cells express differentiation markers such as osteocalcin. Depending on the design of the microarchitecture, these microarchitectures do not allow for cell-cell contact and the deposition of calcium and collagen I is only present in small amounts, if at all.[6,12,36]

In this chapter, a bone-on-chip model is constructed. The device allows for 3D cell culture, while still maintaining the void space for hMSCs to deposit their own ECM during differentiation. These hMSCs can have cell-cell and cell-ECM interactions. Microfluidic devices are suitable for providing such an environment because they offer high levels of control over the geometries at micrometre and millimetre length scales. Earlier microdevices were used to control pressure to induce mechanical stress needed for osteogenesis[8] or to control flow over 2D culture.[37,38]

Our design of the microfluidic device is optimised for long-term cell culture and to differentiate hMSCs towards osteoblasts that deposit an ECM containing calcium.

2.2. Results & Discussion

The geometry of the polydimethylsiloxane (PDMS) microfluidic device was designed based on the typical structure of the long bones in the human body. These bones have a lattice-like structure which surrounds the bone marrow. Trabecular bone, also referred to as cancellous bone, has a high porosity (ca. 75%) with pore sizes up to hundreds of microns.[33] The cells of the bone reside in the pores lining the lamellae from where the cells deposit the ECM. In order to mimic this porosity, an array of 28 pillars with a diameter of 250 µm extending from top to bottom of the channel were fabricated in the main 6 cm^2 cell culture area (**Figure 2.1A & B**). The 28 pillars within the chamber were either arranged in a square or hexagonal pattern (**Figure 2.1D**). The scanning electron microscopy (SEM) images in **Figure 2.2** show pillars with smooth sides, which are suitable for coating with lipid bilayers, and tops, which are suitable to bind the pillar array to a PDMS covered microscopy slide to seal the device.

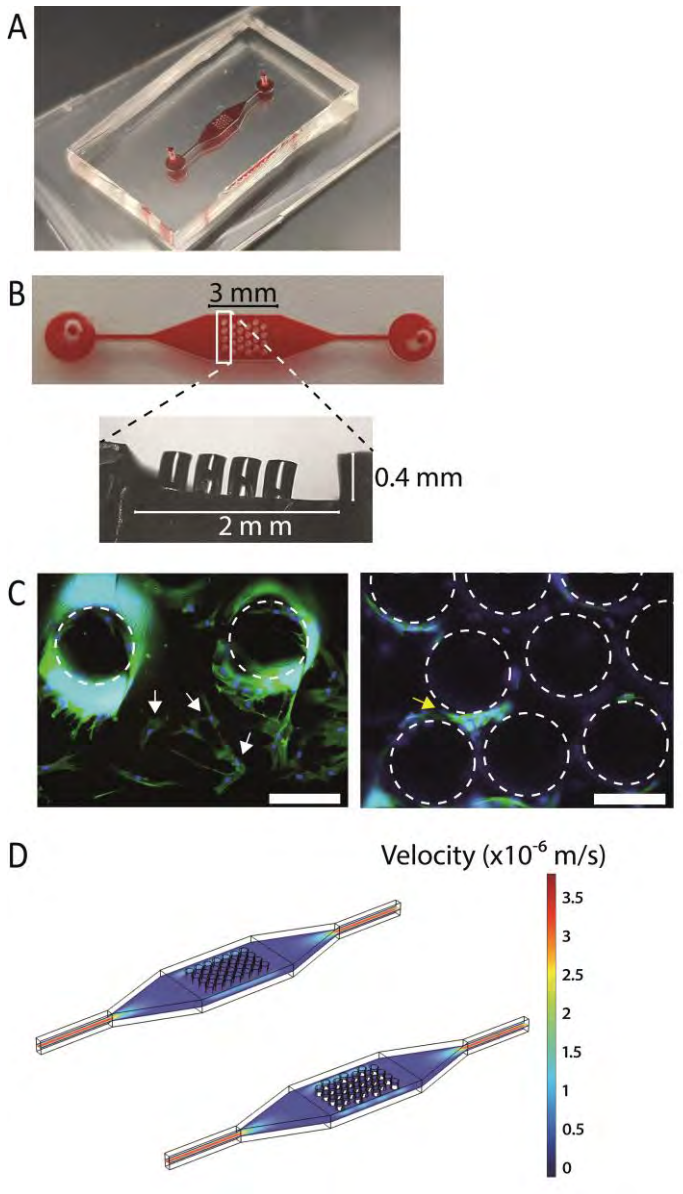

Figure 2.1 Design and characterization of the microfluidic device. A) Overall view of the device when filled with a red dye; B) top and side view (brightfield microscopy) of the device; C) Fluorescence microscopy image showing cells that adhere in a fibronectin-coated device, cells visualised after staining for actin (green) and DAPI (blue). Pillar spacing of 250 µm (left) and 20 µm (right). White arrows indicate examples of stretched cells and yellow arrows indicate examples of flattened cells. Scale bars represent 200 µm; D) Fluid dynamics modelled in devices with a squared (left) and hexagonal (right) pillar pattern. Flow velocity is indicated by colour and shear stress is indicated by the thickness of the lines. As the top flow velocity (indicated by red) is only reached at the inlet and outlet of the device, this is not visible in this representation of the fluid dynamics.

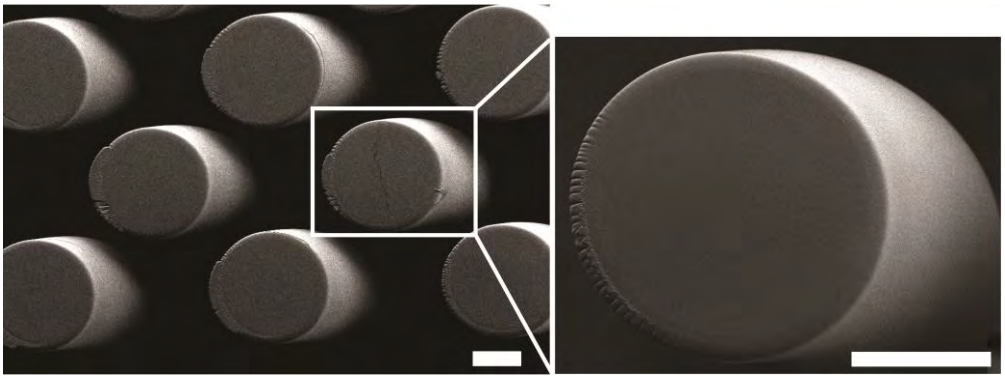

Figure 2.2 Recorded SEM images of an open PDMS device with hexagonal pillar patterns. Scale bars represent 100 µm.

In order to form an integral, three-dimensional tissue, hMSCs need to be able to reach and adhere to multiple pillars, while still having enough space between the pillars for culturing cells. To optimise the spacing of the pillars, hMSCs were seeded in microfluidic devices with pillar distances ranging from 250 to 20 µm, mimicking a porosity between ca. 85% and 35%. The number of cells between the pillars was highest when the distance between the pillars was 50-100 µm (**Figure 2.1C**). With this interpillar distance of 50-100 µm, 130 cells on average were present per image ($9 \cdot 10^5$ µm^2). These hMSCs were elongated, stretching in several directions between the pillars with multiple cell-cell contacts. When the distance was smaller (<50 µm), the number of cells was lower (95 nuclei per image) and only single cells were visible between the pillars and there was no cell-cell contact. In areas where the distance between the pillars was larger (>100 µm), the number of cells was even further reduced (45 nuclei per image) and these cells were found flattened on the bottom of the chamber and had no interaction with the pillars. Therefore, we conclude that optimal cell culturing conditions were achieved in chambers with an interpillar distance of 50-100 µm.

In vivo hMSCs and osteoblasts reside in an environment with almost no fluid flow, while our microfluidic models required daily perfusion of culture medium to maintain a sufficient concentration of nutrients. In order to provide a cell culture environment for the hMSC that had a fluid flow near 0 m/s, but still allows for medium refreshment, the different pillar geometries (square and hexagonal) were explored. Interestingly, despite the fact that there were no differences between these designs in terms of overall cell culture surface area or distance between the

pillars (in this case 50 µm), the patterns of cultured cells showed distinct differences. In the microfluidic device with pillars arranged in a hexagonal pattern, the cells were evenly spread throughout the chamber, whereas the hMSCs cultured in the devices with pillars arranged in a square pattern were only present in the interpillar space parallel to the flow direction and not perpendicular to the flow direction. The pillars arranged in the square pattern allowed for a stronger flow that hindered the hMSC in supporting a cell culture with cells occupying the whole of the available surface evenly as was seen in the hexagonal pattern (**Figure 2.3**). This explanation was also confirmed by computational modelling of fluid dynamics in the devices, which demonstrated that when an input flow velocity of 2.0 µm/s was set, the maximum flow velocity between the hexagonally arranged pillars was 0 m/s, while flow velocities between pillars arranged in a square pattern reached a maximum flow of 0.3 µm/s. Further computational modelling of the devices demonstrated that the flow velocity decreased when going from the inlet channel to the wider chamber where the pillars were arranged. Typical shear rates between the hexagonally arranged pillars of $7 \cdot 10^{-4}$ s^{-1} (shear stress of $6 \cdot 10^{-4}$ mPa when assuming a medium viscosity of 0.8 mPa·s) were estimated (**Figure 2.1D**). These values are ca. 10^5 times below the value of what hMSC can typically withstand in culture.[39–42] Constant shear stress is reported to improve the hMSC differentiation towards osteoblasts.[41] It has been found that hMSCs can withstand 0.2-0.24 Pa of shear stress without deforming.[39,42] This can be 2.5 Pa if the flow velocity is gradually increased.[40,41] However, when the cells are grown in a static environment and only subjected to shear stress when medium is changed, this stress needs to be quite low otherwise the cells will detach from the surface and show a decreased viability.[40,43,44] Our model currently incorporates intermittent flow when refreshing medium, but in the future this can also be used to systematically study the effect of flow and resulting shear stress on the hMSC differentiation process. All further experiments were performed with microfluidic devices with pillars hexagonally arranged, 50 µm apart to ensure the lowest flow velocity and shear rate in culture.

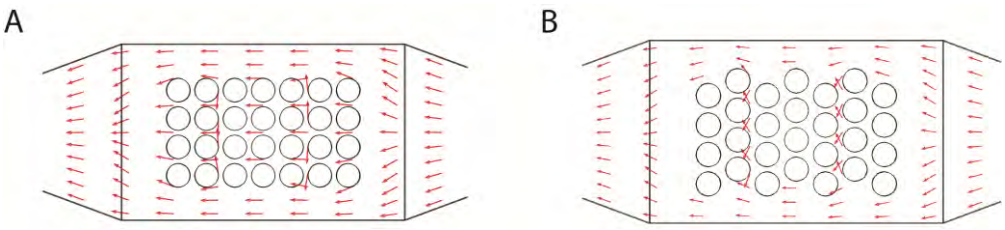

Figure 2.3 Flow profiles in microfluidic devices, with pillar spacing of 50 µm. A) In the device with a squared pillar pattern there is uninterrupted flow profile through the pattern, with a change in direction of the flow behind the pillars, while in B) a hexagonal pillar pattern the flow is interrupted by the pillars, no longer allowing it to go in a straight direction. Arrow size indicates flow velocity.

Next, we compared the clustering of cells in hMSC cell culture on flat PDMS, represented by a PDMS covered microscope slide, to that in the PDMS microfluidic device in more detail. hMSC culture for 72 h on flat, O_2-plasma-treated PDMS slides led to the formation of cell clusters, as indicated by the intense signals when stained for actin, vinculin and DAPI (**Figure 2.4A**). As (plasma-treated) PDMS is not known as a cell adherent material,[45] serum proteins in the medium most likely deposited onto the material, yielding a cell culture surface on which cells could adhere only moderately well. Other cells then adhere to the first cells and create clusters of cells on several locations on the PDMS. In contrast, when the same culturing conditions were applied to the microfluidic device (O_2-plasma treated PDMS, identical cell concentration), no clusters of hMSCs were observed, but hMSCs formed a compact network between the pillars (**Figure 2.4B**). We attribute the observed differences to the structural support offered by the PDMS pillars to the hMSCs resulting in a cellular network that extended into the regions beyond the last row of pillars (**Figure 2.4C**). Inspection of cells in the device using confocal fluorescence microscopy revealed that the hMSCs could migrate up the sides of the pillars to form a three-dimensional culture (**Figure 2.4B & C**). The hMSCs were found to be stretched between several pillars of the device, which mimics the behaviour of the hMSCs in their natural niche. When fibronectin was cast onto the PDMS device surface, hMSCs grew higher up the sides of the pillars compared to when hMSCs were grown in bare PDMS devices. The (near) 3D culture was denser when fibronectin was used on the PDMS (**Figure 2.4B**). Adding fibronectin to flat, plasma-treated PDMS slides before cell seeding resulted in a monolayer of higher cell density without any cell clustering (**Figure 2.4A**).

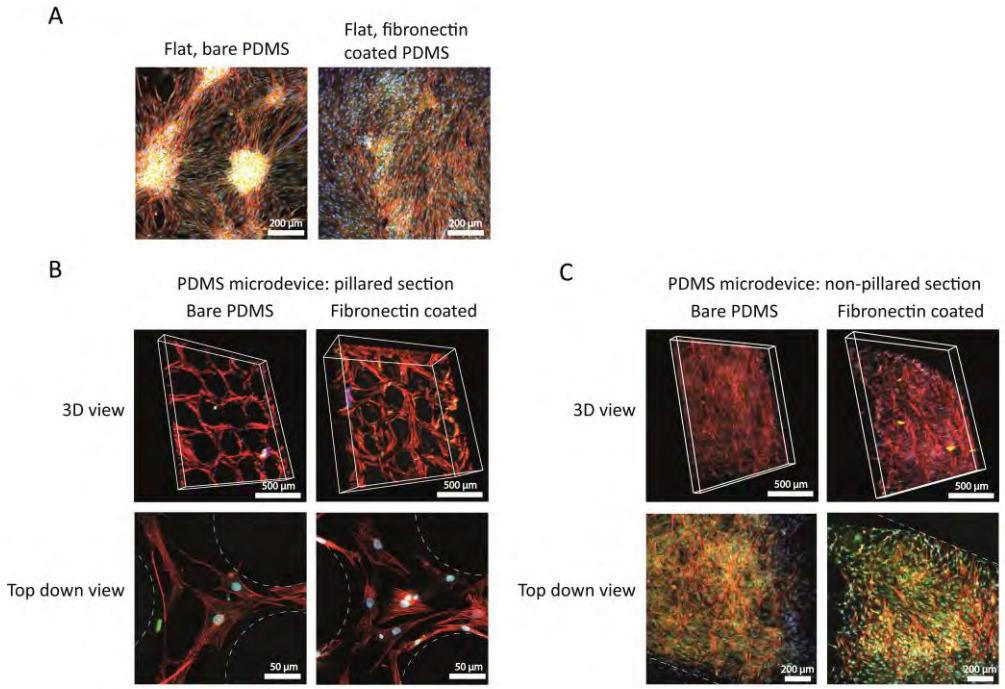

Figure 2.4 Fluorescence microscopy image showing hMSC culture in microfluidic devices for 3 days. Fixated cells visualised after staining for actin (red), vinculin (green) and DAPI (blue). A) Non-functionalised and fibronectin-coated PDMS slides; B) and C) hMSC culture in the microfluidic device with either non-functionalised or fibronectin-coated PDMS.

PDMS, even when plasma-treated to become hydrophilic, is not an ideal surface for cell adhesion.[45] Our results corroborate these findings as the hMSCs clustered together on several locations on flat, hydrophilic PDMS. These clusters then provided the culture with adhesive points that offer some structural support, allowing the entire area to be covered by cells. In contrast, the results presented in this chapter, show that hMSCs adhere to the hydrophilic PDMS pillars in the microfluidic device, forming a network without the use of a surface coating or the formation of clusters. The pillars provide enough structure for the hMSCs to spread out in the entire space and form a tight network, which is pivotal during differentiation.[25,46]

Cultured hMSCs are capable of differentiation in the microfluidic device when proper cell-cell contacts are formed between hMSCs. To demonstrate this, cell differentiation of hMSCs into osteoblasts was monitored during 18 days. The progress of differentiation was analysed on 5 different time points, these time points were divided in three phases: early phase (day 0-4), middle phase (day 5-9) and late

phase (day 10-18). The differentiation assay was normalised for the number of cells present and for the maximal area the cells can occupy. The results of this analysis are plotted in the graphs in **Figure 2.5** and the corresponding confocal microscopy images are shown in **Figure 2.6**. Stem cell markers STRO-1 and CD90 decreased rapidly after the early phase and did not reappear during the middle or late phase of the differentiation. Differentiation marker osterix increased during the early phase, then decreased during the middle phase and kept further decreasing during the late phase. RUNX2 was present during all phases with a clear peak in the middle phase of differentiation. Mineralization marker ALP was not present in the early phase, peaked in the middle phase and decreased again in the late phase of differentiation. Bone induction marker osteocalcin was only present during the late phase of differentiation. Also, calcium deposits were visualised on day 18, while they were absent on day 3 using Alizarin Red staining (**Figure 2.6**).

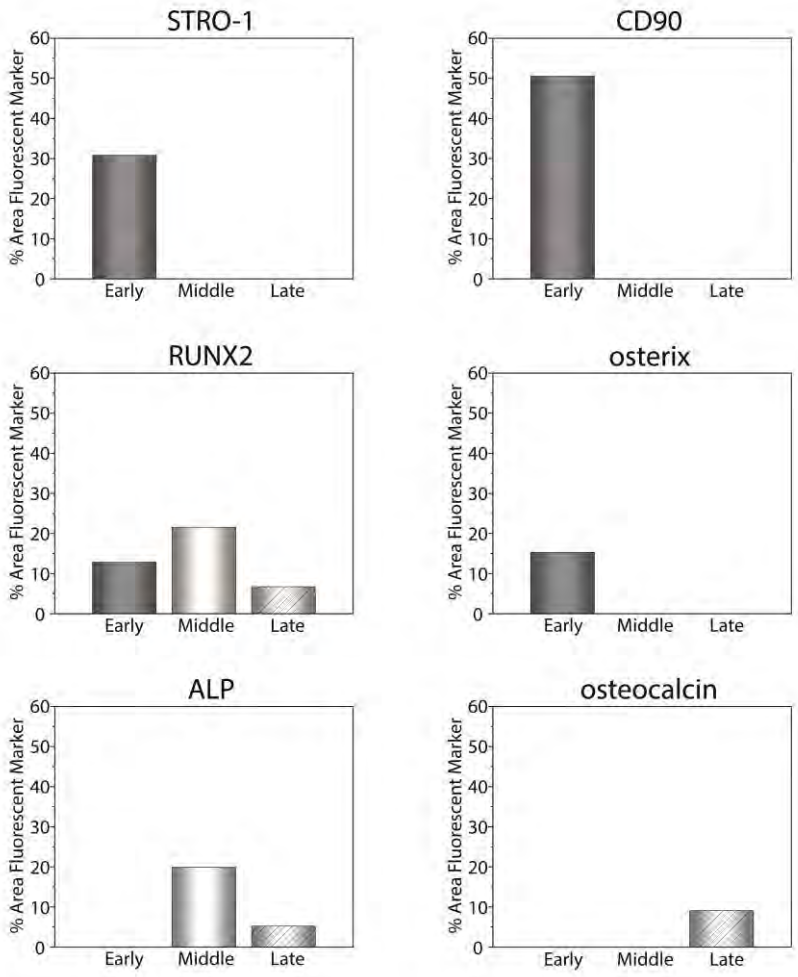

Figure 2.5 Differentiation of hMSCs cultured in microfluidic device. Expression of several differentiation markers during an 18-day differentiation assay of hMSCs to osteoblast in the microfluidic device, normalised for Actin controls.

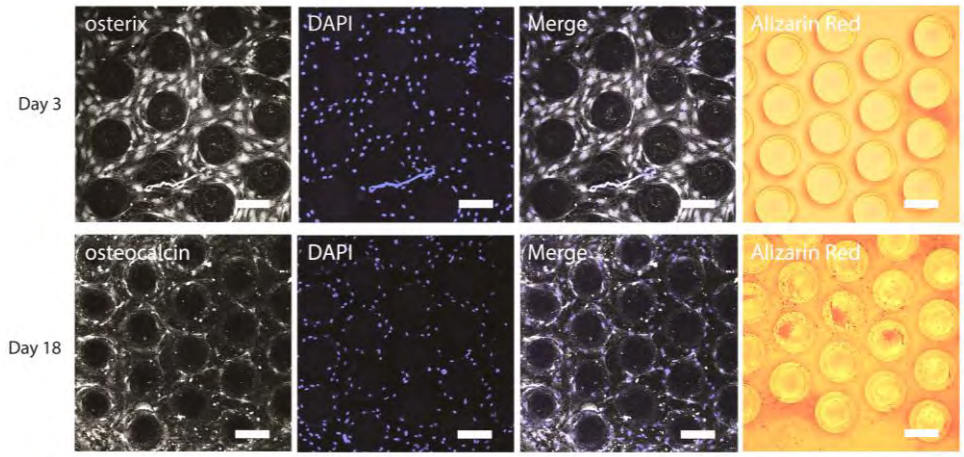

Figure 2.6 Differentiation of hMSCs cultured in microfluidic device. Fluorescence image of osterix expression on day 3 and of osteocalcin expression on day 18; Alizarin Red stain for calcium deposits on day 3 and on day 18. Scale bars represent 200 µm.

The differentiation markers that were used give a good overview of the process of osteogenesis, i.e. the differentiation of hMSCs to osteoblasts and the formation of calcium deposits.[47–51] Expression of stem cell markers STRO-1 and CD90 reduce as soon as differentiation is initiated.[52–54] The early markers RUNX2 and osterix are observed after several days of exposure to differentiation medium, followed by ALP and osteocalcin.[48–50,55] After these osteogenic markers are expressed, calcium deposits are confirmed using Alizarin Red.[50,56–58] In a 3D cell culture, the markers indicate not only cell differentiation, but also that the differentiation is more prominent when compared to 2D cell cultures.[59,60] Our study showed a decline of the stem cell markers after the start of differentiation, indicating that the hMSCs are indeed differentiating in the device. The up-regulation and subsequent down-regulation of early markers and up-regulation of the late markers confirm that osteogenic differentiation is ongoing. This in combination with the positive Alizarin Red staining supports that it is bone material cultured from the hMSCs start culture.

2.3. Conclusion

In conclusion, we have successfully designed and engineered a microfluidic PDMS device in which the seeded hMSCs achieve a (near) 3D cell network that allows for differentiation and deposition of calcium as part of their ECM. The observed hMSC cellular network was assisted by the presence of the microfabricated pillar array

device and the PDMS functionalization with cell-adhesive fibronectin. The homogeneous cell network with calcium deposits is reminiscent of trabecular bone, which consists of an open lattice-like structure. The microfluidic device design and chemistry provide the cells with sufficient adhesion locations and leads to a lower flow velocity. In the future, the surface chemistry could be tailor-made by ligands to direct hMSC in differentiation substituting the use of osteogenic medium.

2.4. Acknowledgements

We thank Mark Smithers for the SEM images, and Dr. Wouter Vijselaar for the cleanroom work.

2.5. Experimental section

2.5.1. Microfluidic device fabrication

A microfluidic device was designed using CleWin 4 (WieWeb Software, Hengelo, the Netherlands) and was constructed using soft lithography. First, a negative mold was constructed using photolithography with a negative photoresist. In short, after cleaning silicon wafers using the UV/Ozone ProCleaner™ Plus (10 min, BioForce Nanosciences Inc., Ames, IA, USA), SU-8 100 photoresist was spin-coated onto them (10 sec at 500 rpm, then 30 sec at 1000 rpm) and then the wafers were placed in an oven for 30 min at 65 °C, followed by 90 min at 95 °C. Then, a mask was placed over the SU-8 coated wafer and exposed to UV-light (power density 12 mW/cm^2) for approximately 30 seconds, after which the wafer was placed on a hot plate (95 °C) for 20 min. Then, the wafer was rinsed with acetone and isopropanol, dry spun and cured on a hot plate (135 °C) for 1 h.

Polydimethylsiloxane (PDMS) was prepared by mixing Sylgard 184 elastomer with its curing agent (Dow Corning Corp, Midland MI, USA) at a 1:10 ratio. This mixture was degassed and subsequently cast on the negative mold wafer to create the microfluidic channels and chamber. PDMS was poured onto a microscopy slide until an even coating of PDMS was reached and cured at 60 °C for 5 h. Then, the PDMS was peeled off the negative mold wafer, cut into blocks and the inlet and outlet were punched using a 1 mm gauge puncher. The microfluidic devices were bonded to the PDMS covered microscopy slides using O_2-plasma activation (40 mA DC current and 200 mTorr vacuum pressure for 60 sec) using the Plasma etcher SPI Plasma-Prep II (SPI Supplies, West Chester PA, USA). Then, the devices were covered in MilliQ water to fill the channels and to preserve hydrophilicity. The devices that served as a positive control were coated with fibronectin from bovine plasma (Sigma-Aldrich) as indicated by the manufacturer.

2.5.2. Computational modelling

Flow dynamics in the microfluidic devices (hexagonal and squared pillar patterns) were simulated using COMSOL (Multiphysics, COMSOL Inc, Burlington MA, USA). For a flow of 2 μm/s at the inlet of the device, flow velocity, flow direction and shear stress were selected as output variables in the simulation.

2.5.3. *In vitro* culture

Human mesenchymal stem cells (hMSC; Lonza, Basel, Switzerland) were cultured in complete medium consisting of α-MEM medium (Gibco) supplemented with 10% FBS (Lonza), 100 U/ml penicillin (Gibco) and 100 µg/ml streptomycin (Gibco) and incubated at 37 °C and 5% CO_2 up to one week before use in the assays. hMSCs (10^6 cells/ml) were cultured in microfluidic devices up to 3 days at 37 °C and 5% CO_2 with enough culture medium on top of the device. Cell differentiation was induced on day 3 of culture. Complete medium was replaced by osteogenic differentiation medium which consisted of α-MEM medium (Gibco) supplemented with 10% FBS, 100 U/ml penicillin, 100 µg/ml streptomycin, 0.2 mM ascorbic acid (Sigma-Aldrich), 100 nM dexamethasone (Sigma-Aldrich) and 10 mM β-glycerophosphate (Sigma-Aldrich). Cells were cultured up to 18 days in differentiation medium, with medium being refreshed daily.

2.5.4. Immunofluorescence

hMSCs were stained for actin (Phalloidin Alexa Fluor 568; 1:200; Thermo Fisher Scientific), vinculin (anti-hVIN-1-FITC, 1:200; Sigma-Aldrich) and the nucleus (DAPI, 1:1000). Stem cell markers STRO-1 (anti-STRO1-Phycoerythrin, 1:50; Abcam) and CD90 (anti-CD90-APC, 1:100; Thermo Fisher Scientific); early differentiation markers RUNX2 (anti-RUNX1 / AML1 + RUNX3 + RUNX2-Alexa Fluor 647, 1:50; Abcam) and osterix (Anti-SP7, 1:50; Sigma-Aldrich) conjugated with R-PE (Abcam); mineralization marker ALP (anti-Alkaline Phosphatase-Phycoerythrin, 1:100; Abcam); and bone induction marker osteocalcin (anti-BGLAP, 1:50; Sigma-Aldrich) conjugated with APC (Abcam) were visualised. Calcium deposits were stained with Alizarin Red (2% w/v in MilliQ) for 5 min and imaged with a confocal microscope (Nikon A1) on day 18.

2.5.5. Image analysis

The expression of the markers was quantified in ImageJ by the calculation of the percentage of the area where the fluorescent label of the marker was detected in 10x images divided by the number of cells. As the pillars in the device also take up a certain percentage of the area of the image, a maximum possible signal was set using the actin expression of the positive control. This maximum was set to 100% fluorescent area, as the abundant expression of actin fibres covered 100% of the available area in the microfluidic device.

2.6. References

1. Bersini, S. *et al.* A microfluidic 3D invitro model for specificity of breast cancer metastasis to bone. *Biomaterials* **35**, 2454–2461 (2014).
2. Drynda, A., Drynda, S., Kekow, J., Lohmann, C. H. & Bertrand, J. Differential effect of cobalt and chromium ions as well as cocr particles on the expression of osteogenic markers and osteoblast function. *Int. J. Mol. Sci.* **19**, (2018).
3. Torisawa, Y. *et al.* Bone marrow-on-a-chip replicates hematopoietic niche physiology in vitro. *Nat. Methods* **11**, 663–9 (2014).
4. Birmingham, E. *et al.* Osteogenic differentiation of mesenchymal stem cells is regulated by osteocyte and osteoblast cells in a simplified bone niche. *Eur. Cells Mater.* **23**, 13–27 (2012).
5. Gong, T. *et al.* Nanomaterials and bone regeneration. *Bone Res.* **3**, 15029 (2015).
6. Kuttenberger, J., Polska, E. & Schaefer, B. M. A novel three-dimensional bone chip organ culture. *Clin. Oral Investig.* **17**, 1547–1555 (2013).
7. Harada, S. & Rodan, G. A. Control of osteoblast function and regulation of bone mass. *Nature* **423**, 349–355 (2003).
8. Park, S. H. *et al.* Chip-based comparison of the osteogenesis of human bone marrow- and adipose tissue-derived mesenchymal stem cells under mechanical stimulation. *PLoS One* **7**, 1–11 (2012).
9. Ehrlich, P. J. & Lanyon, L. E. Mechanical strain and bone cell function: A review. *Osteoporos. Int.* **13**, 688–700 (2002).
10. Specht, A. J. *et al.* XRF-measured bone lead (Pb) as a biomarker for Pb exposure and toxicity among children diagnosed with Pb poisoning. *Biomarkers* **21**, 347–352 (2016).
11. Bogden, J. D., Oleske, J. M. & Louria, D. B. Lead poisoning--one approach to a problem that won't go away. *Environ. Health Perspect.* **105**, 1284–1287 (1997).
12. Palaveniene, A. *et al.* Osteoconductive 3D porous composite scaffold from regenerated cellulose and cuttlebone-derived hydroxyapatite. *J. Biomater. Appl.* **33**, 876–890 (2019).
13. Beier, E. E. *et al.* Heavy metal lead exposure, osteoporotic-like phenotype in an animal model, and depression of Wnt signaling. *Environ. Health Perspect.* **121**, 97-105 9p (2013).
14. Nascimento, C. R. B., Risso, W. E. & Martinez, C. B. D. R. Lead accumulation and metallothionein content in female rats of different ages and generations after daily intake of Pb-contaminated food. *Environ. Toxicol. Pharmacol.* **48**, 272–277 (2016).
15. Beier, E. E., Holz, J. D., Sheu, T. J. & Puzas, J. E. Elevated lifetime lead exposure impedes osteoclast activity and produces an increase in bone mass in adolescent mice. *Toxicol. Sci.* **149**, 277–288 (2016).

16. Stamenkovic, I. Extracellular matrix remodelling: the role of matrix metalloproteinases. *J. Pathol.* **200**, 448–464 (2003).

17. Bonucci, E. & Ballanti, P. Osteoporosis-bone remodeling and animal models. *Toxicol. Pathol.* 1–13 (2013) doi:10.1177/0192623313512428.

18. Soriente, A. *et al.* Effect of inorganic and organic bioactive signals decoration on the biological performance of chitosan scaffolds for bone tissue engineering. *J. Mater. Sci. Mater. Med.* **29**, (2018).

19. Huang, J. *et al.* Bone morphogenetic protein 9 (BMP9) induces effective bone formation from reversibly immortalized multipotent adipose-derived (iMAD) mesenchymal stem cells. **8**, (2016).

20. Elsafadi, M. *et al.* TGFβ1-induced differentiation of human bone marrow-derived MSCs is mediated by changes to the actin cytoskeleton. *Stem Cells Int.* **2018**, (2018).

21. Frith, J. E., Thomson, B. & Genever, P. G. Dynamic three-dimensional culture methods enhance mesenchymal stem cell properties and increase therapeutic potential. *Tissue Eng. Part C Methods* **16**, 735–749 (2009).

22. Cukierman, E. *et al.* Taking cell-matrix adhesions to the third dimension. **294**, 1708–1712 (2001).

23. Baker, B. M. & Chen, C. S. Deconstructing the third dimension-how 3D culture microenvironments alter cellular cues. *J. Cell Sci.* **125**, 3015–3024 (2012).

24. Bao, M., Xie, J. & Huck, W. T. S. Recent advances in engineering the stem cell microniche in 3D. *Adv. Sci.* **5**, (2018).

25. Chen, S. S., Fitzgerald, W., Zimmerberg, J., Kleinman, H. K. & Margolis, L. Cell-cell and cell-extracellular matrix interactions regulate embryonic stem cell differentiation. *Stem Cells* **25**, 553–561 (2007).

26. Jang, K., Sato, K., Igawa, K., Chung, U. Il & Kitamori, T. Development of an osteoblast-based 3D continuous-perfusion microfluidic system for drug screening. *Anal. Bioanal. Chem.* **390**, 825–832 (2008).

27. Qian, W. *et al.* Nanotopographic regulation of human mesenchymal stem cell osteogenesis. *ACS Appl. Mater. Interfaces* **9**, 41794–41806 (2017).

28. Wojak-Ćwik, I. M. *et al.* Synergistic effect of bimodal pore distribution and artificial extracellular matrices in polymeric scaffolds on osteogenic differentiation of human mesenchymal stem cells. *Mater. Sci. Eng. C* **97**, 12–22 (2019).

29. Hernandez, I., Kumar, A. & Joddar, B. A bioactive hydrogel and 3D printed polycaprolactone system for bone tissue engineering. *Gels* **3**, 26 (2017).

30. Chung, S., Sudo, R., Vickerman, V., Zervantonakis, I. K. & Kamm, R. D. Microfluidic platforms for studies of angiogenesis, cell migration, and cell–cell interactions. *Ann. Biomed. Eng.* **38**, 1164–1177 (2010).

31. Heo, D. N., Hospodiuk, M. & Ozbolat, I. T. Synergistic interplay between human MSCs and HUVECs in 3D spheroids laden in collagen/fibrin hydrogels for bone tissue engineering. *Acta Biomater.* **95**, 348–356 (2019).

32. Joshi, J., Abnavi, M. D. & Kothapalli, C. R. Synthesis and secretome release by human bone marrow mesenchymal stem cell spheroids within three-dimensional collagen hydrogels: Integrating experiments and modelling. *J. Tissue Eng. Regen. Med.* 1–15 (2019) doi:10.1002/term.2943.

33. Mescher, A. L. Chapter 8: Bone. in *Junqueira's Basic Histology: Text and Atlas* (eds. Weitz, M., Kearns, B. & Boyle, P.) (McGraw-Hill Education, 2018).

34. Della Bella, E. *et al.* Osteoinductivity of nanostructured hydroxyapatite-functionalized gelatin modulated by human and endogenous mesenchymal stromal cells. *J. Biomed. Mater. Res. - Part A* **106**, 914–923 (2018).

35. Liao, H.-T., Lee, M.-Y., Tsai, W.-W., Wang, H. & Lu, W.-C. Osteogenesis of adipose-derived stem cells on polycaprolactone- β -tricalcium phosphate scaffold fabricated via selective laser sintering and surface coating with collagen type I. *J. Tissue Eng. Regen. Med.* **10**, E337–E353 (2016).

36. Chen, Z. *et al.* Laminated electrospun nHA/PHB-composite scaffolds mimicking bone extracellular matrix for bone tissue engineering. *Mater. Sci. Eng. C* **72**, 341–351 (2017).

37. Leclerc, E. *et al.* Study of osteoblastic cells in a microfluidic environment. *Biomaterials* **27**, 586–595 (2006).

38. Zhang, Y., Gazit, Z., Pelled, G., Gazit, D. & Vunjak-Novakovic, G. Patterning osteogenesis by inducible gene expression in microfluidic culture systems. *Integr. Biol.* **3**, 39–47 (2011).

39. Kaiser, S. C. *et al.* Fluid flow and cell proliferation of mesenchymal adipose-derived stem cells in small-scale, stirred, single-use bioreactors. *Chemie-Ingenieur-Technik* **85**, 95–102 (2013).

40. Dong, J. De *et al.* Response of mesenchymal stem cells to shear stress in tissue-engineered vascular grafts. *Acta Pharmacol. Sin.* **30**, 530–536 (2009).

41. Yourek, G., McCormick, S. M., Mao, J. J. & Reilly, G. C. Shear stress induces osteogenic differentiation of human mesenchymal stem cells. *Regen. Med.* **5**, 713–724 (2010).

42. Julaey, M., Hosseini, M. & Amani, H. Stem cells culture bioreactor fluid flow, shear stress and microcarriers dispersion analysis using computational fluid dynamics. *J. Appl. Biotechnol. Reports* **3**, 425–431 (2016).

43. Stamp, M. E. M. *et al.* Exploring the limits of cell adhesion under shear stress within physiological conditions and beyond on a chip. *Diagnostics* **6**, (2016).

44. Kretzmer, G. & Schügerl, K. Response of mammalian cells to shear stress. *Appl. Microbiol. Biotechnol.* **34**, 613–616 (1991).

45. Zhang, W., Choi, D. S., Nguyen, Y. H., Chang, J. & Qin, L. Studying cancer stem cell dynamics on PDMS surfaces for microfluidics device design. *Sci. Rep.* **3**, 2332 (2013).

46. Arzuaga, X., Gehlhaus, M. & Strong, J. Modes of action associated with uranium induced adverse effects in bone function and development. *Toxicol. Lett.* **236**, 123–

130 (2015).

47. Lu, M. *et al.* Pax2 is essential for proliferation and osteogenic differentiation of mouse mesenchymal stem cells via Runx2. *Exp. Cell Res.* **371**, 342–352 (2018).

48. Sepulveda, H. *et al.* Epigenetic signatures at the RUNX2-P1 and Sp7 gene promoters control osteogenic lineage commitment of umbilical cord-derived mesenchymal stem cells. *J. Cell. Physiol.* 1–23 (2016) doi:10.1002/jcp.25627.

49. Zhang, J. *et al.* Highly dispersed lithium doped mesoporous silica nanospheres regulating adhesion, proliferation, morphology, ALP activity and osteogenesis related gene expressions of BMSCs. *Colloids Surfaces B Biointerfaces* **170**, 563–571 (2018).

50. Go, Y. Y. *et al.* Engineering functional BMP-2 expressing teratoma-derived fibroblasts for enhancing osteogenesis. *Sci. Rep.* **8**, 14581 (2018).

51. Narayanan, K. *et al.* Lineage-specific exosomes could override extracellular matrix mediated human mesenchymal stem cell differentiation. *Biomaterials* **182**, 312–322 (2018).

52. Rosales-Rocabado, J. M., Kaku, M., Kitami, M., Akiba, Y. & Uoshima, K. Osteoblastic differentiation and mineralization ability of periosteum-derived cells compared with bone marrow and calvaria-derived cells. *J. Oral Maxillofac. Surg.* **72**, 694.e1-694.e9 (2014).

53. Simmons, P. J. & Torok-Storb, B. Identification of stromal cell precursors in human bone marrow by a novel monoclonal antibody, STRO-1. *Blood* **78**, 55–62 (1991).

54. Dominici, M. *et al.* Minimal criteria for defining multipotent mesenchymal stromal cells. The International Society for Cellular Therapy position statement. *Cytotherapy* **8**, 315–317 (2006).

55. Teplyuk, N. M. *et al.* Runx2 regulates G protein-coupled signaling pathways to control growth of osteoblast progenitors. *J. Biol. Chem.* **283**, 27585–27597 (2008).

56. Jang, W. G. *et al.* BMP2 protein regulates osteocalcin expression via Runx2-mediated Atf6 gene transcription. *J. Biol. Chem.* **287**, 905–915 (2012).

57. Syftestad, G. T., Weitzhandler, M. & Caplan, A. I. Isolation and characterization of osteogenic cells derived from first bone of the embryonic tibia. *Dev. Biol.* **110**, 275–283 (1985).

58. Duarte Campos, D. F. *et al.* Bioprinting organotypic hydrogels with improved mesenchymal stem cell remodeling and mineralization properties for bone tissue engineering. *Adv. Healthc. Mater.* **5**, 1336–1345 (2016).

59. Shekaran, A. *et al.* Enhanced in vitro osteogenic differentiation of human fetal MSCs attached to 3D microcarriers versus harvested from 2D monolayers. *BMC Biotechnol.* **15**, 102 (2015).

60. Hishikawa, K. *et al.* Gene expression profile of human mesenchymal stem cells during osteogenesis in three-dimensional thermoreversible gelation polymer. *Biochem. Biophys. Res. Commun.* **317**, 1103–1107 (2004).

Chapter 3

Adhesion of human mesenchymal stem cells on polydimethylsiloxane films coated with supported lipid bilayers

Abstract

Human mesenchymal stem cells (hMSCs) in culture critically respond to variations in stiffness of culture substrates. hMSCs differentiate into adipose tissue when cultured on soft substrates, whereas on hard substrates, hMSCs differentiate into bone. Here we demonstrate that when cell-adhesive supported lipid bilayers (SLB) were employed to coat polydimethylsiloxane substrates of different stiffnesses, the mobility of the ligands in the cell-adhesive SLB are instructive to the morphology of the cultured hMSCs. Altering the mobility of the cell-adhesive ligands in the SLB alters the hMSC morphology, ignoring the stiffness of the substrate underneath the SLB.

3.1. Introduction

Human mesenchymal stem cells (hMSCs) can be obtained from adult donors and have the capability to differentiate into multiple cell lineages. They are therefore used extensively as a cell source in regenerative medicine and tissue engineering applications.[1,2] *In vivo*, hMSCs form bone, adipose tissue and cartilage, among others. Understanding the signals that drive the differentiation of hMSCs to a specific cell type is essential for their current and future clinical application.[1–3] It is known that the differentiation of cells is mostly driven by the surrounding cells and extracellular matrix (ECM) through chemical signalling. Cell-cell and cell-ECM interactions are crucial in deciding cell fate. To recreate this multifactorial induction *in vitro* is extremely challenging. Some have tried this by using decellularized tissue,[4–6] others have tried to mimic the ECM with only a small amount of signalling molecules.[5,7,8] One of the major parameters that influences differentiation appears to be cell morphology.[9,10] The morphology of cells is influenced by the stiffness of the surrounding tissue, which determines the amount of force the adhering cell can exert on the binding ligands through its receptors and on the surrounding matrix.[9,10] *In vivo*, the stiffness of the surface, the cell shape and the amount of force the adhering cells can exert, are inherently linked. In a stiffer ECM (Young's modulus of approx. 20 GPa for bone[11]), the ligands will move less when cells exert force onto them via the receptors and, as a consequence, the cytoskeleton of these cells becomes more developed and the shape of the cells becomes more stretched. When the ECM is flexible, such as in adipose tissue (Young's modulus of approx. 1 kPa[12]), the adhering receptor-ligand complexes move around to put no stress on the adhering cells and the cell retains its round shape.[2,4,5,7,13–15] It is challenging to independently study how ECM mechanical properties, ECM ligands and cell force generation contribute to hMSCs differentiation. SLBs have been used as a cell-instructive coating and they consist of phospholipids that can be in various viscoelastic states depending on the type of lipid used (**Figure 3.1**). SLBs made of 1,2-dioleoyl-*sn*-glycero-3-phosphocholine (DOPC) lipids, with a melting transition temperature of -17 °C, are fluidic in which the inserted cell-adhesive ligands are laterally mobile. In contrast, SLBs made of 1,2-dipalmitoyl-*sn*-glycero-3-phosphocholine (DPPC) lipids, with a melting transition temperature of +41 °C, are a gel-state SLB in which cell-adhesive ligands are immobile.

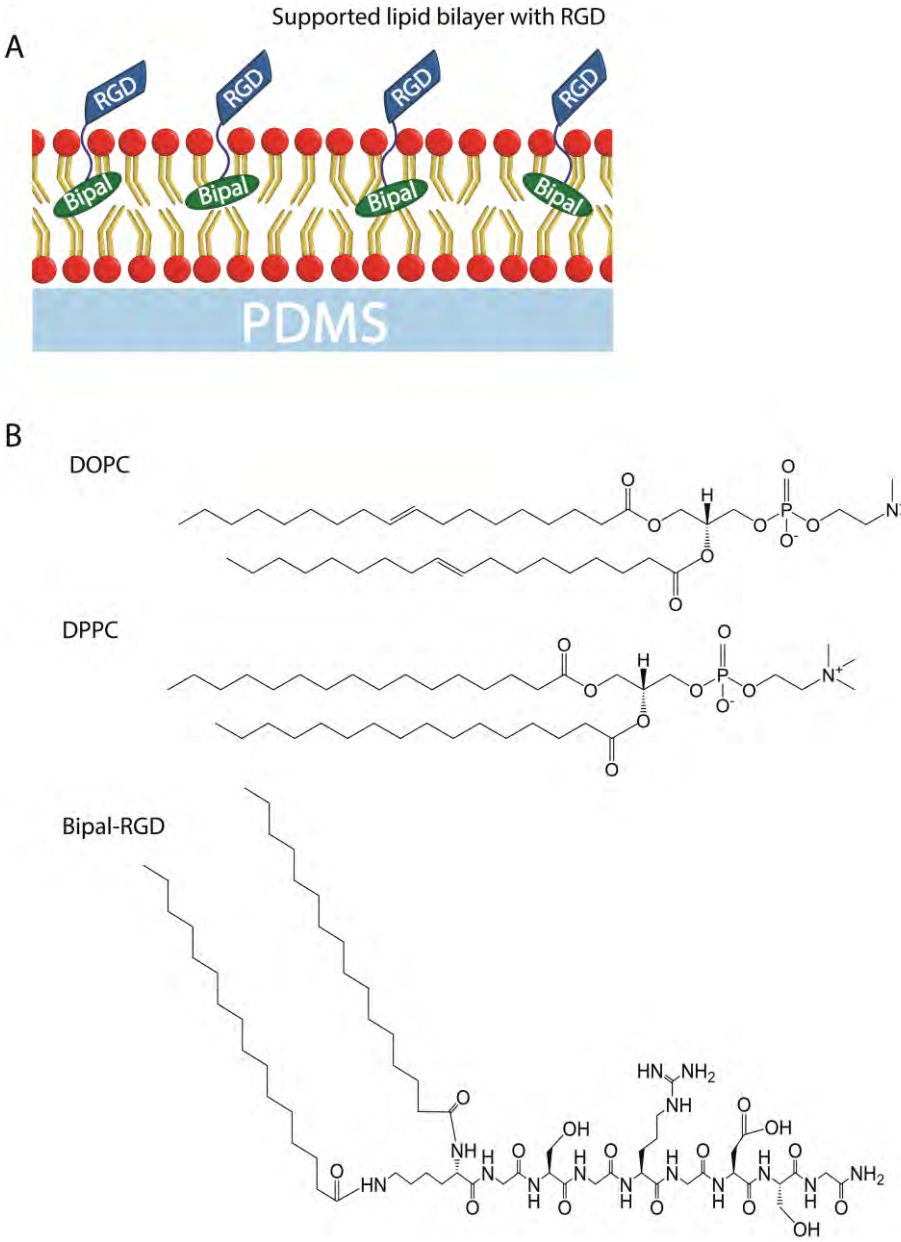

Figure 3.1 A) Coating of plasma-treated PDMS with a supported lipid bilayer (SLB). SLB onto the PDMS substrate functionalised with RGD. B) Molecular structure of the phospholipids 1,2-dioleoyl-*sn*-glycero-3-phosphocholine (DOPC), 1,2-dipalmitoyl-*sn*-glycero-3-phosphocholine (DPPC) and bipalmitic acid-bound Arg-Gly-Asp (RGD).

We have previously demonstrated that when hMSC were cultured on fluidic SLBs functionalized with integrin-binding Arg-Gly-Asp (RGD) peptides, the hMSC would pull on the RGD ligands with high lateral mobility resulting in differentiation towards adipocytes.[16] In contrast, when hMSC were cultured on the gel-state SLBs, the RGD ligands were less mobile and the hMSC showed more differentiation towards an osteogenic lineage.[16] In these experiments the SLBs were applied on glass and they demonstrate that force generation by the hMSC is a dominant stimulus in deciding cell differentiation, independent of ECM ligand density.[16,17] Others have found opposite effects for myoblasts and hepatocytes, which spread more with enhanced nuclear YAP on SLBs with immobile ligands.[18,19] All these studies were carried out with functionalized SLBs on stiff glass substrates. However, no systematic studies have been carried out with SLBs on substrates with varying degrees of stiffness, including those of low stiffness. Therefore, it is currently unknown to what extent SLBs can successfully mask the stiffness of underlying substrates.

^{16,20–22}^{16,20–22}^{16,20–22}(Evans et al., 2013; Koçer & Jonkheijm, 2017; Lautscham et al., 2014; Svedhem et al., 2003)In this chapter, we have studied the cell morphology of hMSCs on polydimethylsiloxane (PDMS) substrates. We selected PDMS because it is the substrate material that is often used in organ-on-chip (OoC) devices and because it can be produced over a wide range of biologically relevant stiffnesses. We covered the substrates with SLBs with varying mobility and density of the cell adhesive ligands. In addition, we varied the PDMS stiffness and studied whether the response of hMSCs in terms of cell-adhesion and spreading when these different types of PDMS were coated with the varying types of SLB.

3.2. Results & Discussion

Different PDMS substrates were prepared in which the stiffness was varied by changing the ratio of curing agent and elastomer. The ratios used were 1:10, which is the standard substrate in OoC devices, 1:33, 1:40 and 1:60. A ratio greater than 1:60 was not useable as the resulting PDMS remained in a liquid state. The stiffness of the PDMS substrates was measured by determining the Young's modulus of the PDMS substrate using atomic force microscopy (AFM) working in the PeakForce Quantitative Nanomechanical Mapping mode (PF-QNM). PDMS Young's modulus maps with representative cross-section analysis and moduli value distributions are shown in **Figure 3.2**. The average values of the Young's moduli were estimated to be 1.87 ± 0.02 MPa for 1:10 PDMS, 0.62 ± 0.01 MPa for 1:33 PDMS, 0.39 ± 0.01 MPa for

1:40 PDMS and 0.19 ± 0.01 MPa for the 1:60 PDMS. Accurate moduli values and a low standard deviation of the means were obtained due to employing calibrated

AFM cantilevers with large spherical tips made of high density carbon. The modulus value of 1.87 MPa for 1:10 PDMS corresponds with earlier findings of a Young's modulus for 1:10 PDMS ranging from 1-3 MPa[23] and is more elastic than glass, which has a Young's modulus of 50 GPa.[9] Increasing the fraction of elastomer in the PDMS mix (1:33, 1:40 and 1:60 PDMS) resulted in an observed decrease of the Young's modulus. This was also found in earlier studies, in which the curing time and thickness of the PDMS was similar.[24–26]

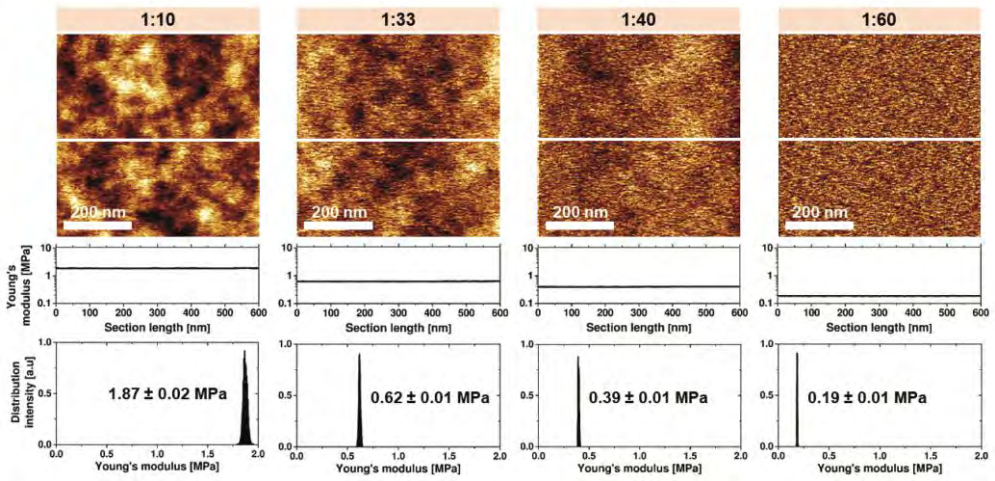

Figure 3.2 AFM analysis of the Young's Modulus of polydimethylsiloxane (PDMS). Mixtures of 1:10, 1:33, 1:40 and 1:60 weight ratio (w/w curing agent to prepolymer) were investigated. The top images display AFM height maps of the PDMS samples, showing the effect on topography of the decrease in the amount of crosslinks from the 1:10 PDMS to the 1:60 PDMS. The graphs in the middle show the Young's modulus obtained along a single scanned line in the image (indicated by a white line in the height images). The graphs in the bottom row show the distribution of Young's moduli indicating little variation in the measured Young's modulus along the cross-section.

As a next step, we hydrophilized the PDMS substrates and applied SLBs to these PDMS substrates and glass using the vesicle fusion method. Making use of a dye-labelled lipid in the SLBs, we performed fluorescence recovery after photobleaching (FRAP) experiments to determine the lateral mobility of the lipids in the SLBs of DOPC and DPPC on different PDMS substrates and glass. The intensity of the radial profile

showed that the bleached area had a Gaussian profile, which allows to use the equation of Kang et al.[27] to determine the lateral mobility of lipids in the SLBs.

As expected, different lateral diffusion rates were derived for the different types of SLBs (**Table 3.1**) when coated on glass substrates. For DOPC fluidic SLBs, we derived a lipid diffusion rate on standard (1:10) PDMS in the same range as was found for DOPC SLBs on glass. In contrast, an SLB consisting of immobile DPPC lipids showed no fluorescence recovery in FRAP, indicating a gel-state SLB. Interestingly, we found that the lateral mobility of SLBs seemed to be unaffected by the underlying PDMS substrate, with similar values found for the SLB derived from DOPC lipids when formed on glass, on 1:10 PDMS or on 1:60 PDMS, all measured at 37 °C (**Table 3.1**). The results indicated that the DOPC lipids in the SLB are free to move around on each of these substrates so there is no apparent drag of the underlying water layer on PDMS compared to glass.

Table 3.1 Diffusion rates on glass, PDMS (1:10 and 1:60) of 1,2-dioleoyl-sn-glycero-3-phosphocholine (DOPC), and 1,2-dipalmitoyl-sn-glycero-3-phosphocholine (DPPC) SLBs estimated from FRAP recovery profiles measured at 37 °C.

	Diffusion rate	
	DOPC	**DPPC**
Glass	1.0 $\mu m^2 s^{-1}$	0.0 $\mu m^2 s^{-1}$
PDMS 1:10	0.82 $\mu m^2 s^{-1}$	0.0 $\mu m^2 s^{-1}$
PDMS 1:60	0.89 $\mu m^2 s^{-1}$	

Subsequently, we cultured hMSCs for 18 hrs in serum-free α-MEM medium on the different PDMS substrates (1:10, 1:33, 1:40 and 1:60) and evaluated the cell morphology (**Figure 3.3**). Bipalmitic acid-RGD was mixed in with the DOPC or DPPC lipids before extrusion of the vesicles in a 1% or 5% (mol%) RGD. All SLBs were applied to the PDMS substrate as above, resulting in SLBs with RGD ligands, that have different mobilities. The resulting culture on the fluidic and gel-state SLBs was influenced by the presence of RGD. When the RGD ligands were absent, hMSC adhesion was low and the cells remained in a rounded morphology, confirming that the SLB is essentially a non-fouling surface. The morphology of the cultured hMSCs differed between the different PDMS substrates, the ligand mobility and ligand concentration. hMSCs cultured on 1:60 PDMS were not adhering well and the few

cells on the substrate showed a rounded morphology regardless of the type of SLB and the concentration of the cell-adhesive ligand (**Figure 3.3**). Furthermore, little to no difference in morphology (small and round) was observed between the 1:10, 1:33 and the 1:40 PDMS when coated with DOPC fluidic SLBs with cell adhesive ligands inserted, while when DPPC gel-state SLBs were used on the different PDMS substrates, a more stretched morphology with longer filopodia were observed (**Figure 3.3**).

Increasing the concentration of RGD ligands on the SLBs, led to an increase in the number of cells that adhered to the surface coating. This observation suggests that RGD-ligand mobility and ligand density are the most important factors for hMSC adhesion and spreading. Cell adhesion and spreading was highest at low RGD-ligand mobility and high RGD ligand density. In culture, hMSCs exert a pull on the RGD-ligands and when the cells encounter sufficient resistance, the hMSCs elongate and form stress fibres and focal adhesions as we observed in actin and vinculin stains (**Figure 3.3**). The mobile ligands in the DOPC SLB presumably provided hardly any resistance as soon as the cells applied force. The cells therefore remained round with no focal adhesions (**Figure 3.3**). In contrast, the DPPC gel-state SLB provided the cells with resistance when force was applied which presumably explains the more stretched morphology of the hMSCs. Increasing the concentration of RGD-ligands from 1% to 5% concentration caused the cells to become more numerous (**Figure 3.3**).

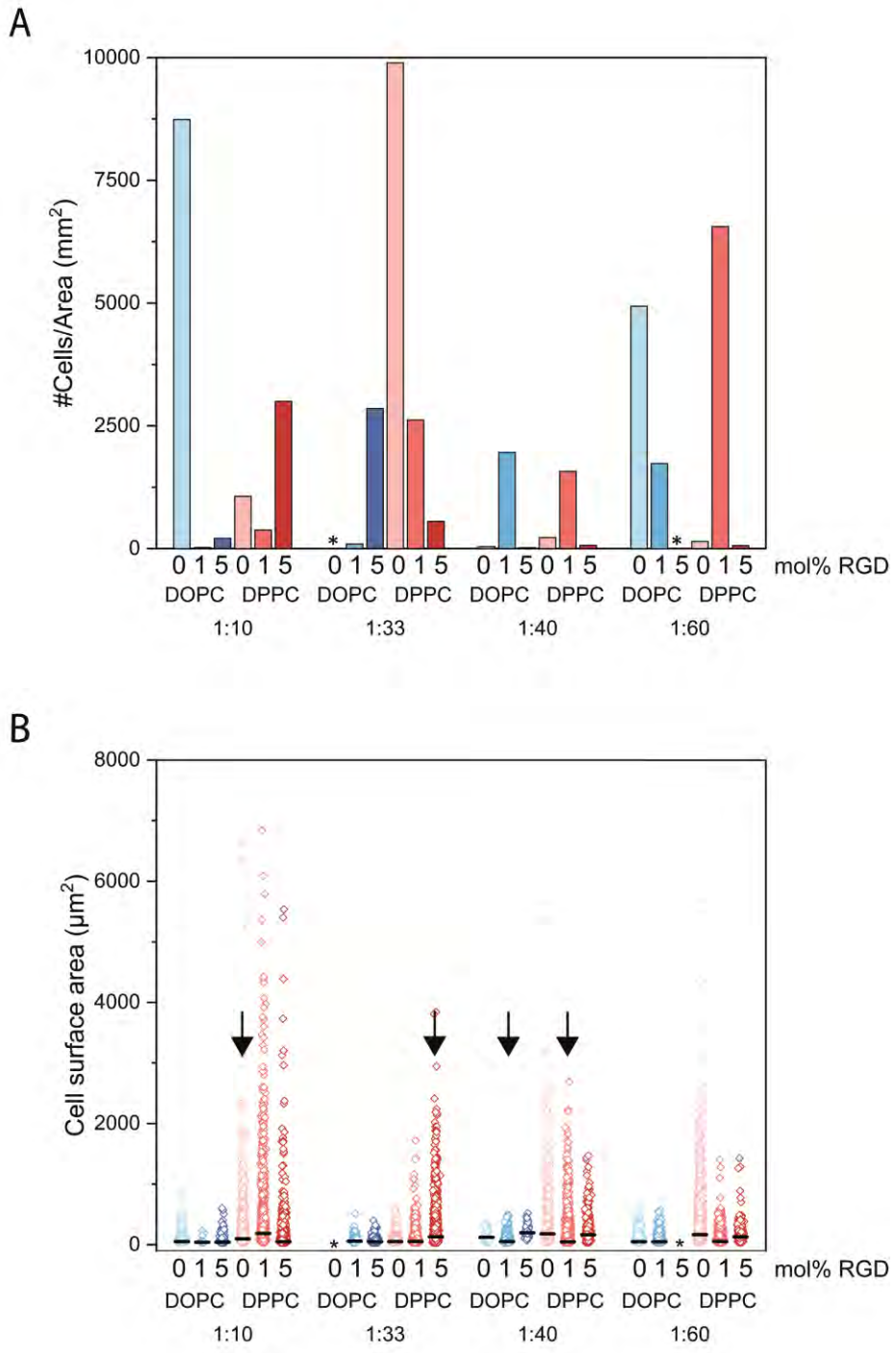
A
#Cells/Area (mm²)
10000
7500
5000
2500
0
0 1 5 0 1 5 0 1 5 0 1 5 0 1 5 0 1 5 0 1 5 0 1 5
mol% RGD
DOPC DPPC DOPC DPPC DOPC DPPC DOPC DPPC
1:10 1:33 1:40 1:60
B
Cell surface area (µm²)
8000
6000
4000
2000
0
0 1 5 0 1 5 0 1 5 0 1 5 0 1 5 0 1 5 0 1 5 0 1 5
mol% RGD
DOPC DPPC DOPC DPPC DOPC DPPC DOPC DPPC
1:10 1:33 1:40 1:60

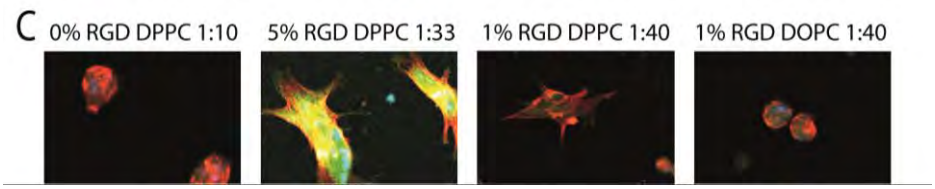

Figure 3.3 Analysis of number of hMSC cells (A) and the cell area (B) when cultured on PDMS with ratios ranging from 1:10 to 1:60, each coated with an SLB with either DOPC and DPPC and functionalised with no RGD, 1% or 5% RGD ligands. *=no data available. C) Examples of fluorescence microscopy images of hMSC culture on PDMS coated with different SLBs (indicated by black arrows), stained for actin (red), vinculin (green) and nuclei (blue), showing differences in morphology. Scale bars represents 100 µm.

The influence of the stiffness of the surface on hMSCs has been previously investigated and it was shown that the morphology of hMSCs was different when cultured on stiffer (50-60 kPa) and softer (8-10 kPa) hydrogels.[2] The hMSCs had a more stretched morphology with long filopodia in the stiffer hydrogel, indicating that there could be more pulling forces applied.[2] Others also connected the stiffness of the surroundings to the development of the cytoskeleton and the cell morphology.[13–15] The mobility of ligands in the SLB appears to have more influence on hMSC morphology than the PDMS stiffness underneath the SLB. While on DOPC fluidic SLBs hMSC appear round, on DPPC gel-state SLBs elongated hMSCs were observed. The RGD ligand density seemed to have a minor influence. The 1% RGD concentration already ensured more cells were present than on bare SLBs. 5% RGD did improve the cell adhesion compared to 1% RGD showing the influence of RGD concentration.

3.3. Conclusions

We observed that hMSCs adhere and spread to the same extent on PDMS of varying stiffness when these PDMS substrates were coated with SLBs in which cell adhesive RGD-ligands were present. Whereas on fluidic SLBs with RGD ligands small and round hMSCs were observed, on gel-state SLBs with the same ligands spread hMSCs were observed. The ability to coat different materials with a cell-instructive layer that introduces similar cell responses is very promising in future developments of organ-on-chip devices and regenerative medicine.

3.4. Acknowledgements

We thank Dr. Ing. Hubert Gojzewski, and Aina Gallemí-Pérez for the AFM measurements. We thank Aukie Hooglught for his contribution to the cell experiments.

3.5. Experimental section

3.5.1. Surface preparation

For all experiments, polydimethylsiloxane (PDMS) surfaces were prepared by mixing elastomer with its curing agent (Sylgard 184 elastomer kit, Dow Corning Corp, Midland, MI, USA) at the desired ratio. The mixtures were degassed, deposited as specified by the experiment and cured at 60 °C for 5 h.

A mobile supported lipid bilayer (SLB) was prepared with 1,2-dioleoyl-*sn*-glycero-3-phosphocholine (DOPC) and a solid SLB with 1,2-dipalmitoyl-*sn*-glycero-3-phosphocholine (DPPC) in chloroform (all Avanti Lipids). The chloroform was evaporated resulting in a lipid cake. The lipids were resuspended in Dulbecco's phosphate-buffered saline (DPBS) in a concentration of 1 mg/ml. The resulting multilamellar vesicles were extruded eleven times through a 100 nm Whatmann filter to form unilamellar vesicles. The unilamellar vesicles were sterilized by filtration (0.2 µm, Whatmann) and added to DPBS to a final concentration of 0.5 mg/ml to rupture and form a bilipid layer by vesicle fusion. After 30 min the excess vesicles were washed off with DPBS, taking care that the SLB was not exposed to air.

For fluorescence recovery after photobleaching (FRAP) the SLBs were made fluorescent by adding 0.2% Texas Red-2-dihexadecanoyl-*sn*-glycero-3-phosphoethanolamine (TR-DHPE, Avanti Lipids) in methanol to the lipids in chloroform. The lipids were extruded as described before to obtain the unilamellar vesicles. For cell culture DOPC lipids or DPPC lipids were mixed with 0, 1 or 5 mol% bipalmitic acid-RGD (KGGRGDS) and extruded as described before to obtain the unilamellar vesicles.

3.5.2. Young's Moduli

PDMS was prepared at a 1:10, 1:33, 1:40 and a 1:60 ratio and characterised by determining the Young's moduli. The uncured PDMS mixtures were cast on atomic force microscopy (AFM) steel mounting disks with silicon barriers (Press to Seal silicon isolators – S/A, 7x7x2mm, Electron Microscopy Sciences, Hatfield US). The disks were placed in 6-wells plate (Greiner) and the PDMS was cured.

A MultiMode 8 AFM instrument with a NanoScope V controller (Bruker) was operated in the PF-QNM mode to record 65.536 force-distance curves per map to be processed further on. The data was collected following a sine-wave sample-tip

trajectory with a frequency of 2 kHz and utilizing a peak-force amplitude value of 300 nm, with the applied forces ranging from 10-30 nN (depending on PDMS type, but kept constant during a particular map generation). The ScanAsyst optimization in the user interface was set to "off" to keep other scanning parameters (e.g. scan rate and feedback loop) constant for each stiffness mapping. Image processing and data analysis were conducted with the NanoScope (version 9.7) and the NanoScope Analysis software (version 1.9), respectively. Measurements were performed in air and at room temperature (~ 21 °C).

Medium soft cantilevers with a calibrated spring constant (range: 3.23 – 3.32 N/m) extracted from Laser Doppler Vibrometer (LDV) measurements were used (Nanotools GmbH, Biosphere B300-FM). The cantilevers were manufactured with a defined spherical tip (diamond-like carbon made) of the radius ranging from 300 to 301 nm (measured by high resolution SEM) for the most accurate data fitting. The large tip-sample contact area leads to a low data scattering in the force-distance curves and guaranties good surface property averaging. The AFM optical sensitivity (deflection sensitivity) was "reverse" calculated based on thermal tune method.[28]

The Young's modulus was determined by fitting the slope of the extended part of force-distance curves, employing the Derjaguin, Muller, and Toporov (DMT) model of contact mechanics,[29] with the following equation:

$$E = (F_L - F_{adh})\frac{3(1-\nu^2)}{4}R^{-\frac{1}{2}}(z-d)^{-\frac{3}{2}}$$

where: F_L – the applied maximum force (load), F_{adh} – the adhesion force, ν – the Poisson's ratio, R – the AFM tip radius, z – the position of the AFM scanner; d – the cantilever deflection.

The equation assumes the contact geometry between a plane surface and a paraboloid indenter ended with a sphere. For the Poisson's ratio a value of 0.49 was used.[30] Other values needed to perform calculation of the Young's modulus from the DMT theory were extracted from force-distance curves.

3.5.3. FRAP

The mobility of the lipids in a supported lipid bilayer was determined by FRAP. PDMS was prepared at a 1:10 ratio and a 1:60 ratio. These mixtures were spin-coated on glass microscopy coverslips (diameter 15 mm) at 2,000 rpm, 300 rpm/s ramp for 2 min (Spin Processor WS-650MZ-23NPP/LITE, Laurell Technologies). The spin-coated samples were placed in a 24- wells sensoplate (Greiner), cured and then activated

using O_2-plasma (SPI Plasma-Prep II, SPI Supplies). The samples were sealed in the wells using silicon O-rings. To preserve the hydrophilicity, all the wells were filled with MilliQ water. A glass bottom 96-wells plate was treated with 1M NaOH for 1 h to activated the surface and the wells were filled with MilliQ water. A mobile, semi-mobile and immobile SLB were prepared with 0.2% TR-DHPE for fluorescence and used for FRAP. FRAP experiments were performed on a Nikon A1 Confocal microscope at 37 °C and the diffusion rate was determined after the data was checked for chromophore recovery using the formula $D_{confocal} = \frac{r_e^2 + r_n^2}{8\tau_{1/2}}$, where r_e is the experimental radius of the bleach spot and r_n the set radius and $\tau_{1/2}$ is the half time of recovery.[12]

3.5.4. Cell culture

The impact of the type of SLB, the ligand density and the stiffness of the underlying substrate on cell morphology was established by analysing cell morphology. The substrates used were PDMS in the 1:10 and 1:60 ratios. This was poured in a 48-wells plate and cured. The resulting substrates were treated with O_2-plasma to activate the surface and to sterilize the surface as well. DOPC lipids or DPPC SLBs with 0, 1 or 5 mol% bipalmitic acid-RGD was added to the 48-wells plate with PDMS surface. Human mesenchymal stem cells (hMSC; Lonza) were cultured in complete medium consisting of α-MEM medium (Gibco) supplemented with 10% FBS (Lonza), 100 U/ml penicillin (Gibco) and 100 µg/ml streptomycin (Gibco) and incubated at 37 °C and 5% CO_2 up to one week before use. The hMSCs were seeded in the 48-wells plate at density of 5000 cells/cm^2 and cultured for 18 h at 37 °C and 5% CO_2. The cells were then fixed using 4% paraformaldehyde for 5 min and stained for actin (Phalloidin Alexa Fluor 568; 1:200; Thermo Fisher Scientific), vinculin (anti-hVIN-1-FITC, 1:200; Sigma-Aldrich) and the nucleus (DAPI, 1:1000). The cells were imaged using the Nikon A1 confocal microscope and analysed with the open-source software CellProfiler™ 4.1.3.

3.5.5. Statistical analysis

Statistical analysis of the data was performed using IBM SPSS Statistics 26, Origin 2019 and the open-source software CellProfiler™ 4.1.3. FRAP data was analysed with Origin to check for Gaussian distribution and to determine the diffusion rate of lipids. The data from CellProfiler™ was analysed using Origin and the difference of cell area assessed with an ANOVA in SPSS.

3.6. Supplemental

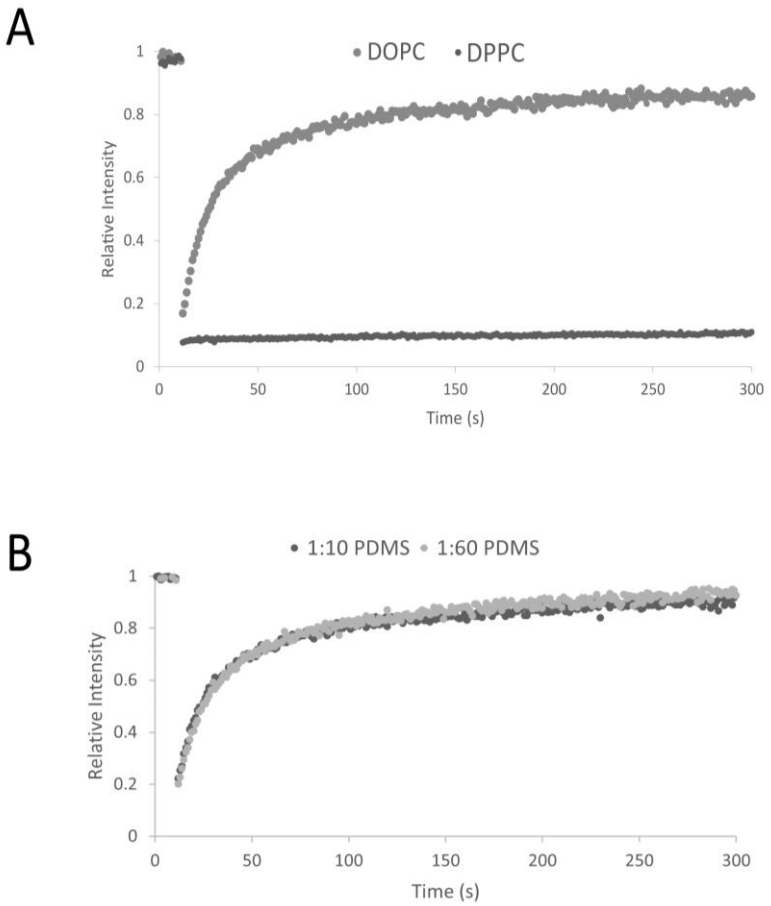

Supplemental 1 Intensity signal of fluorescent SLB after FRAP with A) 1,2-dioleoyl-*sn*-glycero-3-phosphocholine (DOPC) and 1,2-dipalmitoyl-*sn*-glycero-3-phosphocholine (DPPC) on glass, all measured at 37 °C. The graph shows that the mobile DOPC lipids within the SLB move to occupy the bleach spot rapidly with 1.0 $\mu m^2 s^{-1}$, and the immobile DPPC lipids did not move within the SLB at all. B) DOPC lipids on 1:10 and 1:60 PDMS, showing the intensity of the bleach spot and movement of DOPC lipids is equal of an SLB on 1:10 and 1:60 PDMS.

3.7. References

1. Parrotta, E. I., Scalise, S., Scaramuzzino, L. & Cuda, G. Stem cells: The game changers of human cardiac disease modelling and regenerative medicine. *Int. J. Mol. Sci.* **20**, (2019).
2. Whitehead, A. K., Barnett, H. H., Caldorera-Moore, M. E. & Newman, J. J. Poly (ethylene glycol) hydrogel elasticity influences human mesenchymal stem cell behavior. *Regen. Biomater.* **5**, 167–175 (2018).
3. Park, S. H. *et al.* Chip-based comparison of the osteogenesis of human bone marrow- and adipose tissue-derived mesenchymal stem cells under mechanical stimulation. *PLoS One* **7**, 1–11 (2012).
4. Flynn, L. E., Prestwich, G. D., Semple, J. L. & Woodhouse, K. A. Proliferation and differentiation of adipose-derived stem cells on naturally derived scaffolds. *Biomaterials* **29**, 1862–1871 (2008).
5. Lutolf, M. P., Gilbert, P. M. & Blau, H. M. Designing materials to direct stem-cell fate. *Nature* **462**, 433–441 (2009).
6. Lutolf, M. P. & Hubbell, J. A. Synthetic biomaterials as instructive extracellular microenvironments for morphogenesis in tissue engineering. *Nat. Biotechnol.* **23**, 47–55 (2005).
7. Hubbell, J. A. Materials as morphogenetic guides in tissue engineering. *Curr. Opin. Biotechnol.* **14**, 551–558 (2003).
8. Pati, F. *et al.* Ornamenting 3D printed scaffolds with cell-laid extracellular matrix for bone tissue regeneration. *Biomaterials* **37**, 230–241 (2015).
9. Mcbeath, R., Pirone, D. M., Nelson, C. M., Bhadriraju, K. & Chen, C. S. Cell shape, cytoskeletal tenstion and RhoA regulate stem cell lineage committment. **6**, 483–495 (2004).
10. Huebsch, N. *et al.* Matrix elasticity of void-forming hydrogels controls transplanted-stem-cell-mediated bone formation. *Nat. Mater.* **14**, 1269–77 (2015).
11. Rho, J. Y., Ashman, R. B. & Turner, C. H. Young's modulus of trabecular and cortical bone material: Ultrasonic and microtensile measurements. *J. Biomech.* **26**, 111–119 (1993).
12. Comley, K. & Fleck, N. A. A micromechanical model for the Young's modulus of adipose tissue. *Int. J. Solids Struct.* **47**, 2982–2990 (2010).
13. Doss, B. L. *et al.* Cell response to substrate rigidity is regulated by active and passive cytoskeletal stress. *Proc. Natl. Acad. Sci. U. S. A.* **117**, 12817–12825 (2020).
14. Gupta, M. *et al.* Cell shape and substrate stiffness drive actin-based cell polarity. *Phys. Rev. E* **99**, 1–16 (2019).
15. Engler, A. J., Sen, S., Sweeney, H. L. & Discher, D. E. Matrix elasticity directs stem cell lineage specification. *Cell* **126**, 677–689 (2006).

16. Koçer, G. & Jonkheijm, P. Guiding hMSC adhesion and differentiation on supported lipid bilayers. *Adv. Healthc. Mater.* **6**, 1600862 (2017).

17. Sepulveda, H. *et al.* Epigenetic signatures at the RUNX2-P1 and Sp7 gene promoters control osteogenic lineage commitment of umbilical cord-derived mesenchymal stem cells. *J. Cell. Physiol.* 1–23 (2016) doi:10.1002/jcp.25627.

18. Bennett, M. *et al.* Molecular clutch drives cell response to surface viscosity. *Proc. Natl. Acad. Sci. U. S. A.* **115**, 1192–1197 (2018).

19. Vafaei, S., Tabaei, S. R., Biswas, K. H., Groves, J. T. & Cho, N. J. Dynamic cellular interactions with extracellular matrix triggered by biomechanical tuning of low-rigidity, supported lipid membranes. *Adv. Healthc. Mater.* **6**, 2–9 (2017).

20. Lautscham, L. A. *et al.* Biomembrane-mimicking lipid bilayer system as a mechanically tunable cell substrate. *Biomaterials* **35**, 3198–3207 (2014).

21. Svedhem, S. *et al.* In situ peptide-modified supported lipid bilayers for controlled cell attachment. *Langmuir* **19**, 6730–6736 (2003).

22. Evans, S. F. *et al.* Solid-supported lipid bilayers to drive stem cell fate and tissue architecture using periosteum derived progenitor cells. *Biomaterials* **34**, 1878–1887 (2013).

23. Berthier, E., Young, E. W. K. & Beebe, D. Engineers are from PDMS-land, Biologists are from Polystyrenia. *Lab Chip* **12**, 1224 (2012).

24. Schoen, I., Hu, W., Klotzsch, E. & Vogel, V. Probing cellular traction forces by micropillar arrays: contribution of substrate warping to pillar deflection. **10**, 1823–1830 (2011).

25. Carrillo, F. *et al.* Nanoindentation of polydimethylsiloxane elastomers: Effect of crosslinking, work of adhesion, and fluid environment on elastic modulus. *J. Mater. Res.* **20**, 2820–2830 (2005).

26. Wang, Z., Volinsky, A. A. & Gallant, N. D. Crosslinking effect on polydimethylsiloxane elastic modulus measured by custom-built compression instrument. *J. Appl. Polym. Sci.* **131**, 1–4 (2014).

27. Kang, M., Day, C. A., Kenworthy, A. K. & DiBenedetto, E. Simplified equation to extract diffusion coefficients from confocal FRAP data. *Traffic* **13**, 1589–1600 (2012).

28. Hutter, J. L. & Bechhoefer, J. Calibration of atomic-force microscope tips. *Rev. Sci. Instrum.* **64**, 1868–1873 (1993).

29. Derjaguin, B. . V., Muller, V. . M. & Toporov, Y. . P. Effect of contact deformation on the adhesion of elastic solids. *J. Colloid Interface Sci.* **53**, 314–326 (1975).

30. Müller, A., Wapler, M. C. & Wallrabe, U. A quick and accurate method to determine the Poisson's ratio and the coefficient of thermal expansion of PDMS. *Soft Matter* **15**, 779–784 (2019).

Chapter 4

Guiding hMSC differentiation employing supported lipid bilayers in bone-on-chip microfluidic devices

Abstract

Human mesenchymal stem cells (hMSCs) can be differentiated into predetermined tissue. The cues that stem cells receive *in vivo* from the extracellular matrix (ECM) are of chemical and physical nature and they influence the morphology and differentiation of stem cells. In this chapter, we have used a microfluidic device with a pillar microarchitecture that is coated with a supported lipid bilayer (SLB). The SLB is functionalised with cell-adhesive ligands to promote initial hMSC adhesion, which then grows into a three-dimensional cellular network after 3 days in which the hMSCs were stretched. When induced to differentiate by chemical cues, the hMSCs differentiated readily into osteoblasts. First steps to further develop the SLB as an instructive coating were taken by inserting TGF-β1 binding ligands into the SLB and successfully bind TGF-β1 which could be detected by cells. The work in this chapter demonstrates the opportunities to provide the hMSC culture with both physical and chemical cues to steer differentiation toward osteogenesis inside a microfluidic 'bone-on-chip'.

4.1. Introduction

During the development of organs in the embryonic stage, stem cells differentiate into specific tissue cells. The activation or deactivation of genes that regulate this process is influenced by the surroundings of the cell. The location of cells in the tissue and the microenvironment, the opportunity for forming cell-cell contacts and the information given to the cell via the contact of the cell with the extracellular matrix (ECM) are instrumental to guide the differentiation of stem cells.[1–3] In addition, the physical forces exerted on cells, the amount of space available for cells and the presence of cell adhesion points influence the cell morphology and thereby its differentiation process.[4,5] Some of these key chemical and physical cues can be incorporated *in vitro* in organ-on-chip devices to study their influence on cell fate, or, by blocking cues, to perform toxicological studies or to design disease models. For example, controlled delivery of soluble growth factors, surface functionalization with various ECM proteins or control over the mechanical properties of the substrate have been shown to guide differentiation of cultured stem cells.[6–8] Control of the microarchitecture of the cell culture environment is also an efficient method to direct stem cell differentiation.[9] Varying the porosity of a mesh in which stem cells are seeded or the topography of surfaces manipulates the morphology of stem cells and this influences cell differentiation.[4,10,11]

By providing a three-dimensional (3D) microarchitecture in organ-on-chip (OoC) devices, it is possible to offer adhesion sites to form a network of cells, with sufficient space to deposit their own ECM, which will stimulate the cells to further adapt their morphology. Chapter 2 of this thesis describes the formation of a cellular network of human mesenchymal stem cells (hMSC) when hMSCs were cultured in polydimethylsiloxane (PDMS) microfluidic OoC devices that included an array of 28 pillars with a 50 µm spacing and that was covered with ECM protein fibronectin. When these hMSCs were exposed to osteogenic medium, the hMSCs successfully differentiated towards bone cells, as confirmed by osteoblast markers RUNX2, osterix, ALP and osteocalcin, and calcium deposits in the device. The medium that was used in Chapter 2 contained a cocktail of dexamethasone, ascorbic acid and β-glycerophosphate for the osteogenic differentiation of hMSCs,[12] but other important stimuli for osteoblasts are known and could be included to further enhance differentiation. For example, transforming growth factor β1 (TGF- β1) is identified as an essential protein in the differentiation of osteoblasts and could possibly be enough to solely trigger the differentiation pathway towards osteoblasts.[13–16] In Chapter 3, it was shown that a supported lipid bilayer (SLB) coating can be applied

to PDMS, which can then be further tailored with cell-adhesive peptides. The lateral mobility of these active moieties can be tuned by selecting the lipids in the SLB. This mobility is an important factor that determines hMSC differentiation and using this method we were able to assemble cell-adhesive peptides on PDMS films while providing a non-fouling background.[17] SLBs have been applied previously by us as a non-fouling layer in PDMS channels to block the adsorption of drug molecules in PDMS, but there are no reports of using SLBs inside microfluidic OoC devices to control cell adhesion and differentiation by inserting specific ligands in the SLB coating.[18]

In this chapter, the aim is to introduce the SLB coating method into the structured microfluidic OoC device and provide cell-adhesive and TGF-β1 binding ligands to the cultured cells. This design of OoCs provides instruction to the hMSCs to differentiate into osteoblasts via suitable surface functionalization of the OoC device surface.

4.2. Results & Discussion

The PDMS microfluidic OoC device with a pillar array (**Figure 4.1A**, and see Chapter 2) was treated with O_2-plasma for 1 min to hydrophilize the PDMS. After filling the channel with 100 nm unilamellar vesicles of 1,2-dioleoyl-*sn*-glycero-3-phosphocholine (DOPC) with 0.5% TopFluor® PE lipid dye, the device was left to stand for 30 min after which the device was inspected by fluorescence microscopy. This showed that the entire interior surface of the device, i.e. the bottom and top of the chamber and the sides of the pillars, were evenly coated with the SLB (**Figure 4.1B**).

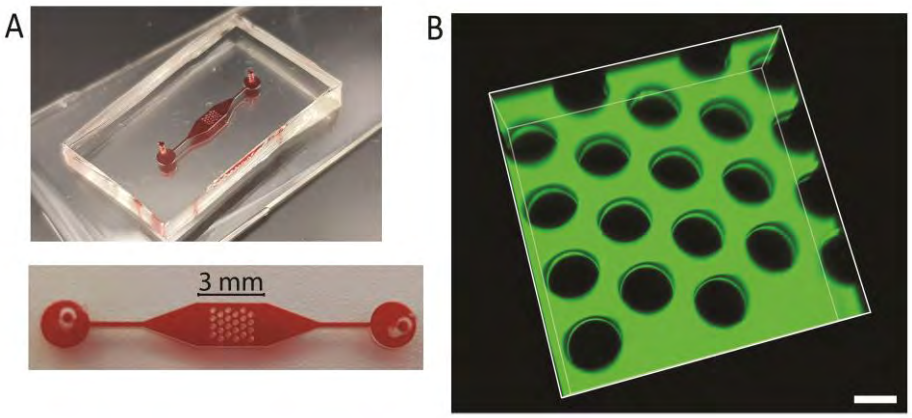

Figure 4.1 A) Photographs of the OoC device with pillar-array microarchitecture. The device is filled with a red-coloured dye. B) Fluorescence microscopy image of the central part of the device. The entire device is coated with an SLB containing a green fluorescent dye (TopFluor® PE). Scale bar represents 200 µm.

Fluorescence recovery after photobleaching (FRAP) experiments were performed on SLBs that contained 0.2% Texas Red dye labelled lipids (TR-DHPE) in the area of the device just adjacent to the pillar array and on the side of a pillar (**Figure 4.2**). Diffusion coefficients were derived to be 1.5 $\mu m^2/s$ and 1.0 $\mu m^2/s$, respectively. These diffusion coefficients of the lipids are comparable to that of the diffusion coefficients of lipids in SLBs that were made on flat PDMS (see Chapter 3).

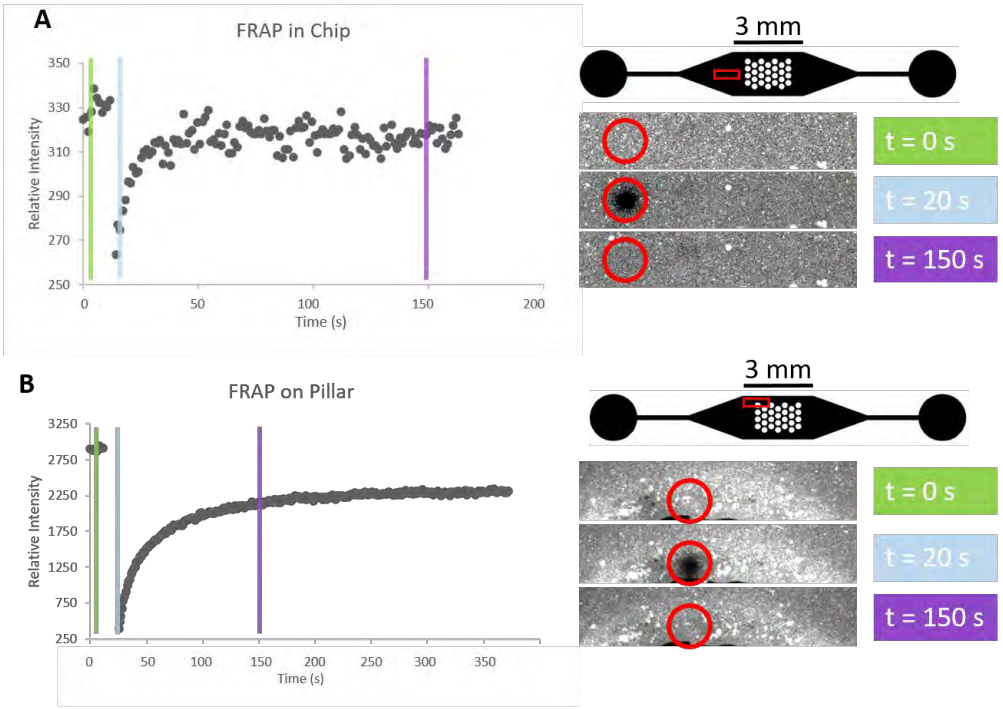

Figure 4.2 FRAP experiments in the OoC device covered with DOPC SLBs complemented with TR-DHPE. Fluorescence recovery profiles and images A) in the area without pillars and B) on the side of a pillar. The graph on the left-hand side depicts the profile of the bleach spot over time. On the right-hand side, the red rectangles indicate the area in the device that was imaged and the red circles indicate the bleached spots. The different timepoints are colour coded (green, blue and purple) and linked to the graph.

In Chapter 2, it was shown that it was possible to culture and differentiate hMSCs in our microfluidic PDMS devices with the pillar arrays when a coating of fibronectin was applied to the surface. hMSCs adhered to the device surface and confluency was reached in 3 days where the cells were stretched between adjacent pillars and covered the entire volume of the device. The cells showed thick actin fibres with vinculin present around the circular nuclei, indicating that the vinculin was not activated to form full focal adhesions for strong adhesion of cells to the surface.[19]

In contrast, when the SLB was applied to the surface of the PDMS in the devices and hMSCs were cultured on them for 3 days, a significant lower number of cells were observed in the device (**Figure 4.3C**) when compared to the devices that were not treated (bare PDMS) (**Figure 4.3A**) or that were coated with fibronectin (**Figure 4.3B**). This result demonstrates that the DOPC SLB in the PDMS devices can be used effectively as an hMSC non-adherent coating in agreement with previous

observations where hMSCs were found to be non-adherent on DOPC-based SLBs on flat PDMS (Chapter 3) and as previously observed by our group on SLBs on glass.[17,20,21] As a next step, the SLBs in the PDMS device were functionalised with cell adhesive Arg-Gly-Asp (RGD) peptides, which constitute the integrin binding site in fibronectin. The RGD peptides were functionalised with a cholesterol (Chol) moiety to enable stable, irreversible insertion into the SLBs.[22,23] After applying the SLBs to the PDMS device, first a solution with Chol-RGD was added to the device (2µM) for 30 min and then cells were seeded in the device in serum-free medium supplemented with Chol-RGD to ensure the binding of hMSCs to Chol-RGD ligands.[24] On day 3, the hMSC culture was observed to be confluent, indicative of cell adherent properties of the SLB coated PDMS device when Chol-RGD is present (**Figure 4.3D**). In the device area with the pillar array cells not only wrapped around the pillars, but also filled the entire volume between the pillars. The morphology of the hMSCs was similar to that observed for the cells in the fibronectin-coated device (**Figure 4.3B**), as is indicated by the actin and vinculin stains. The cell numbers appeared to be slightly lower in the devices with Chol-RGD-functionalised SLBs compared to the fibronectin coated devices. These results indicate that the SLB coatings and their bioactive functionalization can be successfully applied as a coating for hMSC culture inside microfluidic OoC devices.

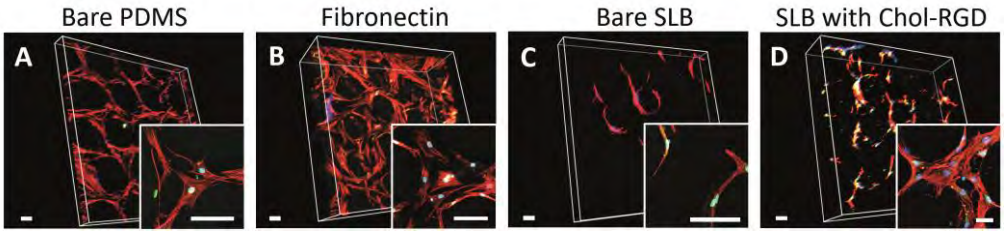

Figure 4.3 Microfluidic devices with hMSC cell culture on A) uncoated, bare PDMS, B) fibronectin coated PDMS, C) SLB coated PDMS, and D) SLB functionalised with Chol-RGD on PDMS. Cells are stained for actin (red), vinculin (green) and the nucleus (blue). All scale bars represent 100 µm.

Alternatively, a palmitoylated RGD (C16-RGD) was reversibly inserted[22,23] into the SLB from solution to study whether the reversibility of the insertion in the SLB influences the cell response in the device.[25,26] After functionalizing the SLBs with either Chol-RGD or C16-RGD, hMSCs were seeded in the devices for 3 days. In the case of Chol-RGD devices, cell confluency was observed which was in strong contrast to the C16-RGD devices, where only cells were observed that adhered to the sides of the pillars while other parts of the device remained empty. These observations are

supposedly caused by with the difference in affinity of the two peptides for the SLB. This difference in affinity leads to Chol-modified ligands that do not desorb from the SLB into the medium, but remain inserted in the SLB, while C16-modified ligands can readily desorb from the SLB into the medium.[22,23,25]

To verify whether the microfluidic OoC devices coated with Chol-RGD SLBs are a suitable microenvironment for long-term culture and cell manipulation, an 18-day hMSC osteoblast differentiation assay was performed in devices coated with Chol-RGD SLBs and devices coated with fibronectin. After an initial attachment period (3 days) in normal cell culture medium, the cells were exposed for 18 days to an osteogenic culture medium, containing dexamethasone, ascorbic acid and β-glycerophosphate. The resulting cell cultures were analysed (at day 0, 3, 6, 11 and 18 of culture) for known osteogenic markers. After 3 days of osteogenic medium, the culture displayed elevated levels of the markers RUNX2 and osterix, which indicates early differentiation of hMSCs to osteoprogenitor cells (**Figure 4.4**). After 18 days of differentiation, the cells displayed elevated levels of ALP, which is a marker for mineralisation, and osteocalcin, which indicates bone induction (**Figure 4.5**). These results demonstrate that the osteoblastic differentiation potential of hMSCs is retained and follows the same time windows in the RGD-functionalised SLB OoC devices as in standard fibronectin coated analogues[27].

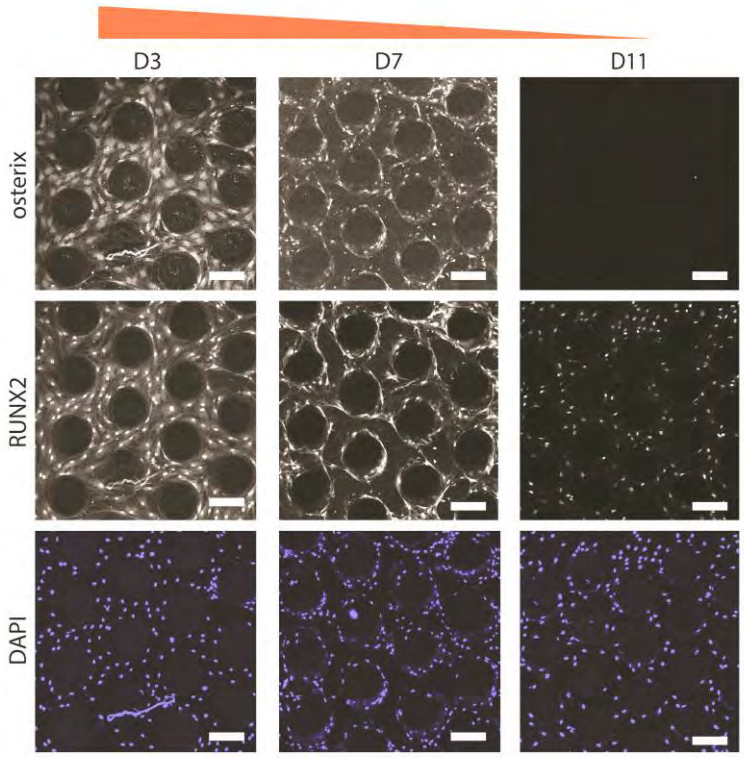

Figure 4.4 Differentiation of hMSC to osteoblasts analysed on day 3, 7, 11 and 18, analysed with fluorescence microscopy. Decrease of early differentiation markers osterix and RUNX2. All scale bars represent 200 µm.

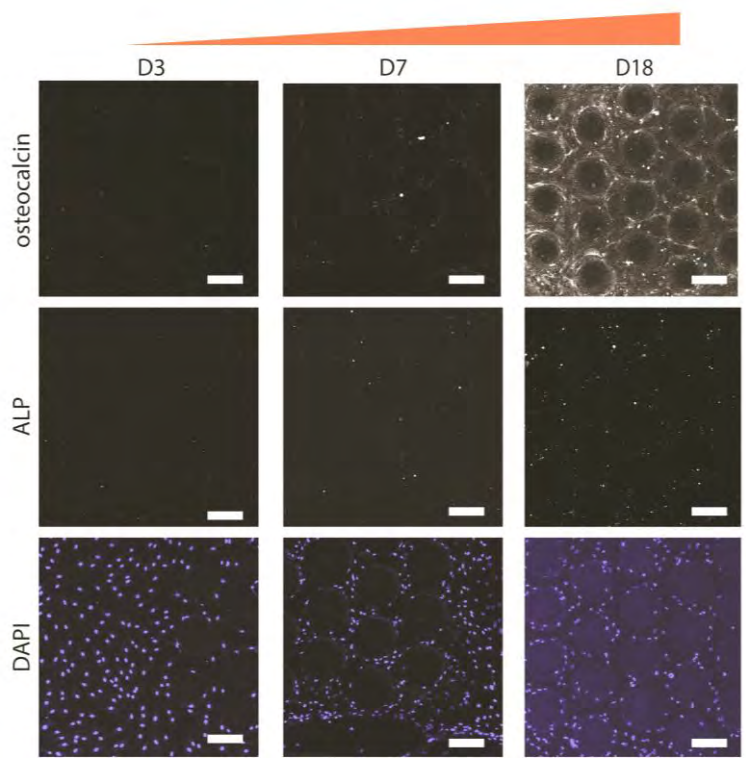

Figure 4.5 Differentiation of hMSC to osteoblasts analysed on day 3, 7, 11 and 18, analysed with fluorescence microscopy. Increase of late differentiation markers ALP and osteocalcin. Nuclei stained with DAPI. All scale bars represent 200 µm.

In a next set of preliminary experiments, we have functionalized the SLBs not only with cell-adhesive RGD ligands, but also with TGF-β1 growth factor binding ligands, as TGF-β1 has a regulatory role in the differentiation of hMSCs in osteoblasts.[13–16] First, it was verified whether TGF-β1 binding ligands could be inserted into SLBs and whether they could bind TGF-β1 onto the SLB surface. After SLBs were formed, palmitoylated TGF-β1 binding ligands were inserted into the SLBs and the binding of TGF-β1 was evaluated using Mink lung epithelial cells (MLEC), which express luciferase when TGF-β1 is taken up.[28] MLEC cells showed higher luminescence when cultured on TGF-β1 binding ligands when compared to when MLECs were cultured on normal culture plates or on PDMS (**Figure 4.6**), indicative of more TGF-β1 available on SLBs.[29]

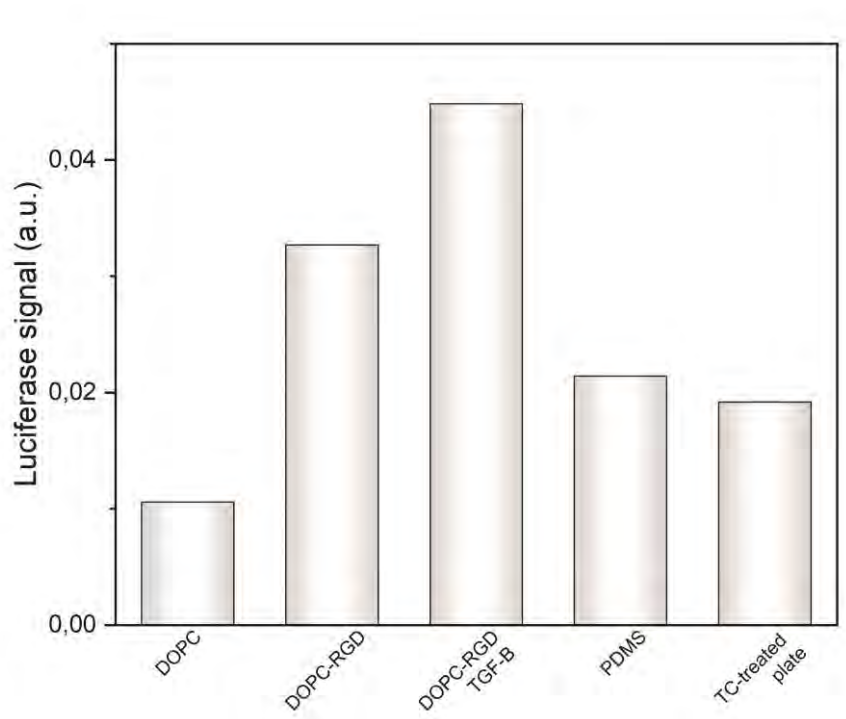

Figure 4.6 Luminescence signal of MLEC cells indicating availability of TGF- β, cultured on SLB. MLEC cells were presented with bare SLB of DOPC lipids, a SLB of DOPC with RGD attachment points, a SLB of DOPC with RGD and TGF-β1 presented, bare PDMS, or were culture on standard culture plate. All were corrected for the number of cells present.

These preliminary results are promising but need to be repeated and further analysed. Prior studies showed that when the cellular pathway is sufficiently

triggered it can continue the cell process without any further instructions, using the established cell-cell and the cell-ECM interactions.[30–32] The TGF- β1 assay with the MLECs is a first step towards achieving such instructive surface coatings.

4.3. Conclusions and Outlook

We demonstrated that the entire surface of the microstructured organ-on-chip devices can be coated with supported lipid bilayers. These DOPC SLB coated OoC devices are non-adherent to hMCSs, but cell-adherent OoC devices have been achieved when SLBs were tailored with cell-adhesive Chol-RGD, which self-assembles in the SLB coating. hMSCs adhered to the entire device surface and formed a near 3D network across the pillars. The SLB can be further functionalised with TGF-β1, showing the possibilities of this versatile coating.

4.4. Acknowledgements

We thank Twan Wildeboer for his help with the peptide synthesis.

4.5. Experimental section

4.5.1. Microfluidic device fabrication

The microfluidic devices were fabricated as before in the *Microfluidic device fabrication* in chapter 2. Completed devices were covered in MilliQ water to fill the channels and to preserve hydrophilicity. The devices that served as a positive control were coated with fibronectin from bovine plasma (Sigma-Aldrich) as indicated by the manufacturer.

4.5.2. Supported lipid bilayer formation in microfluidic devices

A supported lipid bilayer (SLB) was prepared using 1,2-dioleoyl-sn-glycero-3-phosphocholine (DOPC; Avanti Lipids) in chloroform. The chloroform was evaporated resulting in a lipid cake. The lipids were resuspended in phosphate buffered saline (DPBS) in a concentration of 1 mg/ml. The resulting multilamellar vesicles were extruded multiple times through a 100 nm Whatmann filter to form unilamellar vesicles. This vesicle suspension was sterilised by filtration (0.2 µm, Whatmann) to make it suitable for use in cell culture. The microfluidic devices were flushed with sterile DPBS prior to flushing the vesicle suspension through the devices. This vesicle suspension was incubated for 30 min to ensure adherence and rupture of the vesicles. After incubation the devices were rinsed profusely with DPBS. The SLB is then be functionalised when desired with an RGD linked to cholesterol (cholesteryl-KGSGRGDSG; Chol-RGD) by incubating with a 2 µM solution in DPBS for 2 hours. The Chol-RGD inserted itself into the SLB naturally. Another strategy for functionalising the SLB is with C16 linked RGD. 2 µM C16:0-RGD (palmitoyl-KGSGRGDSG) in DPBS was added to the lipid suspension, the suspension with the RGD was extruded and the vesicles used to form the SLB. The devices were used for cell seeding without a rinsing step. The formation of the SLB was checked by adding 0.5% 1-palmitoyl-2-(dipyrromethene boron difluoride) undecanoyl-sn-glycero-3-phosphoethanolamine (TopFluor® PE; Avanti Lipids) to DOPC lipids prior to preparation of the lipid cake.

4.5.3. hMSC culture and differentiation in microfluidic devices

Human mesenchymal stem cells (hMSC; Lonza) were cultured in complete medium consisting of α-MEM medium (Gibco) supplemented with 10% FBS, 100 U/ml penicillin and 100 µg/ml streptomycin (Sigma) and incubated at 37 °C and 5% CO_2 up

to one week before use in the assays. As a positive control, devices were coated with fibronectin. The cell suspension for the microfluidic devices was at a concentration of 10^6 cells/ml. Cell suspension was supplemented with Chol-RGD to a final concentration of 2 µM Chol-RGD in complete medium when used in the SLB-coated microfluidic devices functionalised with Chol-RGD. The hMSCs were cultured in the microfluidic devices up to 3 days at 37 °C and 5% CO_2 with a sufficient amount of culture medium on top of the device to connect both inlet and outlet. The culture medium in the device was changed daily.

Cell differentiation was induced on day 3 of culture. Complete medium was replaced by osteogenic differentiation medium which consisted of α-MEM medium (Gibco) supplemented with 10% FBS, 100 U/ml penicillin, 100 µg/ml streptomycin (Sigma), 0.2 mM ascorbic acid, 100 nM dexamethasone and 10 mM β-glycerophosphate. Cells were cultured up to 18 days in differentiation medium, with medium being refreshed daily. Cell adherence and cell differentiation were checked using immunofluorescence. For cell adherence the hMSCs were fixed with 4% paraformaldehyde for 5 min at 4 °C and washed with DPBS. The hMSCs were permeabilized by 0.5% Triton X in DPBS for 10 min, and stained with Alexa Fluor Phalloidin 568 (Molecular Probes, Thermo Fisher Scientific, 1:100) for actin, monoclonal anti-human vinculin-FITC antibody (anti-hVIN-1, Sigma Aldrich, 1:100) for vinculin in 0.1% Triton X and 5% bovine serum albumin (BSA) in DPBS for 1 h at room temperature. After 3x wash with DPBS the nucleus was stained with DAPI (1:1,000 in DPBS) and after a 2x wash with DPBS before closing the device with a cover glass. This provided information on the shape of the cells and on the formation of focal adhesions. Cell differentiation of hMSCs to osteoblasts was monitored with stem cell markers STRO-1 and CD90; early differentiation markers RUNX2 and osterix; mineralisation marker ALP; and bone induction marker osteocalcin.

4.5.4. FRAP analysis

The movability of the lipids in a supported lipid bilayer within the microfluidic device described in Chapter 2 was determent by fluorescence recovery after photobleaching (FRAP). For this experiment, microfluidic devices were coated with a mobile SLB was prepared by mixing 1,2-dioleoyl-*sn* (DOPC) in chloroform with 0.2% Texas Red-2-dihexadecanoyl-*sn*-glycero-3-phosphoethanolamine (TR-DHPE) in methanol The unilamellar vesicles were prepared as described before and were added to the DPBS in the microfluidic device to rupture and form an SLB by vesicle fusion. After thorough washing the devices were used for FRAP. FRAP experiments

were performed on a Nikon A1 Confocal microscope at 37 °C and the diffusion coefficient was determined after the data was checked for chromophore recovery using the formula $Dconfocal = \frac{r_e^2+r_n^2}{8\tau_{1/2}}$, where r_e is the experimental radius of the bleach spot, r_n the set radius and $\tau_{1/2}$ half time of recovery[33] As the Kang calculation assumes a circle the FRAP analysis on the side of the pillar is a slight estimate, the rounded side of the pillars make the bleaching spot[33] The circular bleaching spot (ø 10 µm) of the analysis is relatively small compare to the pillar (ø 250 µm) and it makes this a valid estimate of the diffusion coefficient.

4.5.5. TGF-β1 binding peptide synthesis

An amino acid peptide with sequence KGLPLGNSH was synthesised in an automated synthesizer (Syro ll, multiSynTech). Fmoc-Rink 4-methylbenzhydrylamine (MBHA) resin (200 mesh, Novabiochem) was loaded at 0.52 mmol/g and 50 mg was swollen in 1-methyl-2-pyrrolidinone (NMP). Amino acids (MultiSynTech) were protected using Fmoc groups and were dissolved in NMP at a concentration of 0.29 M. 20% piperidine in NMP was used as Fmoc-deprotection of the amino acids and resin, 0.3 M hydroxybenzotriazole (HOBt) in NMP was used as racemization suppressor *and 0*.26M N,N,N',N'-Tetramethyl-O-(1H-benzotriazol-1-yl)uronium hexafluorophosphate (HBTU) in NMP and 0.52 M N,N-diisopropylethylamine (DIPEA) were used as coupling reagents. The resin was swollen in NMP for 2 h. The first three coupled amino acids (HSN) were performed with a single coupling for 80 min, on the remaining 6 amino acids (GLP LGK) a double coupling was performed of twice 80 min. The last amino acid was left protected and the peptide sequence was also not yet cleaved from the resin.

4.5.6. Coupling peptide to hydrophobic tail

The resin was reswollen for 2 h in NMP. After removal of NMP, 20% piperidine in NMP was added and reacted for 5 min while shaking at 400 rot/min. This step was repeated with reaction for 15 min. After the removal of piperidine it was washed 3 times with NMP and 3 times with dichloromethane (DCM). 1.1 ml of 0.52 M DIPEA in NMP and 6 ml of 0.52 M NHS-palmitate (Sigma Aldrich) was added, this reaction was carried out at room temperature for 5 h on a shaking plate at 400 rot/min. A Kaisar test was performed on a section of the resin, and after confirmation of the result the peptides were cleaved from the resin and amino acid side groups were deprotected. A fresh cleaving cocktail was prepared of 2.5% MilliQ, 2.5% triisopropylsilane (TIS) and 95% trifluoroacetic acid (TFA). The cleavage was carried

out for 3 h while shaking at 400 rot/min. The peptides were precipitated in cold diethylether and the TFA and ether were removed in a rotary evaporator. The peptides were redissolved in MilliQ water and this solution was freeze-dried in the lyophilizer. The resulting products were analysed with MS (Waters ESI+ToF spectrometer, Micromass LCT) and HPLC with a positive column for acidic conditions. Prior to analysis, the vials were sonicated for 2 min to homogenise the suspension.

4.5.7. MLEC uptake of TGF-β1 from SLB

A supported lipid bilayer was prepared as usual with C16:0 linked TGF-β1 binding peptide (sequence KGLPLGNSH) added to the DOPC lipid suspension prior to formation of the unilamellar vesicles. A TC-treated 96-wells culture plate was prepared by adding a thin layer of PDMS in each well. The surface was activated using O_2-plasma activation (40 mA DC current and 200 mTorr vacuum pressure for 60 sec) using the Plasma etcher SPI Plasma-Prep II (SPI Supplies, West Chester PA, USA) and DPBS was added to preserve hydrophilicity. Unilamillar vesicles (100 mg/ml) with TGF-β1 binding protein were added to DPBS to a final concentration of 50 mg/ml. After formation of the SLB the Chol-RGD was added and left to insert into the SLB naturally. Recombinant human TGF-β1 (HEK293 derived, PeproTech Inc.) was added to the formed SLB. Mink Lung Epithelial Cells (MLECs, a kind gift from DBE laboratory) were seeded at 64,000 cells/cm^2 and incubated at 37 °C and 5% CO_2 for 24 h in DMEM medium supplemented with 10% FBS, 5% L-glut and 1% Pen/Strep. The MLECs expressed luciferase thanks to the Plasminogen activator inhibitor 1 – PAI-1 promoter when the TGF-β gene is activated.[28] The cells were lysed and the luciferase was quantified using the Luciferase assay system (Promega, E4530) and measured with the EnSpire® PerkinElmer Multimode plate reader. Luciferase values were normalized for the number of cells by quantifying DNA with the CyQuant cell proliferation assay (Invitrogen).

4.6. References

1. Chen, S. S., Fitzgerald, W., Zimmerberg, J., Kleinman, H. K. & Margolis, L. Cell-cell and cell-extracellular matrix interactions regulate embryonic stem cell differentiation. *Stem Cells* **25**, 553–561 (2007).
2. Du, M. *et al.* Regulation of human mesenchymal stem cells differentiation into chondrocytes in extracellular matrix-based hydrogel scaffolds. *Colloids Surfaces B Biointerfaces* **114**, 316–323 (2014).
3. Xu, R., Boudreau, A. & Bissell, M. J. Tissue architecture and function: Dynamic reciprocity via extra- and intra-cellular matrices. *Cancer Metastasis Rev.* **28**, 167–176 (2009).
4. Jimenez-Vergara, A. C. *et al.* Refined assessment of the impact of cell shape on human mesenchymal stem cell differentiation in 3D contexts. *Acta Biomater.* **87**, 166–176 (2019).
5. Rens, E. G. & Merks, R. M. H. Cell shape and durotaxis explained from cell-extracellular matrix forces and focal adhesion dynamics. *iScience* **23**, 101488 (2020).
6. Papachroni, K. K., Karatzas, D. N., Papavassiliou, K. A., Basdra, E. K. & Papavassiliou, A. G. Mechanotransduction in osteoblast regulation and bone disease. *Trends Mol. Med.* **15**, 208–216 (2009).
7. Park, S. H. *et al.* Chip-based comparison of the osteogenesis of human bone marrow- and adipose tissue-derived mesenchymal stem cells under mechanical stimulation. *PLoS One* **7**, 1–11 (2012).
8. Shav, D. & Einav, S. The effect of mechanical loads in the differentiation of precursor cells into mature cells. *Ann. N. Y. Acad. Sci.* **1188**, 25–31 (2010).
9. Pati, F. *et al.* Ornamenting 3D printed scaffolds with cell-laid extracellular matrix for bone tissue regeneration. *Biomaterials* **37**, 230–241 (2015).
10. Stoppato, M., Carletti, E., Maniglio, D., Migliaresi, C. & Motta, A. Functional role of scaffold geometries as a template for physiological ECM formation: evaluation of collagen 3D assembly. *J. Tissue Eng. Regen. Med.* **7**, 161–168 (2013).
11. Leferink, A. M., van Blitterswijk, C. & Moroni, L. Methods of monitoring cell fate and tissue growth in three-dimensional scaffold-based strategies for in vitro tissue engineering. *Tissue Eng. Part B Rev.* **22**, ten.TEB.2015.0340 (2016).
12. Langenbach, F. & Handschel, J. Effects of dexamethasone, ascorbic acid and B-glycerophosphate on the osteogenic differentiation of stem cells in vitro. *Stem Cell Res. Ther.* **4**, 117 (2013).
13. Elsafadi, M. *et al.* TGFβ1-induced differentiation of human bone marrow-derived MSCs is mediated by changes to the actin cytoskeleton. *Stem Cells Int.* **2018**, (2018).
14. Wu, M., Chen, G. & Li, Y. P. TGF-β and BMP signaling in osteoblast, skeletal development, and bone formation, homeostasis and disease. *Bone Res.* **4**, (2016).
15. Massagué, J. & Xi, Q. TGF-β control of stem cell differentiation genes. *FEBS Lett.*

586, 1953–1958 (2012).

16. Hall, B. K. & Miyake, T. Divide, accumulate, differentiate: Cell condensation in skeletal development revisited. *Int. J. Dev. Biol.* **39**, 881–893 (1995).

17. Koçer, G. & Jonkheijm, P. Guiding hMSC adhesion and differentiation on supported lipid bilayers. *Adv. Healthc. Mater.* **6**, 1600862 (2017).

18. van Meer, B. J. J. *et al.* Small molecule absorption by PDMS in the context of drug response bioassays. *Biochem. Biophys. Res. Commun.* **482**, 323–328 (2017).

19. Peng, X., Nelson, E. S., Maiers, J. L. & DeMali, K. A. New insights into vinculin function and regulation. *Int Rev Cell Mol Biol* **1**, 191–231 (2011).

20. Bally, M. *et al.* Liposome and lipid bilayer arrays towards biosensing applications. *Small* vol. 6 2481–2497 (2010).

21. van Weerd, J., Karperien, M. & Jonkheijm, P. Supported lipid bilayers for the generation of dynamic cell-material interfaces. *Adv. Healthc. Mater.* (2015) doi:10.1002/adhm.201500398.

22. Richter, R. P., Bérat, R. & Brisson, A. R. Formation of solid-supported lipid bilayers: An integrated view. *Langmuir* **22**, 3497–3505 (2006).

23. Verheijden, M. L. Supramolecular binding of vesicles, viruses and cells to biomimetic lipid bilayers. (University of Twente, 2018). doi:10.3990/1.9789036545501.

24. Mavropoulos, E. *et al.* The impact of the RGD peptide on osteoblast adhesion and spreading on zinc-substituted hydroxyapatite surface. *J. Mater. Sci. Mater. Med.* **24**, 1271–1283 (2013).

25. Kocer, G. Cell-instructive biointerfaces with dynamic complexity. (University of Twente, 2018). doi:10.3990/1.9789036545204.

26. Di Iorio, D., Lu, Y., Meulman, J. & Huskens, J. Recruitment of receptors at supported lipid bilayers promoted by the multivalent binding of ligand-modified unilamellar vesicles. *Chem. Sci.* **11**, 3307–3315 (2020).

27. Bruedigam, C. *et al.* Basic techniques in human mesenchymal stem cell cultures: Differentiation into osteogenic and adipogenic lineages, genetic perturbations, and phenotypic analyses. *Curr. Protoc. Stem Cell Biol.* 1–20 (2011) doi:10.1002/9780470151808.sc01h03s17.

28. Abe, M. *et al.* An assay for transforming growth factor-beta using cells transfected with a plasminogen activator inhibitor-1 promoter-luciferase construct.

29. Crispim, J. *et al.* TGF-β1 activation in human hamstring cells through growth factor binding peptides on polycaprolactone surfaces. *Acta Biomater.* **53**, 165–178 (2017).

30. Flynn, L. E., Prestwich, G. D., Semple, J. L. & Woodhouse, K. A. Proliferation and differentiation of adipose-derived stem cells on naturally derived scaffolds. *Biomaterials* **29**, 1862–1871 (2008).

31. Qian, W. *et al.* Nanotopographic regulation of human mesenchymal stem cell osteogenesis. *ACS Appl. Mater. Interfaces* **9**, 41794–41806 (2017).

32. Grespan, E. *et al.* Effect of geometrical constraints on human pluripotent stem cell nuclei in pluripotency and differentiation. *Integr. Biol. (United Kingdom)* **10**, 278–289 (2018).

33. Kang, M., Day, C. A., Kenworthy, A. K. & DiBenedetto, E. Simplified equation to extract diffusion coefficients from confocal FRAP data. *Traffic* **13**, 1589–1600 (2012).

Chapter 5

Culturing cardiomyocytes in a microfluidic device with defined, biomimetic microarchitecture

Abstract

The use of cardiomyocytes in organ-on-chip devices is particularly interesting as they can be used in modelling cardiovascular disease. When culturing cardiomyocytes in microfluidic devices, it is a challenge to control the three-dimensional shape of the cultures, as they tend to pull together into beating clusters. In this chapter, we used a microfluidic device with defined micro-engineered pillars to control the shape of stem cell-derived cardiomyocyte cultures. Initially, cardiomyocytes evenly covered the device surface while at a later stage, large clusters containing many cells were observed that surrounded the pillar arrays in the device. At the early stage of the culture the beating motion was heterogeneous and independent in different small clusters, but at a later stage larger scale wave-like patterns of contraction in larger clusters interspersed by pillars were observed.

The experiments in this chapter demonstrate that functional cardiomyocytes can be cultured in a microfluidic device with defined microarchitectures. Moreover, the study provides a first step towards modelling cardiac disease processes associated with scar tissue and other defects in cardiac tissue *in vitro*, as the pillars do not conduct electrical signals, analogous to how cardiac defects affect electrical conductivity in the heart.

5.1. Introduction

Cardiovascular diseases are among the leading causes of death worldwide and often cause disability.[1,2] A changing cardiac wall structure due to cardiac remodelling after injury, for instance, is a major health issue and therefore subject to much research.[3–6] Cardiac remodelling is a natural response to cardiac trauma such as ischaemia or necrosis after a myocardial infarction. The scar tissue that forms in response to cardiac injury neither contracts like the cardiac muscle nor does it conduct the electric signal through the cardiac muscle. To still meet the required cardiac output after heart injury, cardiac remodelling occurs. The heart changes in size, shape and structure. Often there is thickening of the cardiac wall, which in turn can lead to a decrease in size of the ventricles. These changes will lead to cardiac dysfunction and eventually to heart failure. Animal models are widely used to study cardiac remodelling, but stem cell-derived human cardiomyocytes (CMs) can also be used to model associated processes *in vitro*.[7–9] By supplying CMs with several surfaces that vary in their stiffness, the influence of a physically changing environment on contraction, conductivity of the electrical action potential and cell morphology can be studied.[10–14] Such experiments are facilitated by using cells that express fluorescent reporter proteins, such as the recently reported Double Reporter mRubyII-α-Actinin GFP-NKX2.5 (DRRAGN) human embryonic stem cell line.[14] CMs derived from this cell line were used in systematic studies to assess the behaviour of cardiac cells to changes in surface stiffness *in vitro*.[15,16] DRRAGN-CMs contain a GFP-reporter for NKX2.5, a key transcription factor in cardiac precursor cells, and fluorescent mRubyII fused to α-actinin, a major cytoskeletal protein in the sarcomeric structure that is important for CM contraction.[17–20] After differentiation of DRAGGN embryonic stem cells, the expression of NKX2.5 identifies the cells that have been derived from a cardiac lineage. α-Actinin and its localization in the sarcomeres allows detailed monitoring of contractile behaviour of DRRAGN-CMs.[21] Long-term culture of CMs in high densities often leads to uncontrolled clumping and formation of 3D cell clusters. A common strategy to control the formation of tissues *in vitro* is to impose a defined 3D cardiac tissue shape by offering specific locations within the modelling devices for the CMs to envelop.

In this chapter, we take advantage of the self-organizing behaviour of cardiac cells in the presence of defined microarchitecture to induce a 3D cell network inside a microfluidic device. The microfluidic device used in this chapter contains a microarchitecture of 28 vertical pillars and has previously been applied in controlling

cultures of human mesenchymal stem cells (hMSCs) (Chapters 2 and 4) and was found to be successful in providing defined attachment locations for the cultured cells. The pillar structures improved the otherwise poor adhesion of hMSCs to the polydimethylsiloxane (PDMS) device surface to form a confluent culture. Since hMSCs do not have a natural tendency to clump together[22], it will be interesting to observe the CMs in a microfluidic device with this microarchitecture. The survival of the high-metabolic CMs in a culture with only a small amount of medium is not certain.[3] This initial study will show how CMs organize themselves in such a structured device and whether a beating motion can be observed. The behaviour of DRRAGN cardiomyocytes in this microfluidic device will be informative for the design of future microfluidic cardiac disease models, for example, when studying the effects of non-conductive areas in the context of cardiac remodelling.

5.2. Results and Discussion

Before harvesting, the DRRAGN-CM cells were visually inspected in the differentiation culture. Cells that were clearly, visibly beating in unison and positive for α-actinin and NKX2.5 were chosen for seeding in the device. The microfluidic device (**Figure 5.1**) containing 28 pillars was prepared with the standard vitronectin and Mouse Embryonic Fibroblasts (MEF) medium surface coating for the DRRAGN-CMs and the cells adhered well to the surface of the microfluidic device upon seeding.

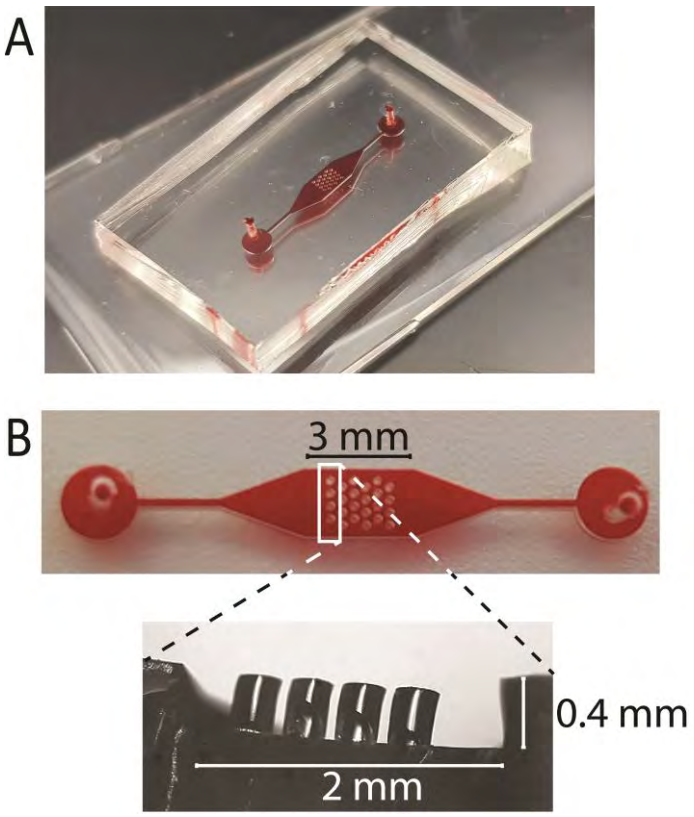

Figure 5.1 Microfluidic device measures 16 mm in total length with a channel height of 400 µm. Inlet and outlet channels measure 200 µm in width. A) Photograph of the device placed on a PDMS covered microscope slide, filled with a red dye; B) Top-view of the microfluidic device, filled with a red dye. Close-up (brightfield image) of the side view of the pillars within the hollow chamber. The surface of the device is coated with vitronectin and MEF medium for DRRAGN-CM culture.

On day 1 of culture, the DRRAGN-CMs occupied the microfluidic device throughout, with the DRRAGN-CMs just starting to come together. (**Figure 5.2**). There were no clear differences in cell occupation of the non-pillared section compared to the pillared section of the device, nor was there any major cell clumping visible throughout the device (**Figure 5.2**). The cells expressed the green NKX2.5 reporter signal and red fluorescent α-actinin. There was no contraction visible in the cells. The microdevice was kept under a 45° angle during culture to provide the highly metabolically active DRRAGN-CMs with nutrients and to remove waste products as the medium was replenished with approx. 100 µl in 24 hours. The medium in the reservoirs mounted on the device as well as in the device itself was refreshed with

new medium every 24 hours by pipetting 200 µl of medium in 5 sec through the device.

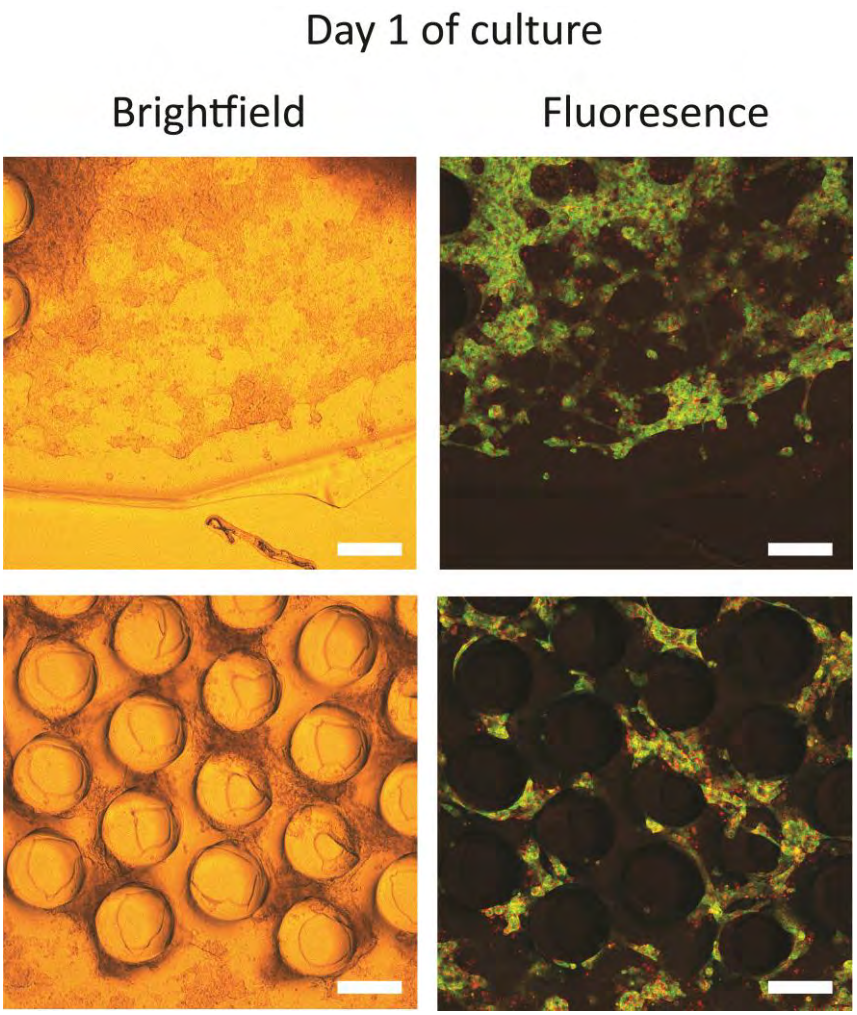

Figure 5.2 DRRAGN cardiomyocytes in a microfluidic device on day 1 of culture at the outlet (top) and in the pillar area (bottom). Brightfield (left) and fluorescence (right) microscopy images with α-actinin in red and NKX2.5 in green. The cardiomyocytes are spread though-out the device and show mild clumping. Scale bars represent 200 µm.

On day 2, after a single medium refresh, the DRRAGN-CMs between the pillars were condensed into small clumps that were spread between the pillars (**Figure 5.3**). The live-cell fluorescent reporter signals were present and a slow and weak contraction

was observed. The DRRAGN-CMs appeared to have moved from their previous location and formed larger cell aggregates in the non-pillared sections of the microfluidic device. Between the pillars, the cell clusters were smaller, as fewer cells were present on the reduced effective culture area.

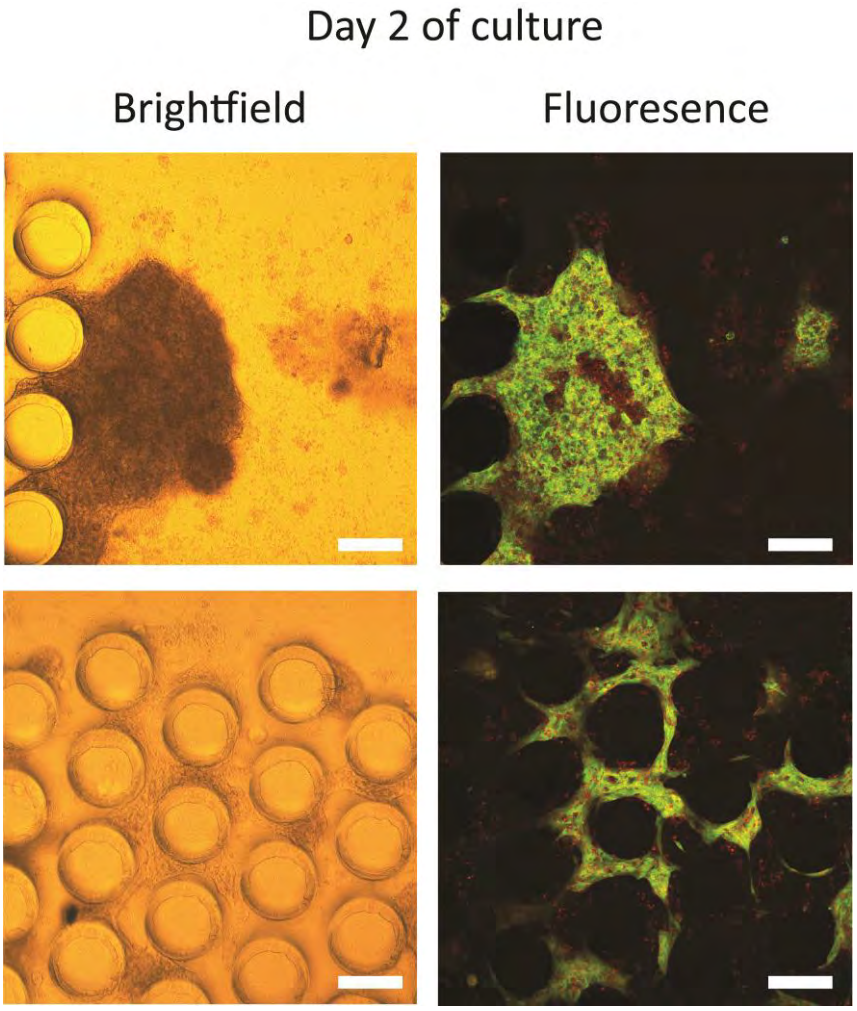

Figure 5.3 DRRAGN cardiomyocytes in a microfluidic device on day 2 of culture at the outlet (top) and in the pillar area (bottom). Brightfield (left) and fluorescence (right) microscopy images with α-actinin in red and NKX2.5 in green. The cardiomyocytes are clumping in between the pillars and in the non-pillared section of the device. Scale bars represent 200 μm.

On day 3, large aggregates were present in the non-pillared section of the device, while the smaller aggregates between the pillars disappeared with only a few very small aggregates remaining (**Figure 5.4** DRRAGN cardiomyocytes in a microfluidic device on day 3 of culture. A) Brightfield microscopy image with the clumping of the cardiomyocytes surrounding the pillars. The cluster contracted around the pillar in a wave-like motion of contraction. Arrows indicate movement direction. B) Brightfield (left) and fluorescence (right) microscopy images with α-actinin in red and NKX2.5 in green at two positions in the device. In comparison to earlier time points, the NKX2.5 expression was decreased. There are a small number of smaller clumps between the pillars and the larger clumping lies in the non-pillared section of the device.). The large aggregates displayed a triangular shape, following the overall shape of the walls of the device and were attached to the outer row of pillars of the device. The larger aggregates of cells surrounded the pillars. As a result of this aggregation with pillars amidst the aggregate, these DRRAGN-CM aggregates did not contract uniformly, but the contraction was coordinated and moved from one side of the cluster to the other in a wave-like motion.

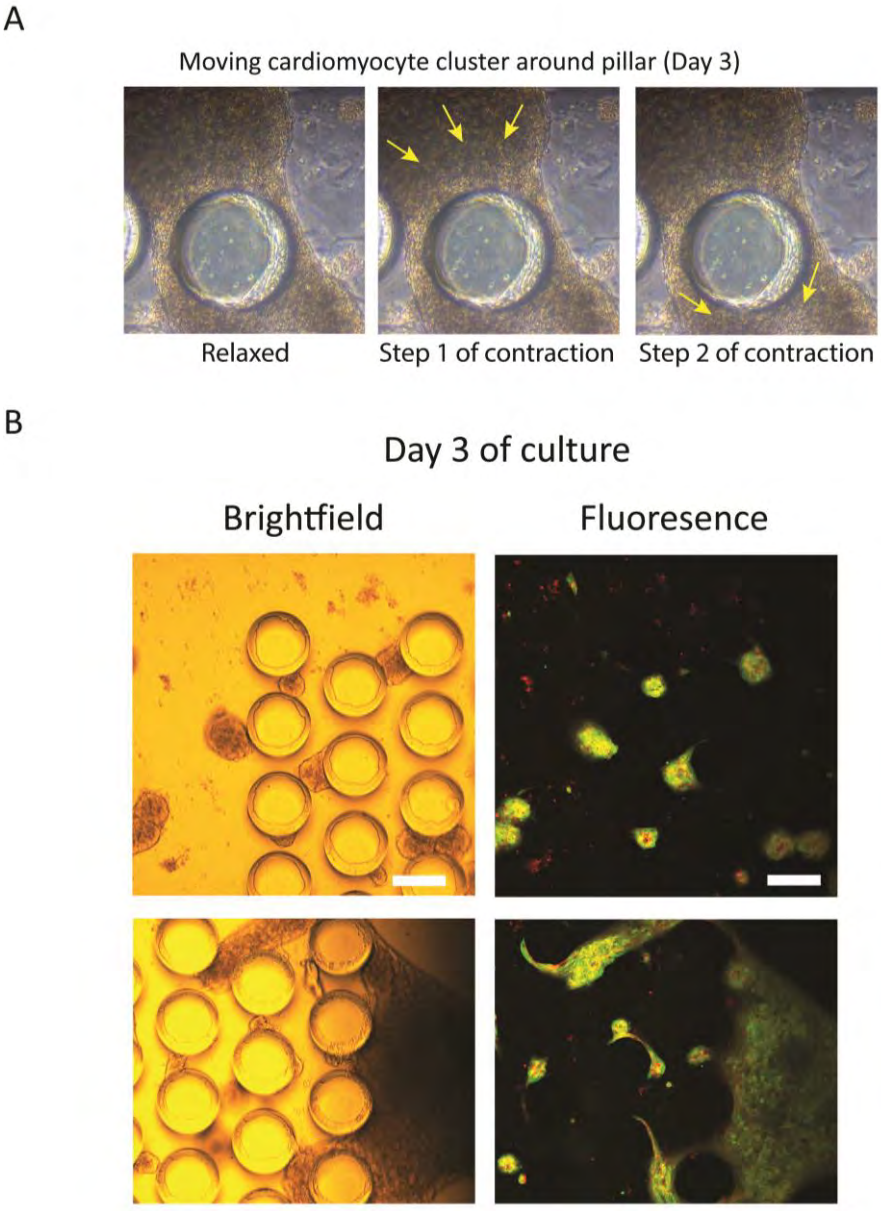

Figure 5.4 DRRAGN cardiomyocytes in a microfluidic device on day 3 of culture. A) Brightfield microscopy image with the clumping of the cardiomyocytes surrounding the pillars. The cluster contracted around the pillar in a wave-like motion of contraction. Arrows indicate movement direction. B) Brightfield (left) and fluorescence (right) microscopy images with α-actinin in red and NKX2.5 in green at two positions in the device. In comparison to earlier time points, the NKX2.5 expression was decreased. There are a small number of smaller clumps between the pillars and the larger clumping lies in the non-pillared section of the device. Scale bars represent 200 µm.

On day 3, fluorescent NKX2.5 was not detected in the smaller aggregates of cells and the small number of single cells. For the larger aggregates however fluorescent NKX2.5 was predominantly detected in the cells on the outside of the aggregates, while in the centre the fluorescence of NKX2.5 was of lower intensity. The contractile movement was discernible on day 2, however there was neither a very visible displacement of the aggregate in the beating motion, nor was it quick (approx. 5 beats/min). On day 3, the displacement of the aggregate was more visible and faster (approx. 7 beats/min). The rounded aggregates contracted uniformly, there was one beat in the aggregate visible. This is in contrast to when the aggregates surrounded one or more pillars. The beating motion moved slower through the cluster as the motion through this aggregate appeared wave-like, moving from contraction at one side of the aggregate towards the other side of the pillar.

Based on these observations, the microarchitecture successfully provided the DRRAGN-CMs culture with a predetermined shape. In areas without pillars, the cardiac tissues followed the tapered shape of the inlet and outlet of the culture chamber to form a triangular shape. In addition, the pillars were clearly affecting the formation and shape of the clusters of DRRAGN-CMs. On day 1 of culture, all cells were evenly spread in the device, also between the pillars. The clustering began between those pillars, resulting in isolated clusters throughout the device. This ensured that the bigger clusters which occurred at the longer culture of 3 days were also more spread through the device and were formed around the pillars.

NKX2.5 expression is usually not lost in cell culture with DRRAGN-CMs,[14] but on day 3 of this experiment this was the case. Contrary to the large cell clusters positioned in areas without pillars, the smaller cell clusters residing between the pillars no longer expressed NKX2.5. This could indicate that these cells have differentiated to different lineages, such as cells of the sinus node.[20]

5.3. Conclusion & Outlook

The design of the microfluidic device allowed for the formation of beating cell clusters around one or more pillars. We observed that the microarchitecture is capable to support the shape of the DRRAGN-CM clusters. The clusters first form between the pillars and then develop into larger clusters without leaving the area between the pillars, resulting in small separate aggregates. The larger clusters however can be found in the non-pillared section, as there are more cells seeded on the larger culturing area. These clumps roughly have a triangular shape, appearing to mirror the tapered shape of the non-pillared section of the device. This means

that the shape of the device could be used to influence the shape of the clusters. The apparent decrease of NKX2.5 indicates that there is a possibility that the CMs change in cell type or specialize in cell function. In future studies, this possibility can be confirmed with for instance real-time reverse transcriptase PCR, where the amount and type of mRNA is quantified to determine changes in gene expression in the cells within the aggregate.

The formation of a large aggregate around and between pillars and its subsequent behaviour of wave-like contraction offers potential for modelling of damaged cardiac wall *in vitro*. The non-conductive damaged tissue causes a beating pattern in the cardiac wall that is recapitulated by the CM aggregates interspersed with non-conducting pillars in the microfluidic device. The pillars within a contracting cluster could therefore function as a model for the non-conductive scar tissue that is present after trauma to the cardiac tissue. In future studies, the device may therefore be used as a disease model for cardiac wall defects.

5.4. Acknowledgements

We thank Simone ten Den and Kim Vermeulen for their help with the cell experiments.

5.5. Experimental Section

5.5.1. Microfluidic device fabrication

A microfluidic device was designed using CleWin 4 (WieWeb Software, Hengelo, the Netherlands) and was constructed using soft lithography. First, a negative mold was constructed using photolithography with a negative photoresist. In short, after cleaning silicon wafers using the UV/Ozone ProCleaner™ Plus (10 min, BioForce Nanosciences Inc., Ames, IA, USA), SU-8 100 photoresist was spin-coated onto them (10 sec at 500 rpm, then 30 sec at 1000 rpm) and then the wafers were placed in an oven for 30 min at 65 °C, followed by 90 min at 95 °C. Then, a mask was placed over the SU-8 coated wafer and exposed to UV-light (power density 12 mW/cm^2) for approximately 30 seconds, after which the wafer was placed on a hot plate (95 °C) for 20 min. Then, the wafer was rinsed with acetone and isopropanol, dry spun and cured on a hot plate (135 °C) for 1 h.

Polydimethylsiloxane (PDMS) was prepared by mixing Sylgard 184 elastomer with its curing agent (Dow Corning Corp, Midland, MI., USA) at a 1:10 ratio. This mixture was degassed and subsequently cast on the negative mold SU-8 wafer to create the microfluidic channels and chamber. PDMS was poured onto a microscopy slide until an even coating of PDMS was reached and cured at 60 °C for 5 h. Then, the PDMS was peeled off the negative mold wafer, cut into blocks and the inlet and outlet were punched using a 1 mm gauge puncher. The microfluidic devices were bonded to the PDMS covered microscopy slides using O_2-plasma activation (40 mA DC current and 200 mTorr vacuum pressure for 60 seconds) using the Plasma etcher SPI Plasma-Prep II (SPI Supplies, West Chester, PA, USA). Then, the devices were covered in MilliQ water to fill the channels and to preserve hydrophilicity.

5.5.2. Cell culture

DRRAGN-CMs were provided by the Applied Stem Cell Technologies department of the University of Twente where cells were differentiated as previously reported.[21,23] Briefly, human induced pluripotent stem cells (hiPSCs) were seeded at a density of 25,000 cells per cm^2 on Matrigel®-coated 6-well plates in Essential 8™ medium (ThermoFisher) on day −1. At day 0, mesodermal differentiation was initiated by addition of Wnt activator CHIR99021 (1.5 µmol/L, Axon Medchem), Activin-A (20 ng/mL, Miltenyi) and BMP4 (20 ng/mL, R&D systems) in serum-free BPEL medium (BSA, polyvinyl alcohol, essential lipids, ThermoFisher). At day 3, Wnt was inactivated

by adding XAV939 (5 µmol/L, R&D Systems) in BPEL medium. In addition, Matrigel® (1:200) was added to promote adhesion of cells. Cell cultures were refreshed on day 7 and 10 with BPEL after the start of differentiation until differentiation was completed on day 13. A visual inspection ensured that the cells were contracting, and displayed NKX2.5 and α-actinin expression. The microfluidic devices were coated with vitronectin in DPBS (500 µg/mL, ThermoFisher) for 1 h, followed by 1 h of coating with Mouse Embryonic Fibroblasts (MEF) medium (DMEM/F12 with GlutaMAX™, 10% FBS, 1% MEM NEAA and 1% penicillin/streptomycin, all from ThermoFisher). The cell suspension for the microfluidic devices was at a concentration of 10^6 cells/ml in cell culture medium. The CMs were cultured in the microfluidic devices up to 3 days at 37 °C and 5% CO_2 with the devices at an angle of 45° to ensure a constant flow of medium. To provide the pressure and the needed medium, 200 µL pipette tips were placed in the inlet and outlet of the devices. The tip at the outlet contained 50 µL medium and the tip at the inlet contained 200 µL medium. Medium was refreshed daily by replacing the medium at the inlet and pull 200 µL through the device with a pipette.

5.5.3. Image analysis

The CMs were imaged with a confocal microscope (Nikon A1) at excitation/emission wavelengths 488/561 nm and 568/561 nm and in brightfield. The images were analysed using Fiji (ImageJ). Movement analysis was done by recording video with an inverted phase-contrast microscope and the stills were analysed for movement with Adobe® Photoshop®.

5.6. References

1. WHO Fact sheet Cardiovascular disease (CVDs). https://www.who.int/news-room/fact-sheets/detail/cardiovascular-diseases-(cvds).
2. Martins, B., Ferreira, D., Neto, C., Abelha, A. & Machado, J. Data mining for cardiovascular disease prediction. *J. Med. Syst.* **45**, 6 (2021).
3. Bagali, S. & Das, K. K. Hypoxia and its preconditioning on cardiac and vascular remodelling in experimental animals. *Respir. Physiol. Neurobiol.* **285**, 103588 (2021).
4. Whitaker, J. *et al.* Standardised computed tomographic assessment of left atrial morphology and tissue thickness in humans. *IJC Hear. Vasc.* **32**, 100694 (2021).
5. Maforo, N. G. *et al.* T1-Mapping and extracellular volume estimates in pediatric subjects with Duchenne muscular dystrophy and healthy controls at 3T. *J. Cardiovasc. Magn. Reson.* **22**, 1–13 (2020).
6. Bocalini, D. S. *et al.* Short-term cigarette smoking in rats impairs physical capacity and induces cardiac remodeling. *Biomed Res. Int.* **2020**, (2020).
7. Lee, M. O. *et al.* Modelling cardiac fibrosis using three-dimensional cardiac microtissues derived from human embryonic stem cells. *J. Biol. Eng.* **13**, 1–17 (2019).
8. Parrotta, E. I., Scalise, S., Scaramuzzino, L. & Cuda, G. Stem cells: The game changers of human cardiac disease modelling and regenerative medicine. *Int. J. Mol. Sci.* **20**, (2019).
9. Schwach, V., Slaats, R. H. & Passier, R. Human pluripotent stem cell-derived cardiomyocytes for assessment of anticancer drug-induced cardiotoxicity. *Front. Cardiovasc. Med.* **7**, 1–12 (2020).
10. Mannhardt, I. *et al.* Human engineered heart tissue: analysis of contractile force. *Stem Cell Reports* **7**, 29–42 (2016).
11. Pandey, P. *et al.* Cardiomyocytes sense matrix rigidity through a combination of muscle and non-muscle myosin contractions. *Dev. Cell* **44**, 326-336.e3 (2018).
12. Wan, W., Bjorkman, K. K., Choi, E. S., Panepento, A. L. & Leinwand, L. A. Cardiac myocytes respond differentially and synergistically to matrix stiffness and topography. *BioRXiV* **52**, 13803–29 (201AD).
13. Boothe, S. D. *et al.* The effect of substrate stiffness on cardiomyocyte action potentials. *Cell Biochem. Biophys.* **74**, 527–535 (2016).
14. Ribeiro, M. C. *et al.* A cardiomyocyte show of force: A fluorescent alpha-actinin reporter line sheds light on human cardiomyocyte contractility versus substrate stiffness. (2020) doi:10.1016/j.yjmcc.2020.03.008.
15. Breckwoldt, K. *et al.* Differentiation of cardiomyocytes and generation of human engineered heart tissue. *Nat. Protoc.* **12**, 1177–1197 (2017).
16. Schwach, V. & Passier, R. Native cardiac environment and its impact on engineering

cardiac tissue. *Biomater. Sci.* **7**, 3566–3580 (2019).

17. Sjöblom, B., Salmazo, A. & Djinović-Carugo, K. α-Actinin structure and regulation. *Cell. Mol. Life Sci.* **65**, 2688–2701 (2008).

18. Hsu, C. P., Moghadaszadeh, B., Hartwig, J. H. & Beggs, A. H. Sarcomeric and nonmuscle α-actinin isoforms exhibit differential dynamics at skeletal muscle Z-lines. *Cytoskeleton* **75**, 213–228 (2018).

19. Behrens, A. N. *et al.* Nkx2-5 mediates differential cardiac differentiation through interaction with Hoxa10. *Stem Cells Dev.* **22**, 2211–2220 (2013).

20. Sizarov, A. *et al.* Molecular analysis of patterning of conduction tissues in the developing human heart. *Circ. Arrhythmia Electrophysiol.* **4**, 532–542 (2011).

21. Ribeiro, M. C. *et al.* A cardiomyocyte show of force: A fluorescent alpha-actinin reporter line sheds light on human cardiomyocyte contractility versus substrate stiffness. *J. Mol. Cell. Cardiol.* **141**, 54–64 (2020).

22. Mushahary, D., Spittler, A., Kasper, C., Weber, V. & Charwat, V. Isolation, cultivation, and characterization of human mesenchymal stem cells. *Cytom. Part A* **93**, 19–31 (2018).

23. Birket, M. J. *et al.* Contractile defect caused by mutation in MYBPC3 revealed under conditions optimized for human PSC-cardiomyocyte function. *Cell Rep.* **13**, 733–745 (2015).

Summary

Identifying physical and chemical cues that regulate cell differentiation in tissues *in vivo* is very valuable in the fabrication of *in vitro* models. These *in vitro* models are fabricated in many ways (**Chapter 1**). Three-dimensional models are a better mimic of the *in vivo* microenvironment compared to two-dimensional cell culture. Further optimized *in vivo*-like mimics have been achieved when incorporating a microarchitecture design in devices and when ligand-functionalized substrate coatings were included.

In this thesis, a microenvironment was constructed in which a microarchitecture improved the formation of a three-dimensional cell network and supported cell differentiation. To accomplish this, a silicone elastomer microfluidic device was fabricated including a microarray of pillars (**Chapter 2**). These pillars provided human mesenchymal stem cells (hMSCs) with the three-dimensional support to form a cellular network, while the hMSCs can survive for up to 3 weeks in the microfluidic device.

Coating the silicone elastomer substrate with cell-adhesive ligands provides hMSCs with instructive information to differentiate. In the different tissues in the body these ligands can move when pulled on in soft tissues (such as adipose tissue) or stay in place in harder tissues (such as bone). The mobility of the cell-adhesive ligands is instrumental for achieving a differentiation-supportive hMSC morphology. We found that different types of stiffness of the silicone elastomer substrate yielded similar hMSC response when these substrates were covered with the same type of cell-adhesive mobile coating. (**Chapter 3**). This difference of morphology of hMSCs can help steer the differentiation towards adipose tissue or bone.

The surface of the pillar microarray and the surrounding Organ-on-Chip (OoC) device surface were coated with the cell-adhesive mobile coatings. The hMSCs cultured in the device again formed the cellular network (**Chapter 4**). Ligands to instruct differentiation to bone (TGF-β1) were added to the coating successfully to arrive at more complex cell-instructive coatings.

Cardiomyocytes were cultured in the OoC devices consisting of a pillar microarray. In a multiday culture, clusters of cardiomyocytes were observed, but the pillar microarrays provided a microstructure that did not synchronize the beating motion of these clusters throughout the device (**Chapter 5**).

We designed a microfluidic OoC device in which a microarray was incorporated and this entire device was chemically coated. This OoC device promoted hMSC network formation and differentiation. Such modular devices are important to construct *in vitro* models for future disease modeling, pharmaceutical studies and biomedical research.

Samenvatting

Het identificeren van fysieke en chemische signalen die differentiatie van cellen in *in vivo* weefsels reguleren is waardevol om zinvolle *in vitro* imitaties te maken. Deze *in vitro* imitaties worden met vele methoden gemaakt (**Hoofdstuk 1**). Driedimensionale modellen bootsen de originele *in vivo* micro-omgeving beter na dan tweedimensionale celkweken. Verdere optimalisatie van deze imitaties wordt bereikt door het aanbrengen van een micro-architectuur in de vloeistofkanaaltjes van microfluïdische chips. Ook door het toevoegen van een laagje met liganden om de aanhechting van cellen te bevorderen kan leiden tot betere imitaties van *in vivo* weefsels in handklare microchips.

In dit proefschrift wordt beschreven hoe micro-architectuur kan worden aangebracht in de chips en hoe deze de vorming van een driedimensionaal netwerk van cellen verbeterde en de differentiatie van de stamcellen ondersteunde. Een microfluïdische chip werd vervaardigd uit een op siliconen gebaseerd elastomeer met kanaaltjes voorzien van meerdere rijen pilaren van hetzelfde elastomeer (**Hoofdstuk 2**). Deze pilaren droegen bij dat menselijke mesenchymale stamcellen (hMSC's) een driedimensionaal netwerk vormden waarin de hMSC's tot wel drie weken in de chip overleefden.

Door het elastomeer oppervlak te bedekken met celhechtende liganden krijgen de hMSC's betere instructie om te differentiëren. In de verschillende weefsels in het lichaam hebben deze liganden verschillende mobiliteit. Deze liganden kunnen bewegen zodra er kracht op uitgeoefend wordt in zachte weefsels (zoals vetweefsel) of juist minder bewegen in hardere weefsels (zoals botweefsel). De mobiliteit van de deze celhechtende liganden is een belangrijk signaal dat de morfologie van hMSC's beïnvloedt en deze morfologie ondersteunt de richting van de differentiatie. We ontdekten dat wanneer verschillende stijfheden van het elastomeer oppervlak worden bedekt met een laag liganden die dezelfde mobiliteit hebben, de hMSC's ook dezelfde reactie geven (**Hoofdstuk 3**). Deze manipulatie van de verschillen in morfologie van de hMSC's kan helpen in het sturen van de differentiatie in de richting van ofwel vet- ofwel botweefsel.

De oppervlakte van de pilaren en de wanden in de chip werden vervolgens bedekt met een laagje celhechtende mobiele liganden. De hMSC's gekweekt in deze microchips vormden een netwerk van cellen (**Hoofdstuk 4**). Liganden welke

instrueren om naar bot te differentiëren (TGF-β1) werden succesvol toegevoegd aan de laag wat kan leiden tot een meer complexe, instruerende laag.

In het laatste hoofdstuk werden cardiomyocyten gekweekt in de microchips voorzien van dezelfde pilaren micro-architectuur. Na een periode van meerdere dagen groeiden de cardiomyocyten bij elkaar en vormden clusters, maar de pilaren zorgden voor asynchrone, samentrekkende bewegingen van de ontstane clusters (**Hoofdstuk 5**).

Al met al, hebben we een microfluïdische chip ontwikkeld met vloeistofkanaaltjes waarin een pilaren micro-architectuur is neergezet welke kan worden voorzien van een chemische laag met liganden om netwerkvorming en differentiatie van gekweekte stamcellen te bevorderen. Zulke modulaire microfluïdische chips waarin op realistische wijze *in vitro* imitaties van weefsels kunnen worden gemaakt lenen zich zeer goed om op relatief eenvoudige wijze toekomstig onderzoek naar oorzaken van en behandeling voor ziekten te versnellen

Acknowledgements

Ik heb een hoop mensen te bedanken. Zonder hun advies, hulp en aanmoedigingen zou ik deze jaren niet succesvol hebben kunnen afsluiten.

Als eerst wil ik mijn promotor Pascal Jonkheijm en co-promotoren Andries van der Meer en Martin Bennink bedanken. Jullie zijn een fantastisch team samen en jullie hebben mij voorzien van advies en de discussies en kritische opmerkingen waren een waardevolle bijdrage aan mijn onderzoek. Pascal, dank je dat je mij de kans hebt gegeven om mijn promotie te doen binnen jouw onderzoeksgroep.

Next of course I would like to thank the graduation committee members, prof. dr. Nico Sommerdijk, prof. dr. Roman Truckenmüller, prof. dr. Robert Passier and prof. dr. Jeroen Cornelissen. Thank you for taking the time to be part of my defence. I also hope that my research can be a step forward in your own field.

Mijn grote dank gaat vervolgens uit naar mijn paranimfen. Ik heb het geluk om twee van mijn beste vriendinnen op de werkvloer te hebben gevonden. Louise en Melissa, jullie zijn mijn grote steunpilaren geweest en zullen dat altijd blijven. Jullie wijsheden in zowel academisch als mentale ondersteuning en jullie idioterie zijn legendarisch. Louise, jij en ik weten met een post-it en 30 minuten ongestoord werk ontzettend veel gedaan te krijgen. Je hield me op de hoogte van de Saxion gebeurtenissen en je hield me in het gareel met alle deadlines waar ik me aan moest houden. Je hebt dubbel zo hard gewerkt om mij de gelegenheid te geven om mijn PhD te doen en daar ben ik je ontzettend dankbaar voor. Melissa, you were like one meter away in the Coop and after the lockdown only one message away. Somehow you always knew what to say and how to help me along if I got stuck in my too many options of how to handle something. The tea breaks were also an eye opener for me, you know so much and you are happy to share. Thank you for your wisdom and your company.

Natuurlijk gaat mijn dank uit naar mijn collega's en het management van Hogeschool Saxion. Peter van Dam en Coby Flier, dank dat jullie achter mijn plan stonden om aan een PhD te beginnen. Peter Schön, dank je dat je zo actief mee dacht waar ik een PhD over zou kunnen doen, om vervolgens meteen je telefoon te pakken en Pascal een berichtje te sturen. Team FO, jullie zijn geweldig geweest. Jullie waren bereid om mij bij te praten wanneer nodig. Jullie maakten het me zo makkelijk mogelijk en

vooral, jullie waren hartelijk en collegiaal. Ook de andere collega's van LS, van praktijkondersteuning tot kerstborrels, ik kon altijd vragen om hulp en kon altijd aanschuiven alsof ik jullie dagelijks tegenkwam.

My time at MnF/BNT would not have been the learning experience what it was without the other staff members. Thank you Jos, Jurriaan, Wim, Nathalie, Tibor and Jeroen for your input during colloquia and at the coffee table. Saskia en Albert, jullie heb ik maar kort mogen spreken. Ik wens jullie en de meest recente toevoegingen in het nieuwe MolMat cluster veel succes.

Mijn onderzoek zou nooit fatsoenlijk van de grond zijn gekomen zonder hart en ziel van de groep: Nicole, Izabel, Regine, Bianca, Marcel en Richard. Jullie hadden altijd een helpende hand in het geval van organisatorische perikelen, labmomentjes en computerdiscussies. Regine, vooral van onze bio-gesprekken heb ik genoten.

I would like to express my gratitude to prof. dr. Julius Vancso and dr. ing. Hubert Gojzewski. Your advice and Hubert your measurements helped make my Chapter 3 reach the next level.

Mijn oud-collega's Milou, Mark en Gulistan, ik dank jullie voor de introductie in het veld van lipids, vesicles en bijlagen. Milou, met jou kon ik mijn plannen voor en twijfels over de cellen bespreken en je had de handigste tips in het maken van PDMS devices. Josh, thank you for introducing me to the making process of PDMS devices. I could always ask you when I encountered a problem. En Wouter, zonder jou zouden de devices niet zo vlot in mijn onderzoek kunnen bestaan. Dank je voor het (herhaaldelijk) maken van de temples in de cleanroom.

Onderzoek doet men nooit alleen. Ik wil dan ook graag mijn stagiaires bedanken: Aukie, Aina en Twan. Ieder van jullie heeft een belangrijke bijdrage geleverd voor mijn onderzoek. Zonder jullie werk was ik niet zo ver gekomen als dat ik nu ben.

Nico, Erik, Naomi, Jos en Richard, samen hebben we de werkweek naar Mainz mogen organiseren. Ik vond het geweldig om dit samen met jullie te doen en het werd een superleuke en leerzame trip.

Mainz is not the only trip I made. Jacopo en Daniele, you were great company to have in Zurich. Daniele, thank you for your patience while you had to handle my navigational skills. You got us there safe!

Naast alle wetenschappelijke bijdragen was er ook tijd voor ontspanning. Ik ben terecht gekomen in een hartelijke groep van PhD's die mij binnen een week includeerden in hun etentjes. Ik heb mij ontzettend welkom gevoeld in jullie club. Janneke, Milou, Rianne, Robin, Erik, Nico, Mark, Mark, Stan en Wouter, ik kan jullie niet genoeg bedanken voor de mooie tijd en ik hoop dat we elkaar snel weer eens kunnen zien. Robin, Erik en Nico, uit dit groepje hebben wij weer een subgroep weten te maken. Ik bak misschien niets van bordspellen, maar jullie gezelschap tijdens de lange weekendjes weg met Melissa, Bea en Elvera was goud waard. Luca, you have a beautiful soul and a wicked sense of humour. It has been a joy to sit next to you in the Coop. Janita, Amber, Elvera en Jeltsje, dank jullie voor de gezelligheid en de bio-gesprekken. Robin, ook jij bent een prachtvoorbeeld dat je je beste vrienden gewoon op de werkvloer kunt vinden. Dank je voor al je humor, wijze raad en je vriendschap en dank je dat ik de eervolle taak mocht hebben jouw paranimf te zijn.

I would like to thank everybody from the MnF/BNT cluster for their scientific discussions and fun at the coffee corner. I wish you all the best of luck and much joy in your endeavours, both in and outside the lab.

Ik ben ook mijn sportvriendinnen dankbaar. Jullie gaven mij een moment van rust, jullie lieten me uitleggen wat ik aan het doen was en jullie hadden soms zelfs de boel alvast voor mij klaarstaan als ik het nog maar net kon redden allemaal. Sandra, jou ben ik vooral dankbaar dat je jouw paardje aan mij toevertrouwt. In mijn afsluitend jaar van mijn PhD, midden in de lockdown, kon ik toch het bos in om even uit te waaien.

En natuurlijk mijn beste vriendin Anouk, al meer dan 20 jaar is het samen lachen en levenservaringen uitwisselen. Er zijn eigenlijk geen woorden goed genoeg om uit te drukken wat jij voor mij betekent, en hoe waardevol jouw vriendschap was in de afgelopen tijd waarin ook nog van alles gebeurde. Ik wens je alle geluk van wereld met je prachtige gezin.

Als laatst, maar het meest waardevolle dat ik bezit, mijn ouders en mijn zus. Jullie hebben je trots en liefde voor me nooit onder stoelen of banken gestoken. Nu is het mijn beurt. Ik ben zo ongelofelijk trots op jullie, op alles wat jullie hebben bereikt en daarmee mij een prachtig voorbeeld hebben gegeven. Tijdens mijn PhD zijn jullie meer dan behulpzaam geweest, hoe en waar ik het ook maar nodig had. Ik ben de

gelukkigste PhD-student met zulke fantastisch ouders en grote zus. Ik kan het niet anders zeggen: ik hou van jullie.

Good goan!